UNIVERSITÀ DI PISA

Ingegneria dell'Energia, dei Sistemi, del Territorio e delle Costruzioni

Corso di Laurea Magistrale in Ingegneria Energetica

Thermal and fluid-dynamic analysis in support to the design of a tokamak breeding blanket

Relatori

Prof. Nicola Forgione

Prof. Walter Ambrosini

Ing. Alessandro Del Nevo

Ing. Ivan Di Piazza

Candidato

Andrea Giovinazzi

ANNO ACCADEMICO 2014/2015

ABSTRACT

The conceptual design of Demonstration Fusion Power Reactor (DEMO) is developed under the leadership of EUROfusion Consortium Agreement with EU H2020 funds. The breeding blanket is a key nuclear component of Demonstration Fusion Power Reactor (DEMO), being in charge of the power extraction, the tritium fuel sustainability and the vacuum vessel radiation shielding. An attractive breeding blanket concept is the Water-Cooled Lithium-Lead Breeding Blanket (WCLL), which is considered a candidate option.

Starting from the experience exploited during previous studies, a new conceptual design has been proposed and is been developed as a multi-module box concept based on DEMO 2015 specifications. The layout of the module is based on horizontal (i.e. radial-toroidal) water cooling tubes in the Breeding Zone (BZ) and on PbLi flowing in radial-poloidal directions. Therefore, besides the caps zone, the central equatorial module is composed by 14 segments having the same geometry.

Within the framework of the DEMO R&D activities, a computational thermal and fluid-dynamic model is developed to investigate the thermal-hydraulic efficiency; to evaluate the temperature distribution in the structures and the thermal field and flow path in the breeding zone. Three-dimensional meshes are set-up, reproducing a toroidal-radial slice of the central equatorial module. It includes six breeder channels in the toroidal direction and one breeder cell in poloidal direction. Solid structures (EUROFER97 and tungsten) and fluid domains (PbLi and coolant) are considered, exploiting the ANSYS CFX (ver. 15.0) solver based on the volume finite method.

Different analyses are carried out changing the mass flow rate distributions in the cooling tubes; the first wall heat load addressing the module performance when limiting temperature conditions are considered and finally the tubes and baffle plate layout in order to optimize the thermal field in the module.

The first series of calculations highlighted where allowable limits are not met and possible criticalities in the PbLi flow paths (i.e. stagnant or low flow zone) giving hints for

enhancements of baffle plate geometry and for the layout of the tubes in the breeding zone. The last simulation demonstrates reduced operating temperatures of PbLi and structures, about 30°C below the tolerable limits and enhanced flow rates and temperatures of coolant in the different arrays of the breeding zone.

SOMMARIO

Il design concettuale del reattore a fusione dimostrativo DEMO è sviluppato sotto la guida del Consorzio EUROfusion attraverso i fondi EC Horizon 2020. Il breeding blanket è un componente fondamentale del progetto DEMO in quanto è indispensabile per l'estrazione della potenza, per garantire la sostenibilità del combustibile trizio, nonché per fornire l'idonea schermatura contro le radiazioni. Il Water-Cooled Lithium-Lead Breeding Blanket (WCLL) rappresenta un possibile candidato per il blanket di DEMO.

Sfruttando l'esperienza dei precedenti studi, un nuovo disegno concettuale del WCLL è stato proposto e sviluppato con approccio modulare basato sulle specifiche di DEMO 2015. Il layout del modulo si basa su tubi di raffreddamento ad acqua orizzontali (radiali - toroidali) nella BZ e su PbLi che scorre in direzione radiale-poloidale. Inoltre, escludendo le zone periferiche, il modulo equatoriale centrale è composto da 14 segmenti aventi la stessa geometria.

Nell'ambito delle attività di ricerca e sviluppo del progetto DEMO, il presente lavoro di tesi ha avuto l'obiettivo di realizzare un'accurata analisi computazionale termo-fluidodinamica al fine di valutare le performance termo-idrauliche, la distribuzione di temperatura nelle strutture, nel breeder e nel coolant ed il campo di velocità nel dominio fluido del breeding blanket del WCLL. A tal fine è stato realizzato un modello 3D semplificato del modulo equatoriale esterno (OB4) del WCLL; il modello riproduce una fetta centrale toroidale – radiale del modulo e include 6 canali breeder in direzione toroidale e una cella breeder in direzione poloidale. Il modello è stato simulato, considerando sia le strutture solide (acciaio e tungsteno) sia domini fluidi (lega eutettica PbLi e refrigerante), utilizzando il software ANSYS CFX (ver. 15.0) basato sul metodo dei volumi finiti.

Sono state effettuate diverse analisi variando la distribuzione delle portate di fluido del refrigerante per valutare differenti condizioni di funzionamento e per determinare il valore limite del flusso termico sulla prima parete tollerabile dal modulo. Infine è stato modificato il layout dei tubi della zona di breeding e la lunghezza della piastra deflettrice per ottimizzare il campo termico e di velocità all'interno del modulo.

La prima serie di analisi ha evidenziato le zone all'interno del dominio dove i limiti imposti ad alcuni parametri termoidraulici non vengono soddisfatti e le criticità riguardanti la presenza di possibili zone di ristagno del PbLi fornendo suggerimenti per migliorare la geometria del deflettore e la disposizione dei tubi nella Breeding Zone (BZ).
L'ultima simulazione mette in evidenzia i miglioramenti ottenuti con la modifica del layout, in particolare temperature del PbLi e delle strutture sono state ridotte di circa 30 °C al di sotto dei valori limite e migliore distribuzione di portate all'interno del modulo e temperature del refrigerante nelle diverse schiere della BZ.

LIST OF CONTENTS

LIST OF FIGURES

LIST OF TABLES

LIST OF ABBREVIATIONS

ALARA	As Low As Reasonably Achievable
BB	Breeder Blanket
BC	Boundary Conditions
BM	Breeder Module
BoP	Balance of Plant
BP	Back-Plate
BSS	Back Supporting Structure
BU	Breeder Unit
BW	Back Wall
BZ	Breeder Zone
CAD	Computer Aided Design
CEA	Commissariat à l'Energie Atomique et aux Energies Alternatives
CEL	CFX Expression Language
CIEMAT	Centro de Investigaciones Energéticas, Medioambientales y Tecnológicas
CFD	Computational Fluid Dynamics
CREATE	Consorzio di Ricerca Energia e Applicazioni Tecnologiche dell'Elettromagnetismo
DCLL	Dual Coolant Lithium Lead
DEMO	Demonstration Power Plant
DWT	Double Walled Tube
EFDA	European fusion development agreement
ENEA	Agenzia nazionale per le nuove tecnologie, l'energia e lo sviluppo economico sostenibile
EU	European Union
FE	Finite Element
FPP	Fusion Powerplant
FW	First Wall
HCLL	Helium Cooled Lithium Lead
HCPB	Helium Cooled Pebble Bed
IB	Inboard Blanket
IFMIF	International Fusion Material Irradiation Facility
ITER	International Thermonuclear Experimental Reactor
KIT	Karslruhe Institute Of Technology
LiPb	Lithium Lead
LOCA	Loss of coolant accident
MHD	Magneto hydrodynamic
MMS	Multi-Module Segmentation
OB	Outboard Blanket
PPCS	Power Plant Conceptual Study
PPP&T	Power Plant Physics & Technology
PWR	Pressurised Water Reactor
R&D	Research And Development
RAFM	Reduced Activation Ferritic/Martensitic Steel
TBM	Test Blanket Module
TBR	Tritium Breeding Ratio
UNIPA	Università degli studi di Palermo
UNIPI	Università di Pisa
VV	Vacuum Vessel
WCLL	Water Cooled Lithium Lead
WPBB	Work Package Breeding Blanket
WPBoP	Work Package Balance Of Plant

1 INTRODUCTION

The growing demand for electrical energy and the need of reducing greenhouse gas emissions has promoted worldwide the interest in nuclear fusion research over the last decades. In fact, fusion power offers the prospect of an inexhaustible source of energy with environmentally attractive and, advantages in terms of safety and sustainability.

The development of fusion technology requires to face and to solve from fundamental scientific challenges to engineering ones. These will be addressed by ITER (under construction in France) that would prove the technology, by IFMIF (Japan leader of the engineering design) that would be employed to solve material issues and, finally, by DEMO that would be the intermediate step of the commercial fusion power plant for electrical energy production.

EUROfusion Consortium Agreement is in charge of the development of concepts for the fusion power demonstration plant DEMO (Fig. 1). The Consortium involves 29 research organizations from 26 European countries (including Switzerland). Among these, Italy, through ENEA, is one of the main stakeholders and University of Pisa is its Linked Third Party. The program is financed by the European Commission and the EURATOM Member States, through Horizon 2020 funds and is pursued on the basis of a roadmap [1]. Within the roadmap the breeding blanket project represent one of the most important and novel part of DEMO.

The breeding blanket is a key component in a fusion power plant in charge of ensuring tritium breeding, neutron shielding and energy extraction. Four design options are considered for DEMO, differing for the coolant (i.e. He, water, and PbLi) and for the breeder/multiplier (i.e. solid or PbLi). The main design drivers are the T self-sufficiency, the thermo-hydraulic efficiency and structural capability to withstand the most severe loading conditions.

Besides EU choice for ITER Test Blanket Module (TBM) program is based on helium as coolant, Water-Cooled Lithium-Lead Breeding Blanket (WCLL) is considered a candidate option in view of the risk mitigation strategy for the realization of DEMO. Indeed, this design might benefit of efficient cooling performances of water as coolant, as well as of a credible program for the power conversion system, based on conventional and reliable balance of plant.

Water Cooled Lithium Lead blanket has been studied, since the idea of producing energy with a tokamak raised. Pros and cons of this design were assessed in the blanket comparison and selection study, funded by DoE, US in 1985 [2].

The design was also developed within the EU during more than 30 years [3][4][5][6]. Among several proposed WCLL blanket concepts the "single-box" concept was chosen by CEA in 1993 as the "reference" one to be further developed. Then, various blanket designs were derived from this study, which were adapted to specific reactor specifications and requirements. The last, in order of time, was the study done during 2012 – 2013 at CEA, based on "multi-modules" concept and adapted to 2012 EU DEMO specifications[7][8].

Since 2014, ENEA is the leader of the design and its design was proposed and studied based on DEMO 2015 specifications.

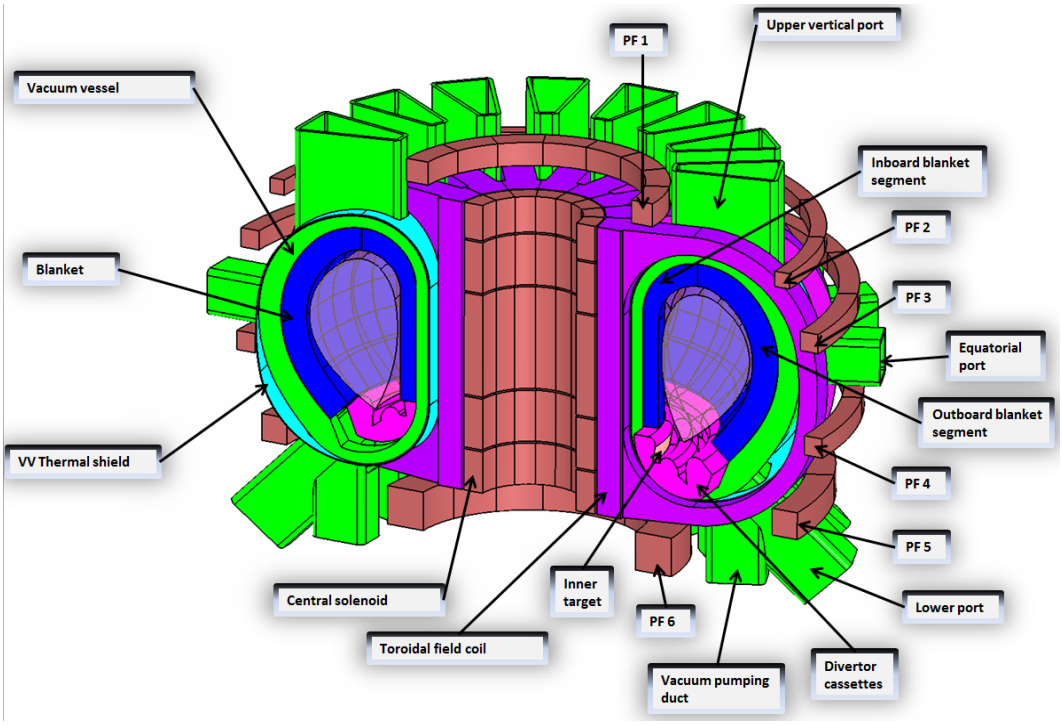

Fig. 1 – DEMO Tokamak plant model [9]

The multi-module box concept was maintained, reviewing the segmentation, but the PbLi flow path and the water cooling system has been changed. The rationale driving the design choices is having a modular design, where a basic geometry is repeated along the poloidal direction of the segment [10].

This approach is pursued by means of

- CAD activities including integration studies;

- thermo-mechanical analyses aimed at ensuring the thermal and mechanical performances fulfil the requirements during normal, off normal and accident conditions;
- neutronic study for demonstrating the achievement of the TBR target (i.e. > 1.1) and sufficient shielding performances;
- thermal hydraulic investigations (including preliminary MHD) devoted to the assessment of the thermal-hydraulic efficiency, to the calculation of the thermal field of the structures and of the LiPb zone, to the evaluation of the flow paths in the breeding zone and in the inlet collector, and to the optimization of the geometry layout.

The activity of this thesis is just focussed on last bullet above. A geometrical domain and spatial discretization of the WCLL equatorial outer module basic geometry has been developed. This reproduces a central toroidal-radial slice of the module and it includes six breeder cells in the toroidal direction and one breeder cell in poloidal direction. The model has been simulated taking by ANSYS CFX (ver. 15.0) code in account solid structures (EUROFER97 and tungsten) and fluid domains (PbLi and coolant).

1.1 Statement of objectives

The main goal of this research activity is the assessment of the thermo-hydraulic analysis of the breeding zone in order to support the module design, highlighting where allowable limits are not met. Design modifications/improvements are identified to solve major issues. In particular, the following objectives have been pursued during the advancement of the research:

- Supporting the water cooling pipes layout.
- Definition of PbLi inlet and outlet orifices.
- Study of PbLi temperature and flow pattern (which will be complemented in future studies through MHD assessment).
- Analysis of water coolant temperature and pipes pressure drops.

2 INSIGHT THE FUSION ENERGY AND MAGNETIC CONFINEMENT DESIGN

Fusion is a form of nuclear energy that involves the merging of light elements, mainly hydrogen (H) and its isotopes deuterium (D) and tritium (T). Ordinarily the energy value for nuclear reactions is in the range 10–100 MeV. The energy released by nuclear reaction is always huger than a chemical reaction with a factor of about one million in energy release between nuclear and chemical reactions. Therefore, huge quantities of energy can be produced from small amounts of material [11].

The fusion of hydrogen is the main reaction that powers the sun through the conversion of matter into energy (Fig. 2).

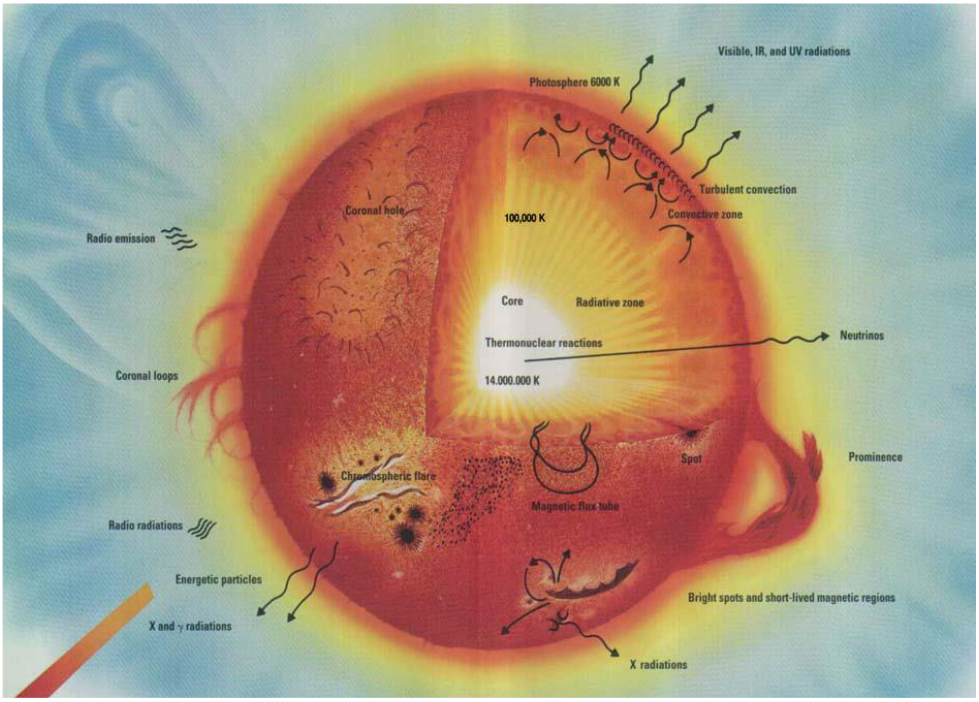

Fig. 2 – Fusion reactions in the sun [11]

There has been an increase in worldwide interest in fusion research in the late 80's considering it an alternative solution for the ever increasing demand for electrical energy. The advantages of fusion from the point of view of environmental impact, safety and fuel reserves are relevant.

The first advantage is the low environmental impact of fusion. Fusion reactions do not produce CO_2 or other greenhouse emissions and do not emit any other harmful chemicals into the atmosphere.

The fuel cycle of fusion does not involve any release of radioactive materials and does not produce long term waste directly. Indeed, the main end product of the fusion reaction is the innocuous and inert gas helium.

The main issue in fusion is that the reaction produces high-energy neutrons (14 MeV), which are partially captured in the fusion blanket, in the manifold region and finally by the vacuum vessel.

Another advantage is the safety. The safety of a fusion reactor is less onerous than the new nuclear fission reactors, thanks to the higher intrinsic safety. In fact, any accident in fusion reactors leads the reaction to stop as first consequence.

Considering first fuel reserves, there is no problem about resources. Deuterium is in plentiful supply and can be easily extracted at a very low cost. Deuterium occurs naturally in ocean water and there is enough energy generated to power the earth for billion years.

However, since tritium is a radioactive isotope with a half-life of only about 12.4 years, there is no natural tritium to be found on earth. Tritium can be obtained by breeding with the lithium isotope Li^6, which is one of the components in the fusion blanket. Lithium is widely available being present in good quantities in the earth crust.

The issue to be considered is the complexity of the fusion from the phenomenological point of view. Specifically, the process must be carried out at very high temperatures because the two nuclei require large amounts of energy to overcome their tendency to repel each other. The temperatures must reach 150×10^6 K, hotter than the center of the sun. At these temperatures the fuel is fully ionized becoming a plasma, a high-temperature collection of independently moving electrons and ions dominated by electromagnetic forces [12].

The plasma temperature is too high that there is no possibility to contain the hot plasma in any conventional vessel with ordinary material, hence other methods are required. One option is the magnetic confinement in which a magnetic field is used to create a barrier between the hot fuel and the wall. In this way, a magnetic field can be used to guide the charged particles and prevent them from hitting the surrounding solid walls.

There are also engineering challenges:

- Low-activation materials need to be developed that can withstand the neutron and heat loads generated by the fusion plasma.

- Large high-field, high-current superconducting magnets need to be developed to confine the plasma.
- New technologies to provide heating power have to be developed in order to raise the plasma temperature to the enormously high values required for fusion.

Many of the critical issues will be addressed in a new experiment known as the International Thermonuclear Experimental Reactor (ITER) and in the longer term, in the Fusion Demonstration Power Plant (DEMO).

2.1 Nuclear reactions

Nuclear reactions produce changes in the basic structure of the nuclei of the atoms involved, in fact a nuclear reaction changes atoms of one element into atoms of another.
The energy release in a nuclear reaction, usually in the form of either the kinetic energy of the end particles or gamma rays, represents the decrease in nuclear "potential energy". The final state is more stable with a decrease in the final total nuclear mass; this difference in mass is transformed into energy:

$$\Delta E = \Delta m \cdot c^2$$

The world's fusion energy research program is focused on the D–T reaction because it is the easiest fusion reaction to initiate.
The D–T reaction involves the fusion of a deuterium nucleus with a tritium nucleus, both hydrogen isotopes; the end products consist of an alpha particle and a neutron (Fig. 3) [11].

$$D + T \rightarrow He^4(3.5) + n(14.1) + 17.6\ MeV$$

Where:

$$D = nucles\ of\ the\ deuterium = H^2$$
$$T = nucles\ of\ the\ tritium = H^3$$
$$He^4 = nucles\ of\ the\ helium = \ \alpha\ particle$$
$$n = neutron$$

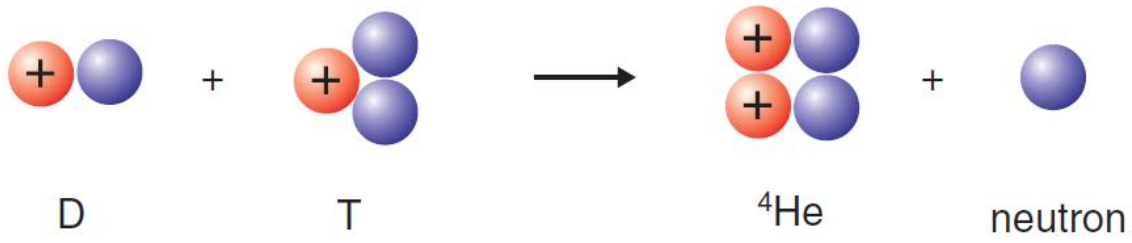

Fig. 3 – Deuterium and tritium fusion reaction [11]

Significant amount of nuclear energy is produced (E = 17.6 MeV), and these large amounts of energy released in fusion reactions appear in the form of kinetic energy of the end products. The kinetic energy of the alpha particle is equal to 3.5 MeV (20% of total E) while that of the neutron is equal to 14.1 MeV that is 80% of total energy [12].

The alpha particles remain stuck into the plasma and give it their energy; neutrons instead, as electrically neutral, are not affected by magnetic field effects and, therefore, escape from the plasma, by crossing the first wall and depositing their kinetic energy in the blanket or shields.

The main problem is the tritium supply, in fact there is no natural tritium on earth, so the solution is to breed tritium in the blanket surrounding the region of D–T fusion reactions. The chemical element that is most favorable for breeding tritium is lithium. Natural lithium comprises 7.4% Li^6 and 92.6% Li^7.

The Li^7 undergoes a first reaction to the fast neutron (14 MeV) from the D–T reaction. The resulting thermal neutron is used to perform further reaction with the Li^6.
The nuclear reactions are:

$$Li^7 + n \rightarrow He^4 + T + n - 2.5\ Mev$$

$$Li^6 + n \rightarrow He^4 + T + 4.8\ MeV$$

Both reactions produce tritium although the second reaction generates energy while the first one consumes energy.
Nuclear data show that the Li^6 reaction is much easier to initiate and as a result it is this reaction that dominates in the breeding of tritium. So the breeding tritium from Li^6solves the problem of sustaining the tritium supply [12].

In order to start the fusion reaction, it is necessary that the two nuclei to be melted are quite close together so that the short-range nuclear forces can act leading to the compound nucleus formation, from which both the energy and the reaction products are generated.

This implies that the two nuclei must be equipped with a sufficient energy to overcome the potential barrier due to the Coulomb repulsion (being the nuclei ionized and thus positive charged).

This energy is given by heating and determines the increase of particles kinetic energy. In fact, the only possibility to get particles closer is the thermal agitation. The kinetic energy due to thermal motion is written depending on the temperature using the Boltzmann relation:

$$E_{kinetic} = \frac{3}{2} K_B T$$

$$K_B = Boltzmann\ constant = 8.61 \cdot 10^{-5} \cdot eV/K$$

$$T = Temperature\ [K]$$

Looking at the probability that a fusion reaction will take place (cross section) for a range of energies of deuterium ions reported in Fig. 4, it is possible to note as at lower energies the probability for the D-T reaction is much higher than D-D (deuterium plus deuterium) and D-He^3 (deuterium plus helium-3). Despite this, the D-T fusion reaction requires at least a kinetic temperature of about 10 keV corresponding to 116 million degrees Kelvin (Fig. 4).

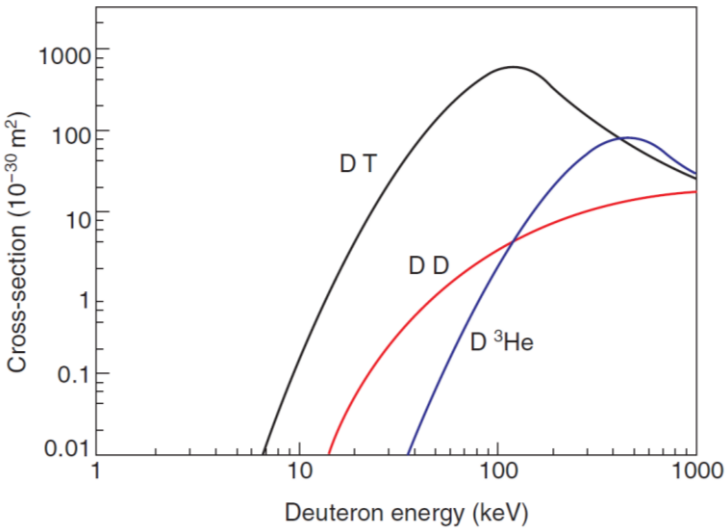

Fig. 4 – Cross section of fusion reactions [11]

2.2 The Plasma physics

When a gas is heated to high temperature it breaks up into a mixture of negatively charged electrons and positively charged nuclei or ions. At this temperature the kinetic energy associated to agitation of the molecules is comparable to the energy of ionization. The electrons and the ions are separated and can move freely as can be seen in Fig. 5.

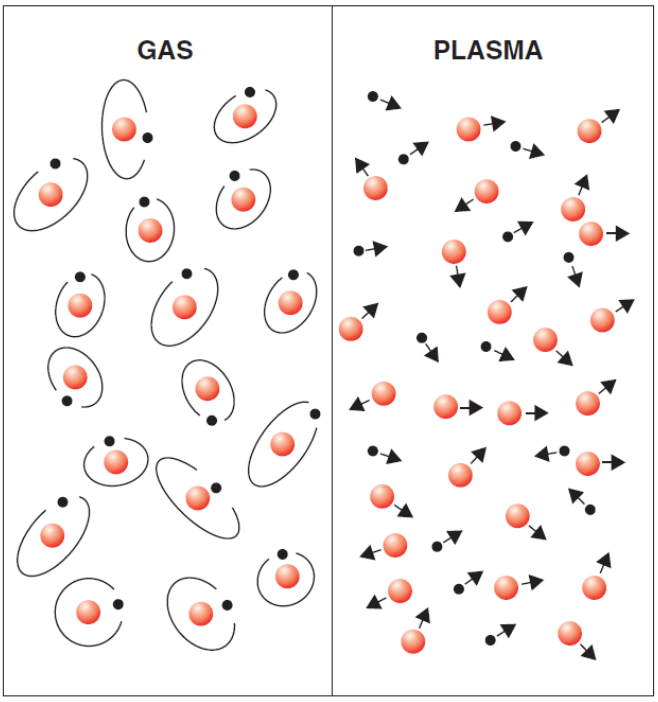

Fig. 5 – Gas state and plasma state [11]

The ionization energy, i.e. the energy that should be provided to an electron to leave the atom, is obtained by multiplying the potential of ionizations and the electron charge $e = 1.6 \cdot 10^{-19}\ C$.
For the hydrogen atom:

$E_i \cong 2.1 \cdot 10^{-18} J = 13.5 eV$

The temperature required to ionize a gas can be estimated equating the ionization energy with the average kinetic energy of a molecule:

$$E_i = E_{kinetic} = \frac{3}{2} \cdot K_B \cdot T$$

For the hydrogen: $T \cong 1.5 \cdot 10^5 K$[13]

Therefore, at the temperatures required for fusion, the gas is fully ionized and consists of a mixture of negative electrons and positive nuclei: the gas is called plasma.
The Plasma is one of the four fundamental states of matter (solid, liquid, gas and plasma) and has different properties than a normal gas. One important property of plasma is that can conduct electricity so it responds strongly to electromagnetic fields.

In a nuclear fusion reactor, the energy of the alpha particle released by deuterium plus tritium reaction can be used to heat the plasma. Initially an external source of energy is needed to raise the plasma temperature until the fusion reaction becomes self-sustaining (the alpha heating is sufficient by itself). This point is called *ignition* and this condition, in a magnetic confinement, is calculated setting the alpha particle heating equal to the rate at which energy is lost from the plasma.

The largest energy losses from the plasma are due to:

- thermal conduction between plasma and the FW in the BB;
- energy associated with particles crossing magnetic field;
- radiation through various forms [13].

2.3 Magnetic confinement

Due to the high temperature, the plasma can't be in direct contact with any solid material. Magnetic confinement is the ideal solution for plasma confinement because magnetic fields can interact with separated ions and electrons.

A particle of charge q moves with velocity $\vec{v}$ in the presence of a magnetic field $\vec{B}$ (Fig. 6), then it will experience the Lorentz force $\vec{F}$:

$$\vec{F} = q\vec{v} \wedge \vec{B}$$

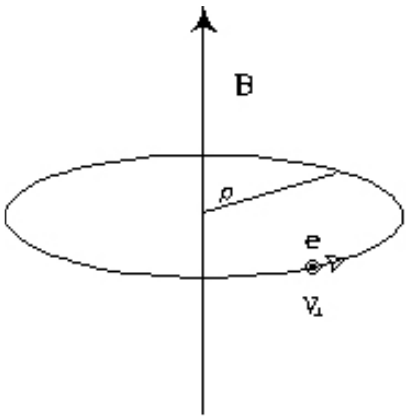

Fig. 6 – Interaction between charge q and magnetic field [13]

The interaction between the electric current flows through a conductor, in this case the plasma, and a magnetic field generates centripetal forces that constrict the plasma and pull it away from the walls avoiding the contact between plasma and material surfaces.

So in magnetic confinement, hundreds of cubic meters of D-T plasma at a density of less than a milligram per cubic meter are confined by a magnetic field.

The tokamak (torus-shaped magnetic chamber) is an axisymmetric torus with a large toroidal magnetic field, a moderate plasma pressure and a relatively small toroidal current (Fig. 7).

The toroidal magnetic field, due to an electric current induced through a transformer, is curved around to form a closed loop. It is currently the most promising design to become the world's first fusion reactor due to brilliant physics performance.

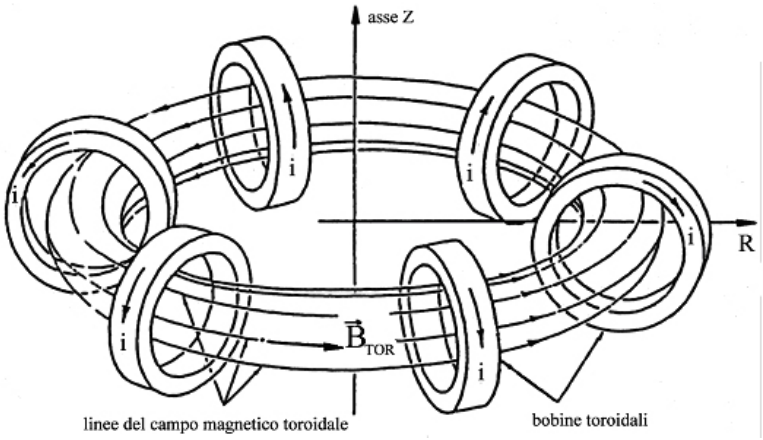

Fig. 7 – Toroidal magnetic field in a tokamak [13]

2.4 ITER Project

ITER (International Thermonuclear Experimental Reactor) is an international nuclear fusion research and engineering project funded and run by the European Union, India, Japan, China, Russia, South Korea and the United States. The mission of ITER project is to prove the scientific and technological feasibility of fusion energy for peaceful purposes.

ITER will be the world's largest magnetic confinement plasma physics experiment, which is currently building adjacent to Cadarache in the south of France.
Plasma experiments will initiate in 2020 with full deuterium–tritium fusion experiments starting in 2027.

The ITER Tokamak will be a machine specifically designed to:

- Produce 500 MW of fusion power for pulses of 400 s,
- Demonstrate the integrated operation of technologies for a fusion power plant,
- Achieve a deuterium-tritium plasma in which the reaction is sustained through internal heating,
- Test tritium breeding,
- Demonstrate the safety characteristics of a fusion device.

In a fusion reactor and therefore also in the ITER the following structures are defined from the plasma to the outside (Fig. 8):

- blanket modules to produce tritium through reaction of Li^6 with neutrons produced during fusion reaction; moreover to shield the steel vacuum vessel and external machine;
- vacuum vessel is the central part of the ITER machine: a double walled steel container in which the plasma is contained and acts as a first safety containment barrier;
- positioned at the bottom of the vacuum vessel, the divertor controls the exhaust of waste gas and impurities form the reactor and withstands the highest surface heat loads of the ITER machine,
- superconducting magnets will produce the magnetic field to initiate, confine, shape and control the ITER plasma;
- cryostat to surround the vacuum vessel and superconducting magnets in order to provide a super-cool vacuum environment [14].

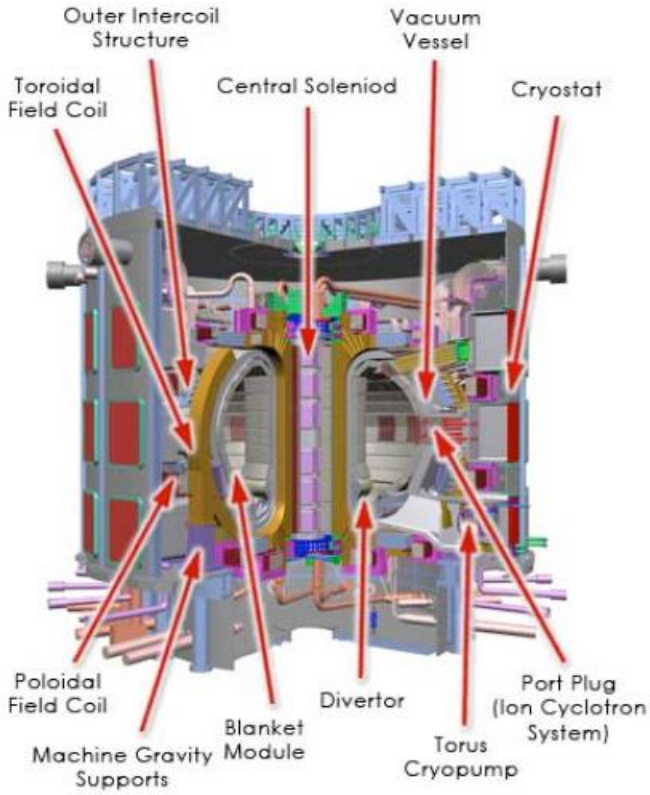

Fig. 8 – Main parts of ITER reactor *[12]*

PARAMETER	ATTRIBUTES
Plasma current	15 MA
Max Toroidal Field	5.3 T
Total Fusion Power	500 MW
Fusion Power Gain	≥10 (for 400 s inductively driven burn) ≥ 5 (for steady-state objective)
Auxiliary heating	73 MW
Plasma major radius	6.2 m
Plasma minor radius	2.0 m
Plasma Volume	830 m^3
Plasma Surface	680 m^2
Plasma Cross Section	22 m^2

Tab. 1 – Main features of ITER [15]

Tab. 1 summarizes the main features of ITER

.

3 BREEDING BLANKET DESIGNS IN DEMO PROJECT

Power Plant Physics and Technology (PPPT) department of the European Fusion Development Agreement (EFDA) is in charge of the development of DEMO (Demonstration Power Plant) fusion reactor which is considered the ITER successor device and will be the nearest-term fusion reactor design capable of producing electricity, operating with a closed fuel-cycle. It can be considered the last step before a commercial reactor (Fig. 9) [16].

Currently DEMO project is under research and development, as well as its design is constantly reviewed conceptually. In fact, reactor design has not been formally selected and detailed operational requirements are not yet available.

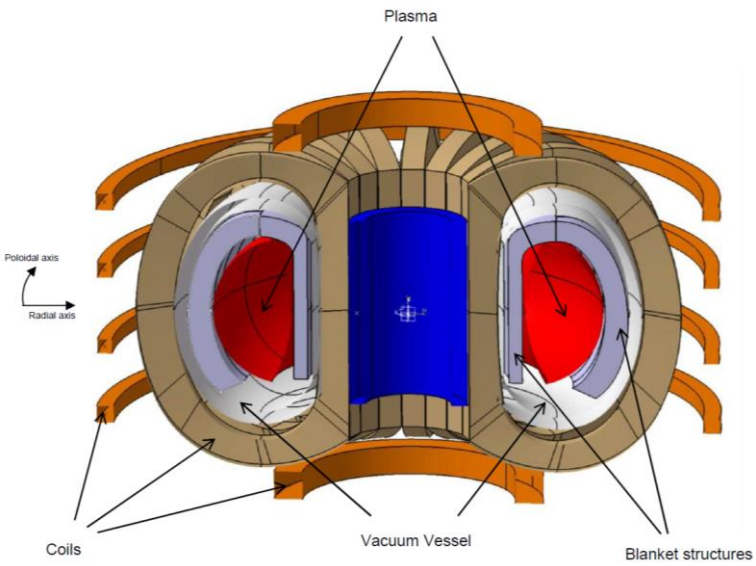

Fig. 9 – Main parts of DEMO reactor [17]

DEMO reactor must:

- demonstrate production of 500 MW of electrical energy;
- resolve all physics and technical issues foreseen in the plant and demonstrate reactor relevant technologies;
- achieve tritium self-sufficiency and tritium extraction/control;
- demonstrate the economic feasibility of electric power generation from nuclear fusion reactions;

- demonstrate nuclear safety and acceptable environmental impact with only low radioactivity waste;
- prove adequate Reliability/Maintainability/Availability/Inspectability (RAMI) with remote maintenance of fusion core components [18].

In Tab. 2 the suggested features of DEMO are reported:

PARAMETER	ATTRIBUTES
Plasma current	19.6 MA
Max Toroidal Field	5.7 T
Total Fusion Power	2037 MW
Plasma major radius	9.072 m
Plasma minor radius	2.927 m
Plasma Volume	2502 m^3
Plasma Surface	1428 m^2
Av. Neutron wall load	1.05 MW m^{-2}

Tab. 2 – Summary of parameters for DEMO [19]

3.1 Breeding blanket designs

The blanket system is one of magnetic confinement reactor components. It is located adjacent to the vacuum vessel and it constitutes the first structure surrounding the plasma.
The blanket is a key component of the DEMO reactor and its key features are summarized as follow:

- Neutron kinetics energy transformation into heat and collection of the heat for electricity production (allowing the extraction of generated thermal power and make it available to a thermodynamic cycle);
- Tritium production through irradiation of lithium and extraction from the blanket to then be re-inserted in the plasma;
- Shielding contribution of the magnetic coils from the high neutron flux coming from the fusion neutrons and biological shielding of the entire machine [20].

Therefore, the design is featured in order to achieve a low maintenance time, sufficiently long lifetime, a high safety level with low environmental impact and a reasonable direct cost also during the operational phase.

The material within blanket intended for the tritium generation is called breeder. It must have the following features:

- good capacity to generate tritium;
- good release properties of tritium;
- chemical stability;
- compatibility with the other materials constituting the blanket;
- security to the problems due to possible incidental causes.

Many blanket concepts have been proposed worldwide over the past 40 years using different combinations of materials and principles of operation and currently four DEMO blanket concepts are under design and development in Europe. The finalization of all the four breeding concepts is scheduled for 2020, in order to choose the more promising blanket to test and finally implement in DEMO [20].

Candidate designs for the EUROfusion Breeding Blanket Project to be developed are:

- WCLL Water-cooled Lithium Lead (described in section 3.2);
- HCPB Helium-cooled Pebble Bed (described in section 3.1.1);
- HCLL Helium-cooled Lithium Lead (described in section 3.1.2);
- DCLL Dual-Cooled Lithium Lead (described in section 3.1.3).

3.1.1 HCPB – Helium Cooled Pebble Bed

The European helium cooled pebble bed breeding (HCPB) blanket concept has been deeply investigated since 1994 [21] [22]. It is a solid breeder concept, developed by KIT (Karslruhe Institute of Technology), that uses ternary ceramic breeders like Li_4SiO_4 (orthosilicate) or Li_2TiO_3 (metatitanate) in pebbles with a typical diameter of 0.4-0.6 mm and beryllium in pebbles with a diameter in the range of 1 mm as neutron multiplier. The concept is based on the use of ferritic martensitic steel with reduced activation features (RAFM) as structural material with Helium as coolant that flows at high pressure (around 8 MPa) in small channels directly in the steel structure of the blanket (Fig. 10). The structural material design window temperature between 300 and 550 °C limits the maximum He temperature at about 500 °C. This reduces efficiency of the power generation system, based on conventional Rankine cycle, through a primary He loop and a steam generator [23].

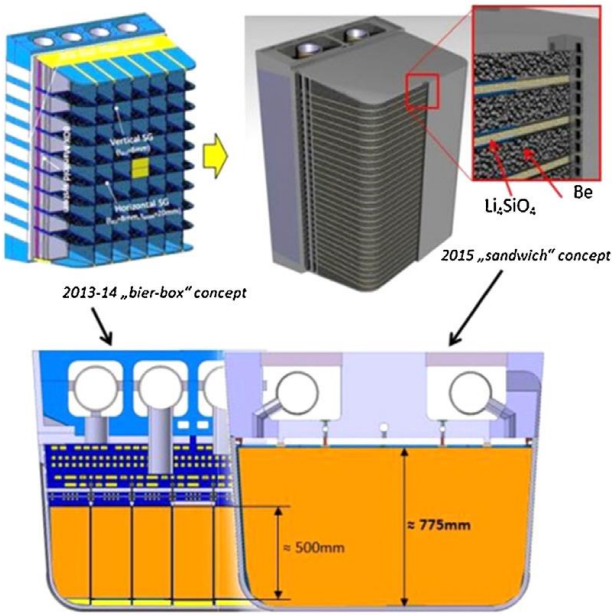

Fig. 10 – Evolution of the HCPB design (2013-2015) [24]

The blanket system is a Multi-Module Segment (MMS) concept subdivided on 16 sectors in toroidal direction; each blanket sector is made of 5 segments: three for the Outboard and two for the Inboard. Each sector is divided in 6 modules in the inboard and 6 in the outboard, along the poloidal direction.

The HCPB blanket concept is showed in Fig. 11. Helium flows in the FW channels and in the cooling plates that divide the module in boxes containing the breeder material and neutron multipliers in form of a pebbles bed. An independent low pressure helium flow provides the purging of Tritium from the pebble beds for recovery outside the blanket. The purge flow velocity is low to limit pressure drops, practically no heat removal is provided by the helium circulating in the loop [23].

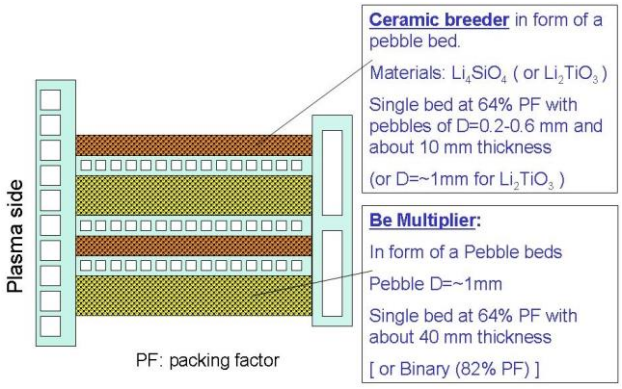

Fig. 11 – Conceptual scheme for the HCPB [23]

3.1.2 HCLL – Helium cooled Lithium Lead

The DEMO HCLL breeding blanket was proposed in 2003 [25] and now it is developed by CEA (Commissariat à l'Energie Atomique et aux Energies Alternatives). It is a separately cooled liquid-metal blanket model. The Pb15.8Li eutectic alloy serves exclusively as a breeder and neutron multiplier, while the entire thermal power is removed by helium cooling system at a pressure of 8 MPa. The module uses RAFM steel as structural material. The blanket system is divided into 16 identical sectors of 22.5° in toroidal direction. Each sector is made of 2 Inboard (IB) and 3 Outboard (OB) segments and is divided in 8 modules in the inboard and 8 in the outboard along the poloidal direction.

The generic HCLL blanket module is subdivided by a helium cooled stiffening grid into an array of 90 rectangular breeder units (BUs): 9 in the toroidal direction and 10 in the poloidal direction (Fig. 12) [9].

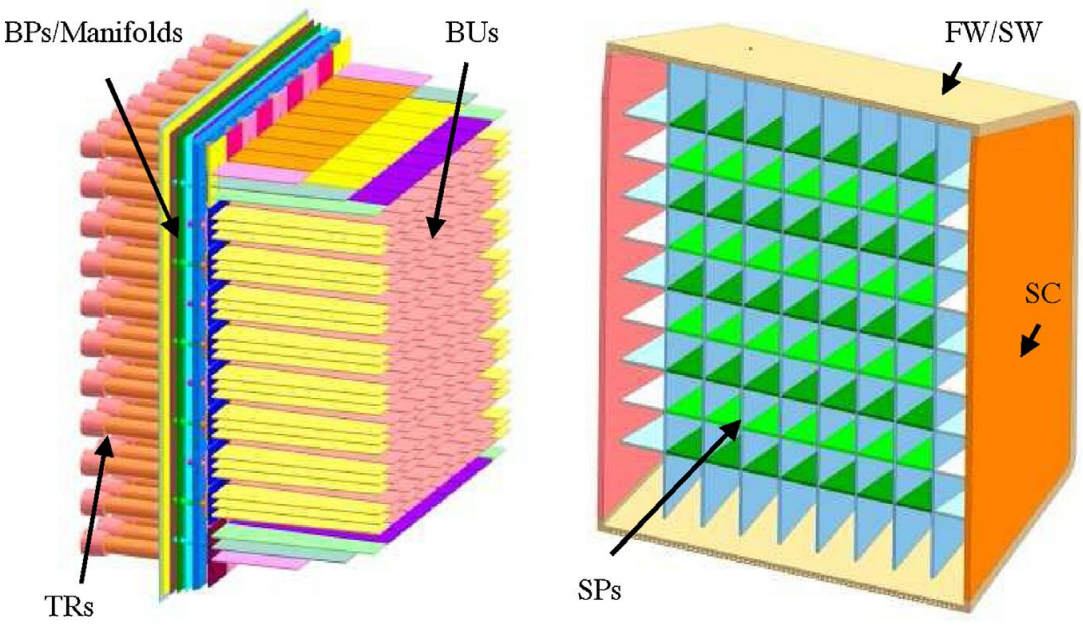

Fig. 12 – HCLL design [9]

The PbLi enters at the bottom of the module through a pipe connected to the common manifold/BSS. PbLi, in the BUs around parallel horizontal cooling plates, flows at low velocity radially towards the FW gradually increasing the tritium concentration, goes to the BU immediately above and then radially flows to the outlet common column in manifold (Fig. 13). Since the liquid-metal velocity in BUs is very small, the interaction of the electrically conducting PbLi with the plasma-confining magnetic field is weak and MHD pressure drop in BUs is not an issue.

The helium enters from the back of the module through pipes connected to the common manifold. It arrives in the first distribution chamber where it enters the cooling channels of the FW/SWs.

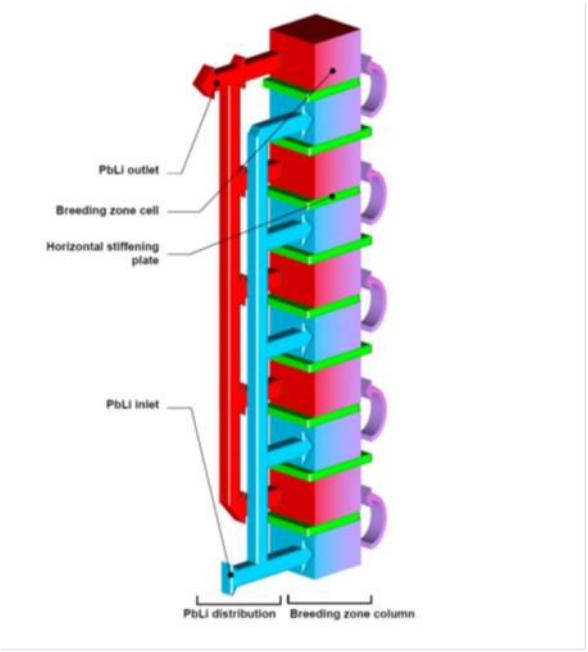

Fig. 13 – Principle of PbLi circulation in one breeding column [9]

3.1.3 DCLL – Dual Cooled Lithium Lead

The DCLL breeding blanket concept was studied in EU since 1994 (see Refs. [26], [27]). CIEMAT (Centro de Investigaciones Energéticas, Medioambientales y Tecnológicas) has been working on the new design since 2014.

The DCLL is an attractive high-temperature and high-efficiency breeding blanket concept using RAFM steel as structural material. In this concept, a high-temperature PbLi alloy flows in large poloidal rectangular ducts to remove the volumetric heat and produce tritium, while the pressurized He (typically to 8 MPa) is used to remove the surface heat flux and to cool the first wall and other blanket structures.

The design is based on a multi-module segment, having 8 different modules attached to a common BSS, while the BZ consists of 4 parallel PbLi circuits, separated by radial stiffening grid (Fig. 14).

A key element of this design is a flow channel insert (FCI) composed of steel/alumina/steel layers placed on the wall to be used as an electrical and thermal insulator for decoupling electrically conducting structural walls from the flowing PbLi to reduce magneto hydrodynamic pressure drop.

The concept is interesting for the potentiality to operate at high PbLi temperatures (up to 700 °C) with consequently a high thermal efficiency by enabling the use of a Brayton power conversion cycle.

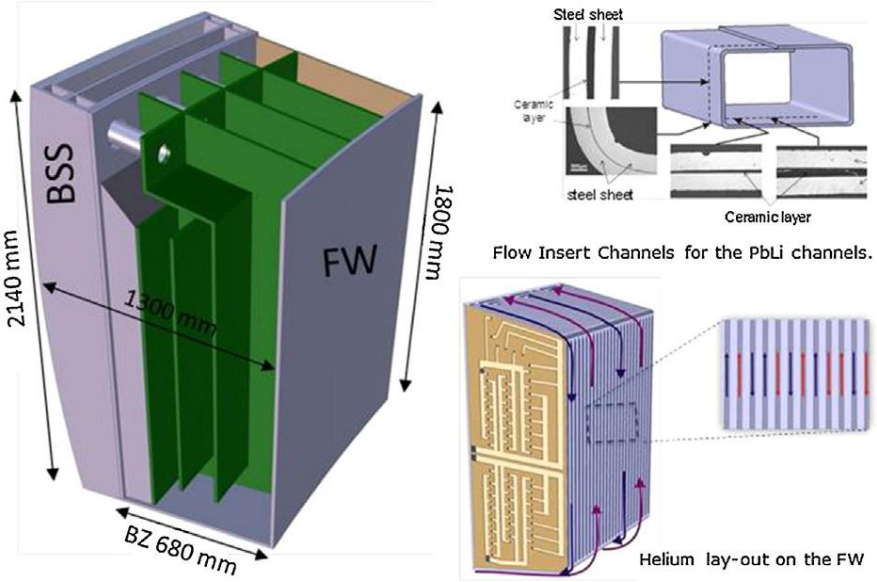

Fig. 14 – DCLL design 2014-2015 [24]

3.2 WCLL – Water Cooled Lithium Lead

The WCLL has been identified as a feasible blanket candidate for DEMO fusion power plant. It is investigated in the EUROfusion Breeding Blanket Project. ENEA, CREATE and the Universities of Palermo, Pisa and Roma are in charge of developing the conceptual design.

It is designed as a modular concept to limit manufacturing issues, thermo-mechanical and electromagnetic loads on the structural elements, PbLi pressure drop and tritium permeation into the coolant. The blanket structure is segmented in small modules with straight surfaces, attached to a common Back Supporting Structure (along the poloidal direction) housing feeding pipes, in order to form a blanket segment which can be removed from the upper port, through remote handling.

The WCLL BB uses reduced activation ferritic-martensitic steel Eurofer as structural material filled with Lithium-Lead (PbLi) as breeder, neutron multiplier and tritium carrier, and water at typical Pressurized Water Reactor (PWR) conditions (T_{in} = 285 °C, T_{out} = 325 °C at 15.5 MPa) as coolant.

Concerning the breeding zone cooling loop, water flows in Double-Wall Tubes (DWT), which are used to minimize the probability of water/PbLi interaction. Besides the inherent

safety reasons, they are mainly used to enhance the reliability of the system. The front part of the WCLL BB System is the First Wall (FW), which is cooled with a separate loop. The coolant flows in channels inside the steel along the radial-toroidal directions.

The module box is attached to the back supporting structure and the manifolds through its Back Plate. This is in charge to withstand the box inner pressure and external loads due to postulated accident conditions [10].

All structures (i.e. module box, stiffening plates, first wall and refrigerant pipes, manifolds and BSS) are realized in Eurofer 97, an oxide dispersion strengthened ferritic-martensitic steel developed specifically to withstand the blanket environmental conditions. Its main features are the resistance to neutron irradiation, reduced activation and the capability to maintain good mechanical properties up to 550 °C.

The WCLL blanket concept is based on near-future technology requiring limited extrapolation from present-day knowledge both on physical and technological aspects, expected to be available in medium term with moderate R&D requirements. In fact, for the refrigeration circuit and its components (steam generator, pressurizer, pumps and valves) it can refer to the already well-established technology of PWR, while for some components of the Pb-17Li circuit can use the acquired knowledge from the LMFBR reactors. Moreover, the tritiated water treatment system can take advantage of the experience gained in CANDU reactors.

Other advantages of the blanket WCLL are:

- the extraction of tritium from the PbLi, which is the career, outside of the Vacuum Vessel;
- the low speed of liquid metal, which implies negligible issues connected with the magneto hydrodynamics.

3.2.1 Poloidal segmentation

The blanket segmentation, the dimension and shape of the module are realized considering the following rationales:

- To have straight surfaces, approximating as much as possible the plasma profile;
- Number of modules minimized, to increase Tritium Breeding Ratio (TBR);
- Small modules with max height of 2.4 m;
- Modularity of breeding blanket.

The DEMO WCLL blanket system is divided in 18 sectors in toroidal direction. A blanket sector comprises three segments in the outboard blanket (OB) and two segments in the inboard (IB) with 20 mm gap between the modules to allow the operational thermal expansion. Thus, there is a total of 54 segments in the outboard blanket and 36 in the inboard blanket along the toroidal direction. The segment is divided in 7 modules in the inboard and 7 in the outboard, along the poloidal direction, as shown in Fig. 15. Therefore, the blanket system has 378 modules in the outboard and 252 modules in the inboard, totaling 630 modules. The dimensions of each module radial thickness, FW area and volume are summarized in Tab. 3 [10].

Module	**Module Thickness [m]**	**FW area [m^2]**	**Volume [m^3]**
IB1	0.55	1.439	0.796
IB2	0.55	1.650	0.889
IB3	0.55	1.650	0.865
IB4	0.55	1.650	0.889
IB5	0.55	0.831	0.487
IB6	0.55	0.940	0.563
IB7	0.55	1.020	0.613
OB1	0.80	1.416	1.038
OB2	0.80	2.456	2.504
OB3	0.85	3.036	3.069
OB4	0.90	3.133	3.155
OB5	0.90	3.032	3.031
OB6	0.90	2.748	2.620
OB7	0.90	2.474	2.323
Total (7x36)+(7x54)		**1318.34**	**1141.63**

Tab. 3 – Poloidal segmentation of the blanket [10]

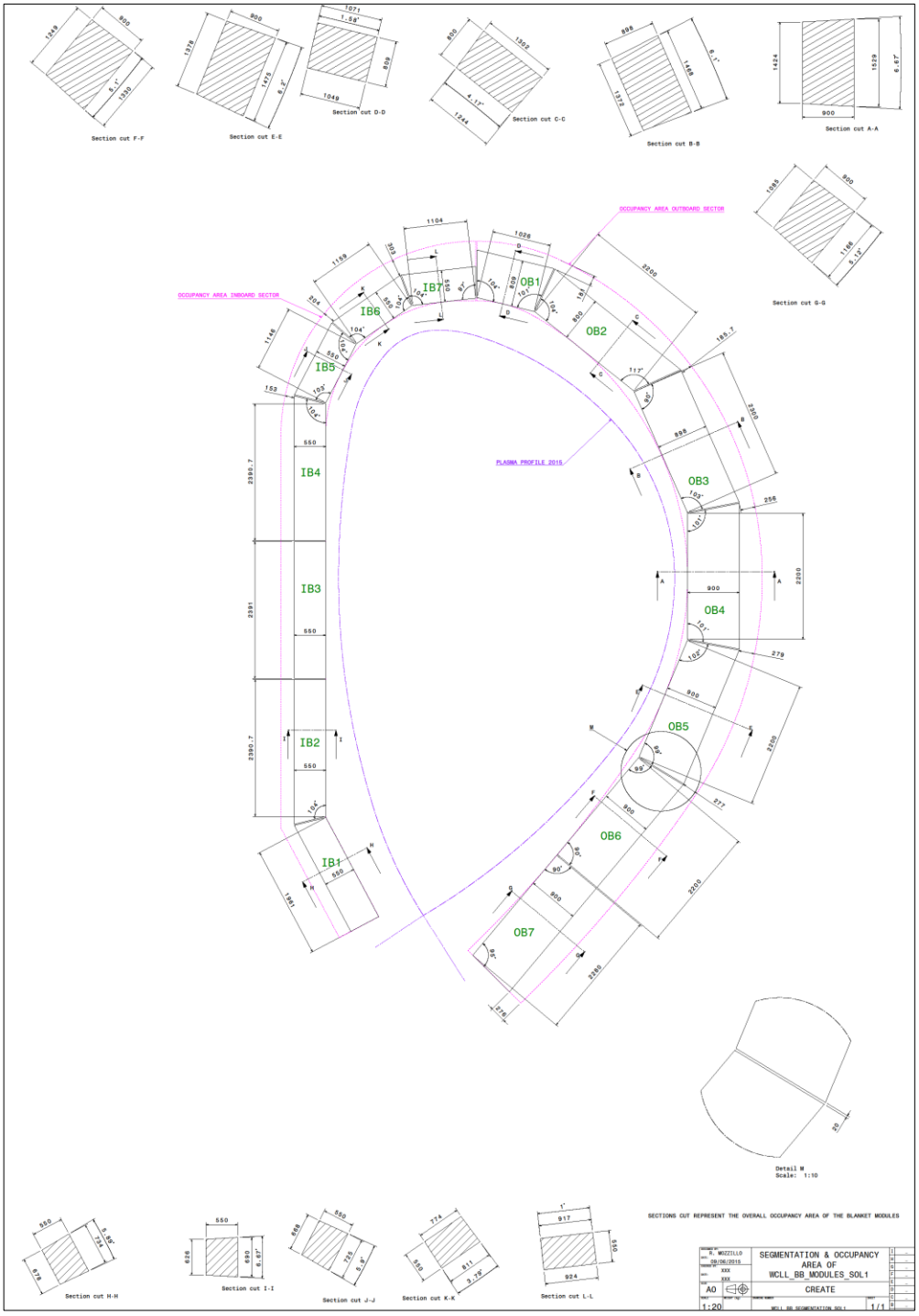

Fig. 15 – WCLL poloidal segmentation [10]

3.2.2 Sources of power in blanket modules

The WCLL breeding blanket design in DEMO 2015 configuration design has an average neutron wall load (NWL) of 1.05 MW m^{-2} [19].

The poloidal distribution of the NWL, as well as the heat power volumetric density profiles in the blanket materials to simulate power deposited by neutrons and photons, have been deducted from the PPCS [28] by scaling the results to the ratio of the average NWLs.
A heat flux of 0.5MW m^{-2} is postulated on the plasma-facing wall of the blanket modules to take in account heat power deposition due to particles and radiations arising from plasma.

Accordingly with the consideration above, the geometry and the material composition, the WCLL breeding blanket power is evaluated by the heat power volumetric density and the heat flux. The overall data are reported in Tab. 4, where the missing term is the power deposited in the manifold region and vacuum vessel structures. The power deposited in the divertor is neglected and can be added to the total power to complement the energy flow map.

Module	Tot Power (MW)	FW (NWL+HF) (MW)	Blanket (MW)
IB1	2.26	0.89	1.31
IB2	2.59	1.02	1.50
IB3	2.79	1.04	1.67
IB4	2.79	1.04	1.67
IB5	1.35	0.51	0.80
IB6	1.52	0.58	0.90
IB7	1.65	0.63	0.98
Total	***14.94***	***5.72***	***8.82***
OB1	2.69	0.90	1.78
OB2	4.67	1.56	3.09
OB3	5.77	1.93	3.81
OB4	6.20	2.02	4.15
OB5	6.00	1.96	4.02
OB6	5.17	1.75	3.41
OB7	4.66	1.57	3.07
Total	***35.15***	***11.68***	***23.32***
Reactor 36*IB+54*OB	**2436.0**	**836.7**	**1577.1**

Tab. 4 – WCLL BB Power [10]

3.2.3 Outline of central outer segment equatorial module design

The outboard equatorial OB4 module, shown in Fig. 16 and Fig. 17, consists of an Eurofer steel box, reinforced by an internal grid of radial-poloidal and radial-toroidal plates in order to withstand water pressure (15.5 MPa) in case of accidental pressurization. In the

breeder unit there are 15 stiffening plates of 12 mm in radial-toroidal direction and 5 stiffening plates of 16 mm. The module box results divided in 16 elementary cells in poloidal direction and 6 channels in toroidal direction. Each elementary cell is divided in the middle with a baffle plate that allows PbLi to flow in radial-poloidal direction. An inlet chamber between the Back Plate (BP) and the breeding zone ensures the PbLi distribution in the elementary cells through 6 orifices. The PbLi enters from 8 feeding pipes linked to the manifold, and exits through 32 pipes linked to the two central channels.

The water coolant flows in radial-toroidal tubes in the breeding zone: enters from the manifold in the right and exits from the manifold in left. There are 21 pipes in each elementary cells. While in the FW Zone, the water flows in square channels (7x7 mm) in counter current direction [10]. Tab. 5 summarizes the main parameters of WCLL BB project.

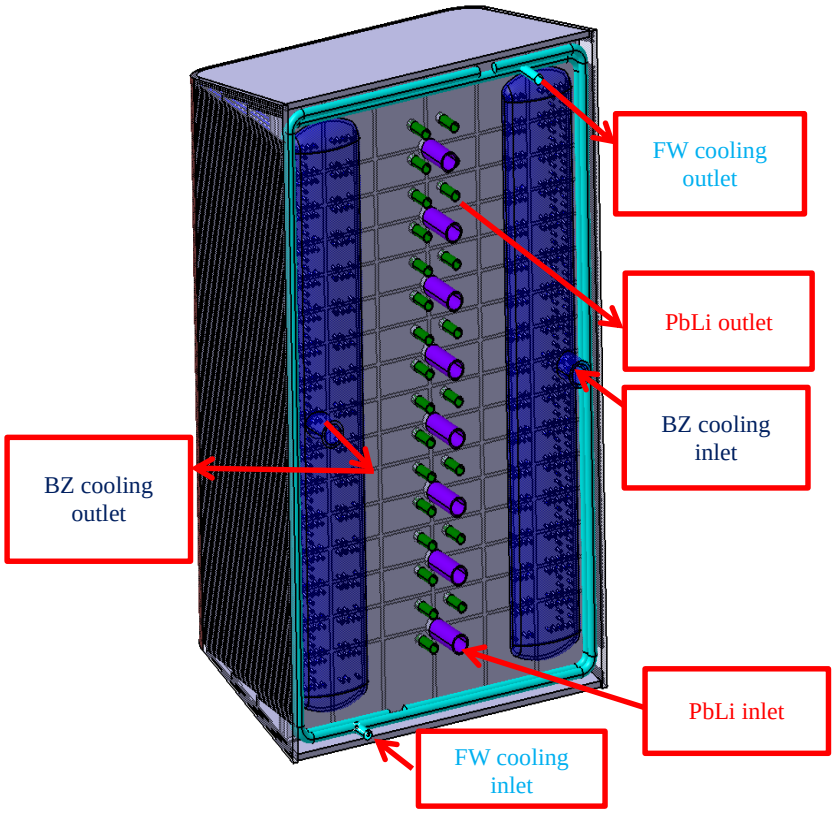

Fig. 16 - WCLL outboard module isometric view [10]

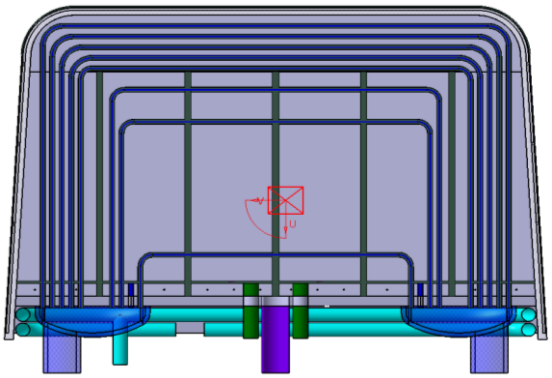

Fig. 17 – WCLL outboard module [10]

T_max Steel	550 °C
T_max PbLi	550 °C
T_outlet PbLi	325 °C
T_outlet coolant	325 °C
v_max coolant	7 m/s
v_max inlet PbLi	5 mm/s
Delta P coolant system	1 Mpa

Tab. 5 – Main parameters of WCLL BB project [10]

4 CFD ANALYSES

The CFD analyses are carried out by ANSYS® Workbench software (vers.15.0) exploiting the ANSYS CFX solver (ver. 15.0). The code is based on a finite volume method, where the numerical algorithm consists of the following steps:

- integration of the governing equations of fluid flow over all the finite control volumes of the domain;
- discretization – conversion of the resulting equations into a system of algebraic equations;
- solution of the algebraic equations by an iterative method.

In order to set the simulations, the following steps have been carried out:

- definition of the geometry of the region of interest (computational domain) through the Design Modeler of ANSYS;
- grid generation - the division of the domain into a number of smaller sub-domains: a mesh of elements through ANSYS ICEM;
- selection of the physical phenomena that need to be modelled;
- definition of fluid properties and specification of appropriate boundary conditions through CFX.

Seven simulations have been performed under various operating conditions (see Tab. 6):

- Sim I - 0.5 MW/m^2 nominal Heat Flux on the FW surface with constant mass flow rates in each tubes of the breeding zone. Mass flow rate in each zone is estimated assuming no heat exchange between breeding zone and FW zone.
- Sim II - the same operating conditions of simulation I activating buoyancy forces in the fluids domains.
- Sim III - 0.5 MW/m^2 nominal Heat Flux on the FW surface with non-constant mass flow rate in the tubes of the breeding zone. The mass flow rates have been calculated analytically by imposing total flow rate and constant pressure drops between input and output for each tube of breeding zone (manifold approach).
- Sim IV - 0.5 MW/m^2 nominal Heat Flux on the FW surface with non-constant mass flow rates in the breeding zone tubes. The mass flow rates flowing in BZ tubes and

in FW channels have been estimated through an energetic balance to achieve fluid outlet temperatures set as project conditions.

- Sim V - 1.5 MW/m^2 nominal Heat flux on the FW surface to assess the performance of the FW with respect to the Eurofer temperature limit.
- Sim VI - Fluid dynamic analysis (isothermal) of the PbLi domain to evaluate the possibility to let PbLi exiting only through the central outlets of the module.
- Sim VII - A new layout of the tubes is proposed in the breeding zone, setting 0.5 MW/m^2 normal heat flux on the FW surface with non-constant mass flow rate in the tubes of the BZ. The mass flow rates have been calculated analytically by imposing total flow rate and constant pressure drops between input and output for each tube of BZ (manifold approach).

The simulations were carried out at the ENEA "Centro Ricerche Brasimone" using a HP Z800 Workstation with 12 processors Intel Xeon X5670 2.93 GHz and a total of 47.2 GB of RAM available.

	Nominal heat flux (MW/m^2)	**Volumetric heat power (W/m^3)**	**Buoyancy forces**	**BZ coolant mass flow**
Sim I	0.5	f (r)	no	constant
Sim II	0.5	f (r)	yes	constant
Sim III	0.5	f (r)	no	manifold approach
Sim IV	0.5	f (r)	no	orifices
Sim V	1.5	f (r)	no	manifold approach
Sim VI	0	0	no	
Sim VII	0.5	f (r)	no	manifold approach

Tab. 6 – Simulations performed

4.1 Mathematical Model

The set of equations solved by ANSYS CFX in the fluids domains are the Navier-Stokes equations, in their conservation form. The equations are:

- continuity equation

$$\frac{\partial \rho}{\partial t} + \nabla(\rho \vec{v}) = 0$$

$where: \rho = density;\ \vec{v} = velocity\ vector$

- x - momentum equation

$$\frac{\partial(\rho u)}{\partial t} + \nabla(\rho u\vec{v}) = -\frac{\partial p}{\partial x} + \nabla(\mu \nabla u) + S_{Mx}$$

- y – momentum equation

$$\frac{\partial(\rho v)}{\partial t} + \nabla(\rho v\vec{v}) = -\frac{\partial p}{\partial y} + \nabla(\mu \nabla v) + S_{My}$$

- z – momentum equation

$$\frac{\partial(\rho w)}{\partial t} + \nabla(\rho w\vec{v}) = -\frac{\partial p}{\partial z} + \nabla(\mu \nabla w) + S_{Mz}$$

$where: \mu = dynamic\ viscosity;\ p = pressure; \vec{S}_M = source\ term$

- energy equation

$$\frac{\partial(\rho h)}{\partial t} + \nabla(\rho h\vec{v}) = -p\nabla\vec{v} + \nabla(\lambda \nabla T) + S_{thm}$$

$$\rho \cdot c_p \left[\frac{\partial T}{\partial t} + (\vec{v} \cdot \nabla)T\right] = \lambda \nabla^2 T + S_{thm}$$

$where: h = enthalpy;\ T = Temperature;\ \lambda = thermal\ conductivity;$
$S_{thm} = source\ term$

The turbulence models seek to modify the original Navier-Stokes equations by the introduction of averaged and fluctuating quantities to produce the Reynolds Averaged Navier Stokes (RANS) equations. These equations represent the mean flow quantities only, while modeling turbulence effects without a need for the resolution of the turbulent fluctuations. All scales of the turbulence field are being modeled [29].
In the momentum and energy equations, the dynamic viscosity and the thermal conductivity need to be replaced with their effective counterparts due to turbulence effect:

$$\mu_{eff} = \mu + \mu_t$$

$$\lambda_{eff} = \lambda + \lambda_t$$

Two-equation k-omega Shear Stress Transport (SST) model is used to simulate the turbulence effects.

Two-equation turbulence models are widely used, as they offer a good compromise between numerical effort and computational accuracy. Both the velocity and length scale are solved using separate transport equations.

k-ω model solves two transport equations, one for the turbulent kinetic energy, k, and one for the turbulent frequency, ω.

The k-ω models assumes that the turbulence viscosity is linked to the turbulence kinetic energy and turbulent frequency via the relation:

$$\mu_t = \rho \frac{k}{\omega}$$

In the solid regions, the equations for heat transfer are solved with no flow. This is known as conjugate heat transfer. The conservation of energy equation can account, within solid domains, for heat transport due to solid motion, conduction, and volumetric heat sources:

$$\frac{\partial(\rho h)}{\partial t} + \nabla \cdot \left(\rho \vec{U} h\right) = \nabla \cdot (\lambda \nabla \mathrm{T}) + S_E$$

$$where: h = entalpy; \vec{U} = solid\ velocity; S_E = volumetric\ heat\ source$$

The solid motion advection term (the term including $\vec{U}$) is optional and is added only when a solid motion velocity is set; in our case is zero [29].

There is no exchange of matter to the solid/fluid interfaces; besides there is conservative heat flux on interface, this implies that the heat flux will flow between the current boundary and the boundary on the other side of the interface (ideal approach in the absence of contact resistance).

High resolution advection scheme is adopted for Continuity, Energy and Momentum equations, while upwind advection scheme for Turbulence Eddy Frequency and Turbulence Kinetic Energy equations.

ANSYS CFX uses a coupled solver, which solves the hydrodynamic equations (for u, v, w, p) as a single system and subsequently the energy equation (Fig. 18). This solution approach uses a fully implicit discretization of the equations at any given time step. For steady state problems, the time-step behaves like an 'acceleration parameter', to guide the approximate solutions in a physically based manner to a steady-state solution. This reduces the number of iterations required for convergence to a steady state [29].

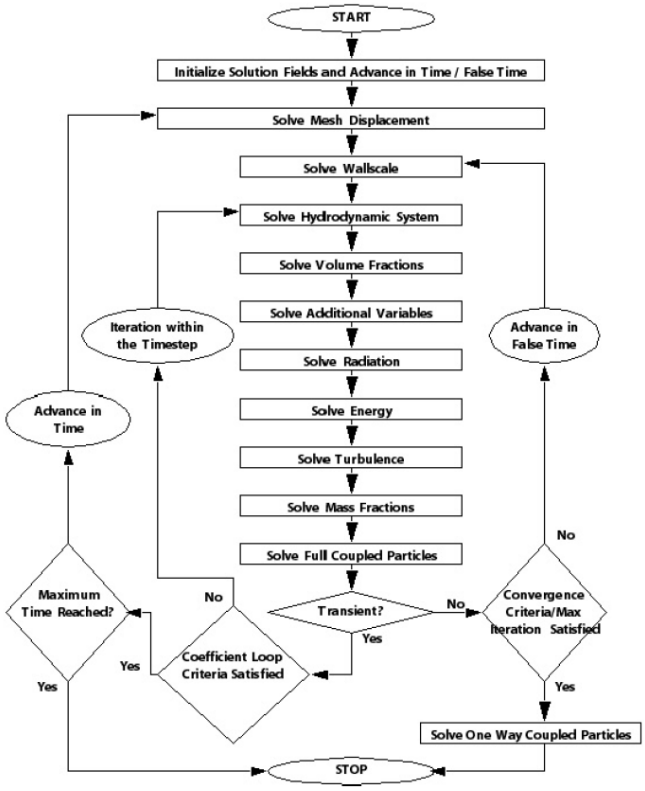

Fig. 18 – Solution algorithm of CFX [29]

4.2 Geometric domain

A three-dimensional finite volume model of the equatorial module of the DEMO-WCLL breeding blanket outboard segment was set-up in order to assess the thermo-hydraulic behaviour of the WCLL-DEMO blanket concept. The model reproduces a central toroidal-radial slice of the module and includes six breeder cells in the toroidal direction and one breeder cell in poloidal direction.

The water coolant flows in counter-current mode along the SW-FW-SW in eleven square section channels and the BZ cooling loop is based on twenty-one circular section double walled C-shaped tubes flowing in radial-toroidal-radial direction.

The mesh accounts for solid structures and fluids, as hereafter listed.

- Solid domain (Fig. 19.a):
  - Stiffening plates
  - Baffle plate
  - Double walled tubes
  - First wall

- Fluid domain:
  - Water coolant (Fig. 19.b)
  - PbLi breeder (Fig. 19.c)

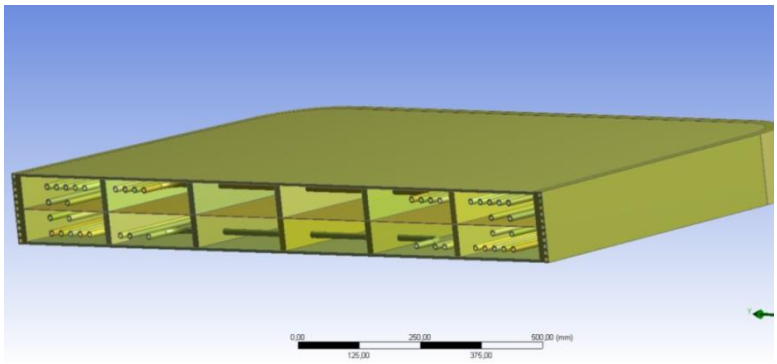

(a) Solid structures domain

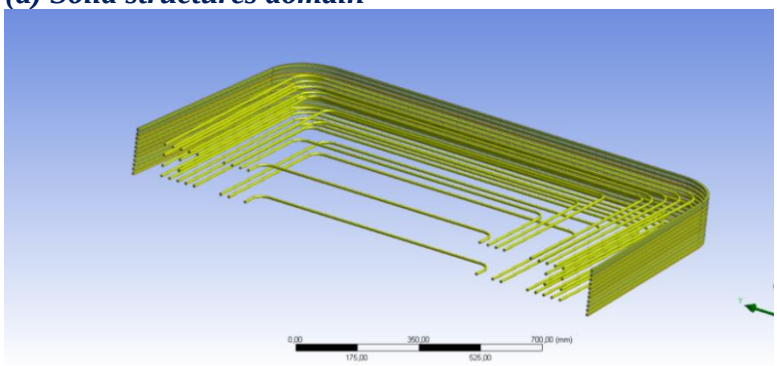

(b) Water coolant domain

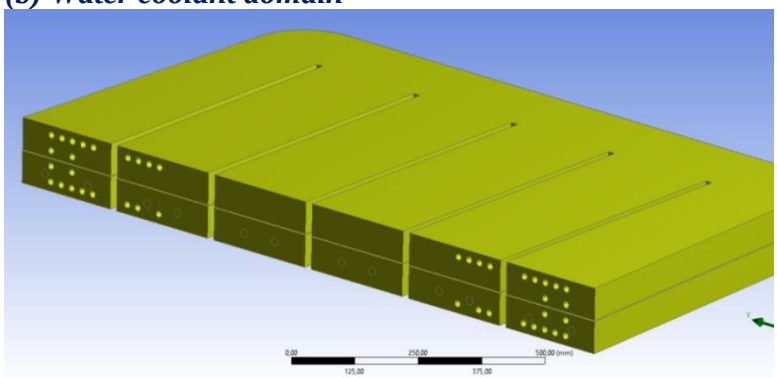

(c) PbLi breeder domain

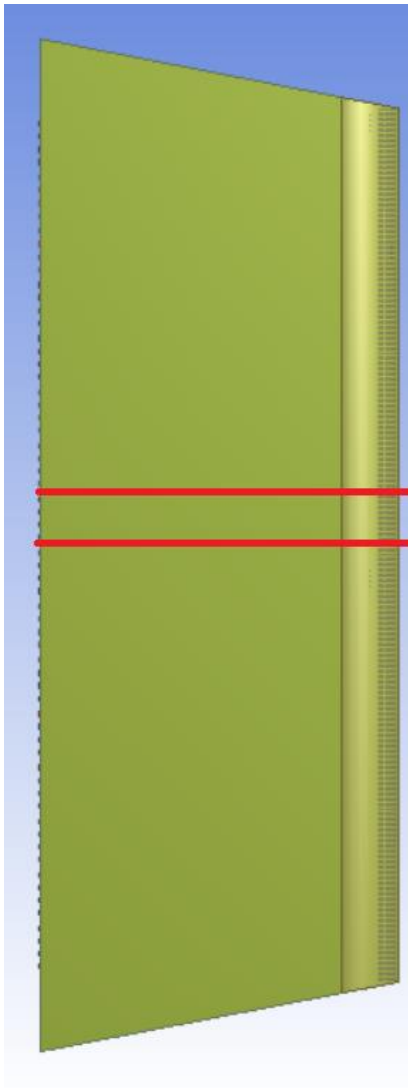

(d) Toroidal – radial slice of the module

Fig. 19 –WCLL breeding blanket model : details of geometry

The geometry is realized through the Design Modeler in ANSYS using the information in the CAD drawing of the entire outboard equatorial module (OB4). Indeed, this has made easier modifications of the mesh for sensitivity analyses. 69 bodies are created and grouped into two parts:

- Breeding zone including the PbLi, 21 coolant tubes, 21 tubes and 13 plates (Fig. 20);
- FW zone containing sidewall/first wall plate with 11 coolant channels and tungsten domain (Fig. 21).

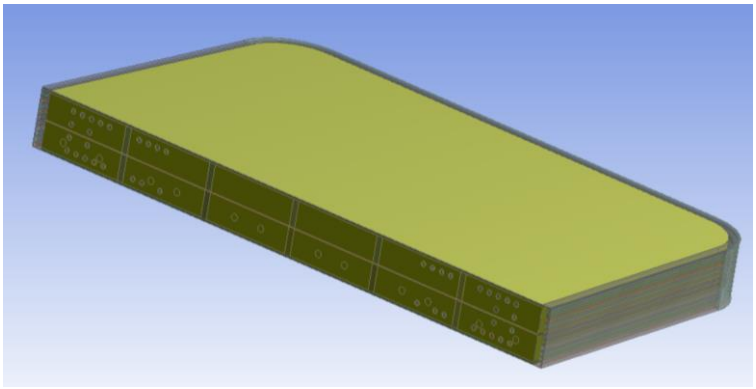

Fig. 20 – Breeding zone

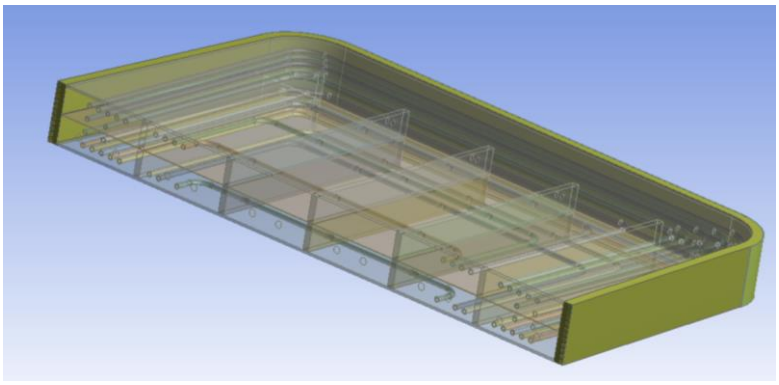

Fig. 21 – FW zone

The maximum overall dimensions of the model are 146.4 mm in poloidal direction, 827 mm in the radial direction and 1520 mm in toroidal direction. The total volume is of about 0.17 m^3.

Tab. 7 shows the main geometric parameters characterizing the model (Fig. 22).

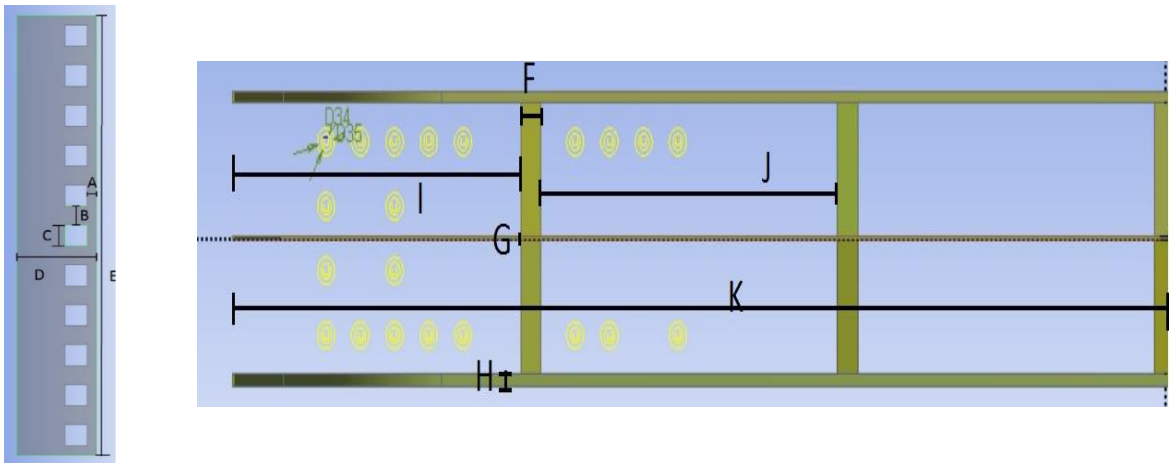

Fig. 22 – Sketches of FW zone and stiffening Plate

Parameter	Length[mm]
A	3
B	6.3
C	7
D	25
E	146.4
F	16
G	2
H	6
I	227
J	234
K	735
D34	8
D35	13.5

Tab. 7 – FW zone and stiffening plates geometric parameters

The 21 tubes of the coolant are divided into 9 arrays. They have different lengths. Indeed, they develop differently in the radial direction to cool adequately the several zones of the module (Fig. 23), to cover the volumetric power deposition distribution. The extension in the radial direction is summarized in Tab. 8.

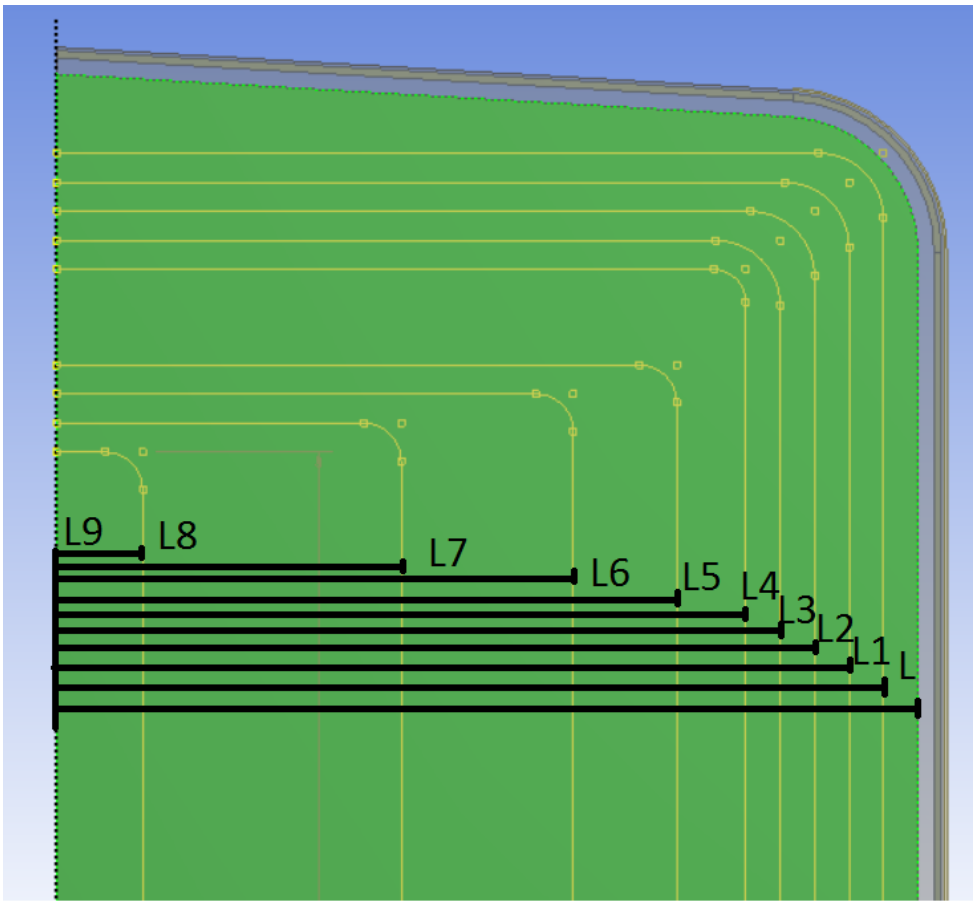

Fig. 23 – Sketch of BZ coolant pathlines

Parameter	Length[mm]
L	800
L1	768
L2	736
L3	704
L4	672
L5	640
L6	576
L7	480
L8	320
L9	80

Tab. 8 – Breeding zone coolant geometric parameters

Within the CAD model, the details of the inlet and outlet of PbLi were not provided, therefore they were postulated on the basis of design constraint on the breeder velocity. The flow area of the PbLi inlet is calculated to guarantee a crossing speed of less than 5 mm/s and subsequently two circular sections for each PbLi elementary channel have been added.

For the definition of the PbLi outlet, the whole PbLi surface available in the exit area is adopted. This is not a realistic design solution, but it is suitable for fulfilling the objectives of the analysis, thus to assess the effectiveness of the tubes layout and the flow paths of the PbLi inside the module.

Afterwards, the VI simulation addresses the fluid dynamics of PbLi in the outlet sections, to provide feedbacks to designers about the proposed configuration of the outlet manifolds. This is based on the assumptions that PbLi exits only from the two central positions. Hence, it is necessary to drill the poloidal radial stiffening plates to allow the fluid flowing from the side channels of the module towards the center. More details are discussed in section 5.6.

A new arrangement of the BZ tubes is proposed and analyzed in simulation VII. The geometry and change local controls of the mesh are modified according with the outcomes from the other simulations (see section 5.7).

4.3 Mesh set-up

4.3.1 Mesh independence and convergence

A mesh independency analysis has been performed for the finite volume model to select optimized spatial discretization allowing accurate results and saving calculation time.

A first independent analysis is conducted to identify the suitable mesh of coolant in the BZ and in the FW zone channels. For this purpose, simulations are conducted with one tube and a single channel.

Five different meshes (A, B, C, D, E) are set-up, modelling the FW channel. They are evaluated with increasing degree of detail, as reported in Tab. 9.

The heat transfer between the coolant flowing in the channels and the structural material is simulated. The coolant flow rate is set 0.055 kg/s and the inlet temperature 285 °C. A constant temperature of 350 °C is set in the wall.

Mesh	n. nodes
A	45632
B	59520
C	87296
D	**142848**
E	244528

Tab. 9 – Single channel coolant grids details

The pressure drops between inlet and outlet and the average temperature of the fluid are reported in a section placed at 0.5 meters from the entrance. Analyzing the results (Fig. 24 and Fig. 25), the Mesh D is evaluated as the "optimum compromise" and therefore selected for modelling the coolant channels of the FW.

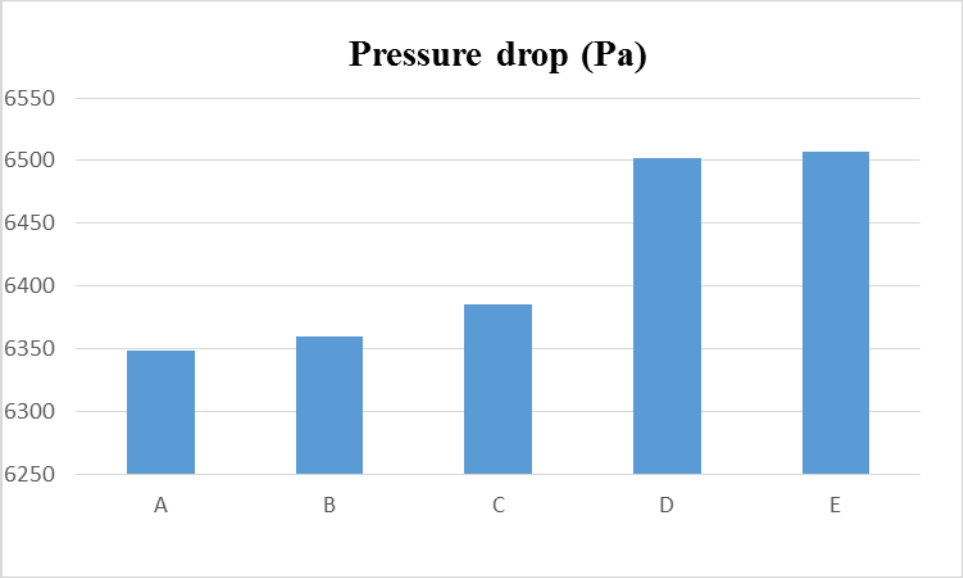

Fig. 24 – Single channel coolant pressure drop

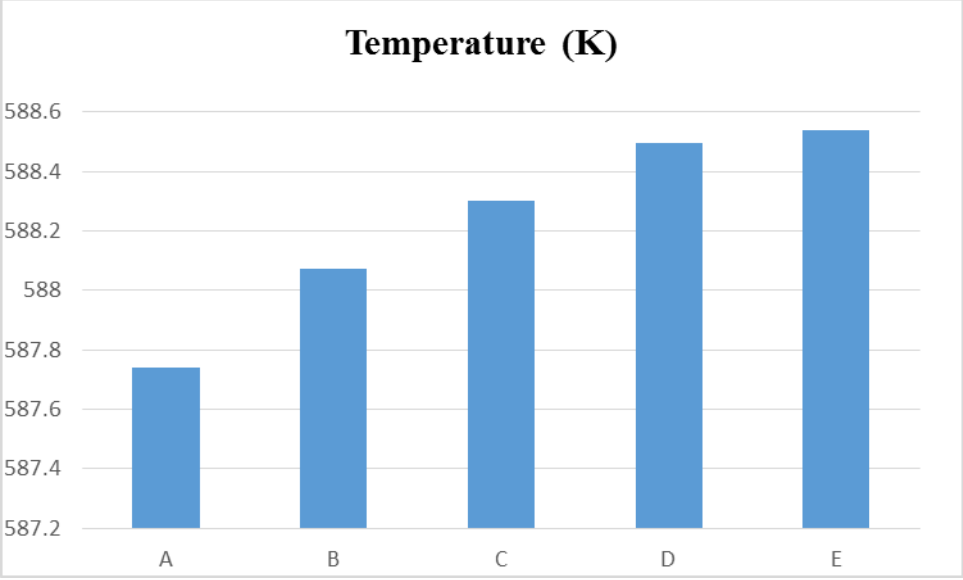

Fig. 25 – Single channel coolant temperature

Five meshes (1, 2, 3, 4, 5), modelling the double wall tubes in the breeding zone, have been also assessed (Tab. 10), evaluating the prediction of the heat exchange and the pressure drop at 0.45 meters from the entrance. A mean velocity of 1.5 m/s and inlet temperature of 285 °C have been set, while a constant temperature of 350 °C has been set for the wall.

Mesh	n. nodes
1	36296
2	91438
3	124244
4	**178688**
5	256166

Tab. 10 – Single tube coolant grids details

Analyzing the results, reported in Fig. 26 and Fig. 27, the detail degree of Mesh 4 is adopted for the coolant of the BZ in the complete model.

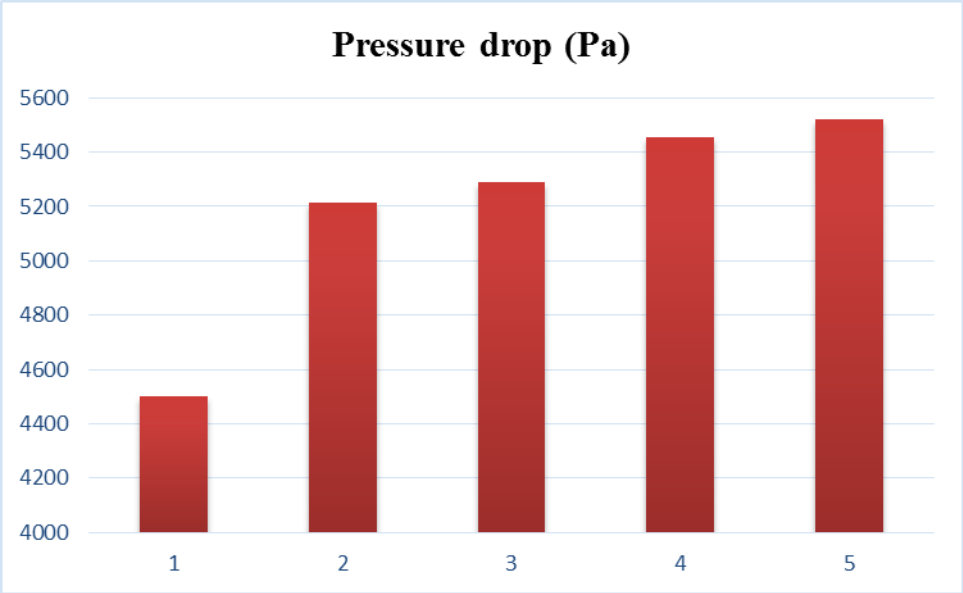

Fig. 26 – Single tube coolant pressure drop

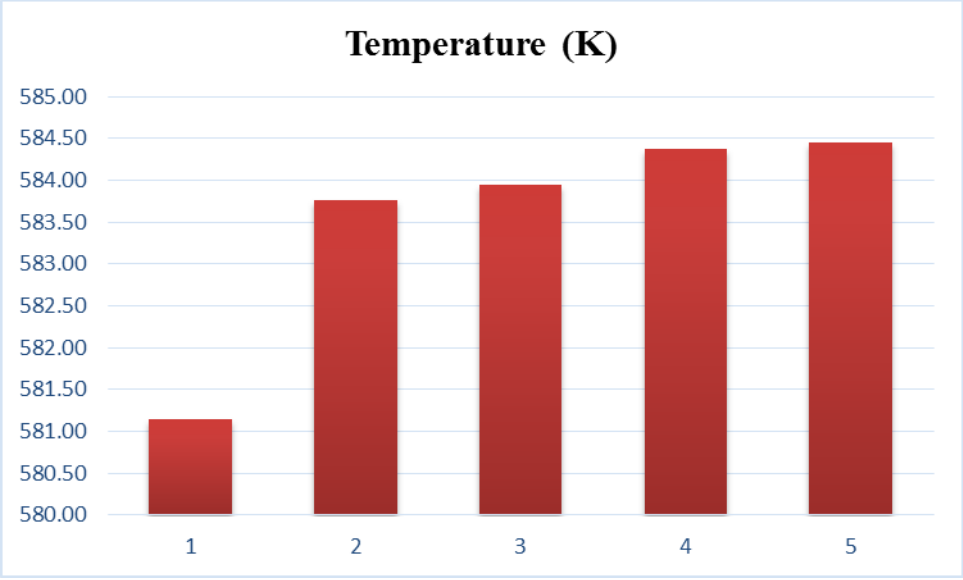

Fig. 27 – Single tube coolant temperature

Afterwards, a sensitivity analysis is conducted using the complete computational domain setting up 3 different meshes, identified as C1, C2, C3 in Tab. 11. They differ for the level of detail in the PbLi domain, as well as in the solid structures, i.e. stiffening plates and FW zone.

The analysis is performed accounting for the thermal loads, the boundary conditions and the inlet conditions as specified for "Sim I" run (see sections 4.5 and 4.6).

Mesh ID	n. nodes
C1	8.2 M
C2	**10.3 M**
C3	12.8 M

Tab. 11 – Complete module grids details

The maximum and the average output temperatures in the PbLi domain are those parameters used for the evaluation of the mesh. The results are reported in Fig. 28 and Fig. 29.

The mesh C2 was chosen, because it represents a good compromise between the degree of detail and the computational time efforts.

This is the reference mesh adopted in the simulations described in section 5.

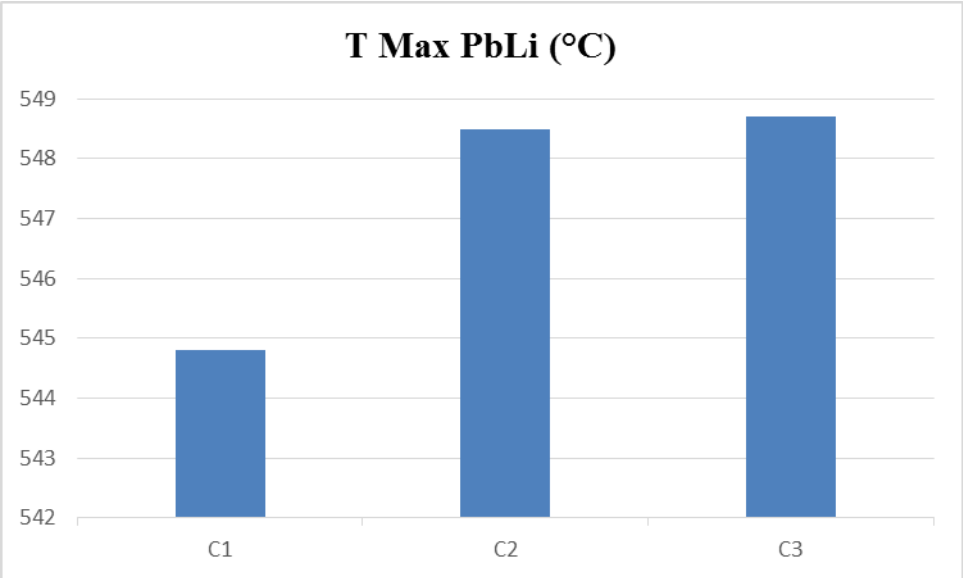

Fig. 28 – Max PbLi temperature

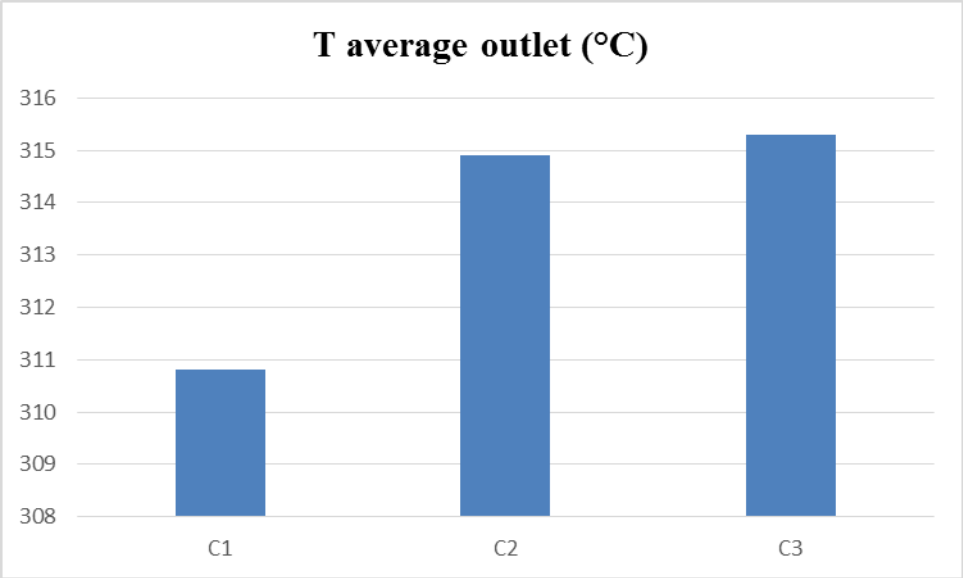

Fig. 29 – Average PbLi temperature in outlet section

Three are the conditions considered for assessing the convergence of the results of the simulations. Therefore, the steady state calculation was interrupted when:

- residual RMS error values are below an acceptable value, i.e. 10^{-5};
- monitor points for selected parameters of interest achieve steady solutions;
- mass, momentum and energy imbalances (measure of the overall conservation of quantity) are less than 1% in the entire domain.

4.3.2 Mesh details

Hexahedral and tetrahedral elements are adopted taking into account the geometrical features of the domains to be meshed and the required optimization of the nodes number and mesh quality.

A conformal mesh between the different domains (i.e. PbLi, plates, tubes and coolant) is used within the BZ; instead a non-conformal interface between the PbLi and FW zone is adopted. This solution does not involve issues because there is no exchange of matter at this interface.

The main features of the mesh are the following:

- Structured hexahedral mesh in the BZ coolant (Fig. 30) and FW zone coolant domain (Fig. 31); inflation layers at the coolant\solid interface are present and the mesh follows the channel profile in radial-toroidal-radial direction.
- Structured hexahedral mesh in solid structure as showed in the Fig. 32 details.

- Structured hexahedral blocks (in the zones around the tubes and walls) and unstructured tetra blocks in PbLi domain with inflation layers at the PbLi\solid material interface to allow a better description of the system because those are the zones that require a greater degree of detail due to higher velocity gradients (Fig. 33).

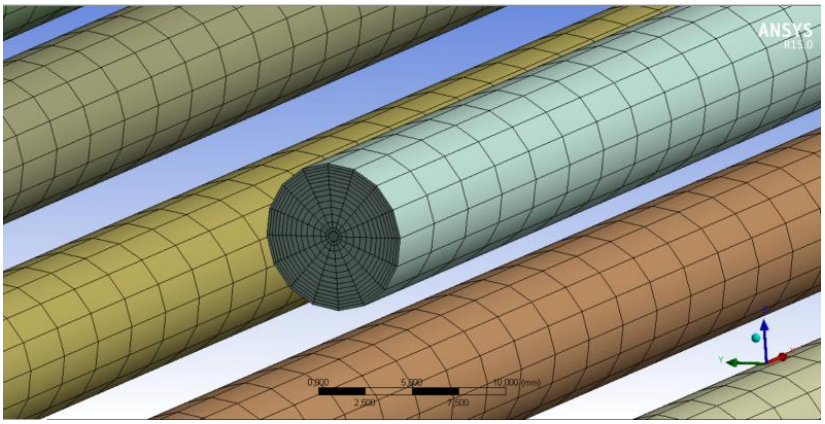

Fig. 30 – BZ water coolant mesh detail

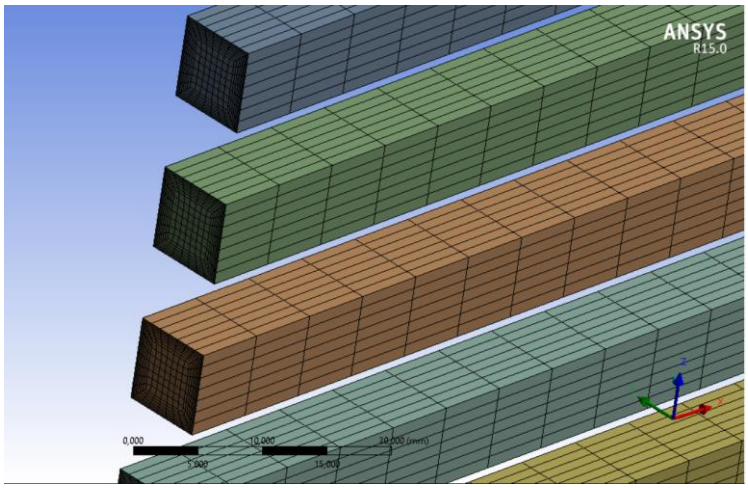

Fig. 31 – FW water coolant mesh detail

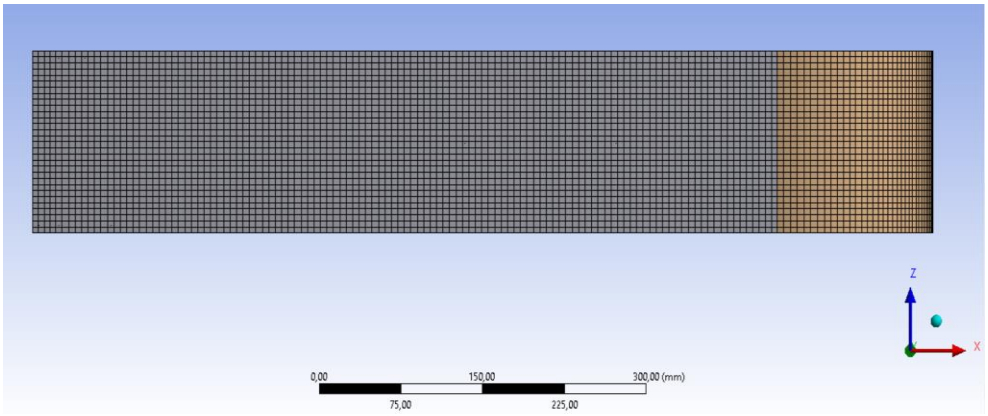

Fig. 32 – Solid structure mesh detail

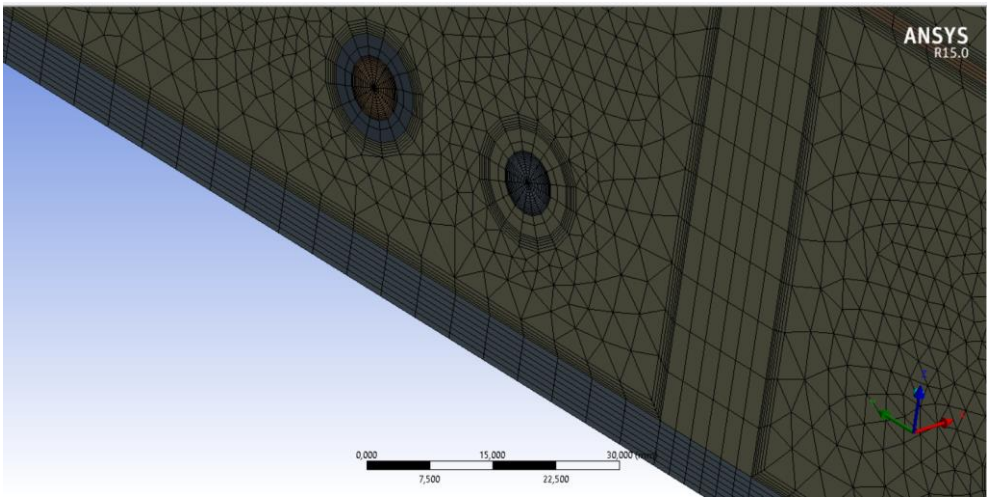

Fig. 33 – PbLi mesh detail

The mesh was created through the software ANSYS ICEM CFD and many local mesh controls are inserted to define appropriately the complex geometry. For this purpose, different code tools are exploited, such as the sizing control, the sweep method, the mapped face, and the inflation control.

The mesh is generated separately for each body defined in the Design Modeler. The order in which the body are meshed is very important because this choice leads to different results and may determine incompatibility of the set controls. For this purpose, the Worksheet function has been exploited.

Despite the complexity of the domain, due to the number of tubes within the PbLi, a satisfactory result in terms of quality of the mesh was reached, as demonstrated in Tab. 12.

Mesh statistics	
Nodes	10.3 M
Skewness average	0.2938
Orthogonal quality average	0.831

Tab. 12 – Mesh details

4.4 Material properties

PbLi, Coolant, Eurofer steel and tungsten, fluids and materials involved in the simulation are not implemented in CFX code database, so it needs to include these materials in the model and to characterize their physical properties. For a correct representation the solids are specified in terms of density, specific heat, thermal conductivity, while fluids require also the dynamic viscosity.

The operating temperature range of the Pbli and Eurofer is expected to be very wide. Therefore, a correct representation of the physical phenomenon it is necessary to introduce the properties as a function of temperature. Furthermore, the properties of the coolant have a relevant dependence from the temperature, thus also for water is essential to describe the properties as a function of this variable.

CEA data [8] reported in Tab. 13, Tab. 14 and Tab. 15 are taken as reference, and a polynomial fitting of data is used for different materials minimizing the sum of the square of the deviations of data. The properties are assumed depending from the temperature. Appendix A shows the Matlab's curve fitting tool.

Temperature (K)	543.15	553.15	563.15	573.15	583.15	593.15	603.15	613.15
Density (kg m^{-3})	782	765	747	727	705	680	651	616
Specific heat (j kg^{-1} K^{-1})	4895	5043	5232	5481	5818	6290	6977	8036
Thermal conductivity (W m^{-1} K^{-1})	0.607	0.593	0.577	0.559	0.539	0.516	0.491	0.462
Dynamic viscosity 10^{-6} (kg m^{-1} s^{-1})	102	98.2	94.9	91.7	88.3	84.5	80.4	76

Tab. 13 – Coolant thermal properties [17]

Temperature (K)	573.15	623.15	673.15	723.15	773.15	823.15	873.15	923.15	973.15
Density (kg m^{-3})	9839	9779	9720	9661	9601	9542	9482	9423	9363
Specific heat (j kg^{-1} K^{-1})	190	189	189	188	187	187	187	187	186
Thermal conductivity (W m^{-1} K^{-1})	13.18	14.16	15.14	16.12	17.10	18.08	19.06	20.04	21.02

Tab. 14 – Pb-15.7Li thermal properties [17]

Temperature (K)	573.15	623.15	673.15	723.15	773.15	823.15	873.15
Density (kg m^{-3})	7666		7633		7596		7558
Specific heat (j kg^{-1} K^{-1})	551	566	584	612	655	721	801
Thermal conductivity (W m^{-1} K^{-1})	30.2		29.3		29.5		31.2

Tab. 15 – Eurofer steel thermal properties [17]

The coefficients of the fitting function are reported in Tab. 16, Tab. 17 and Tab. 18. These values are used in the code through CEL language and are reported in Appendix B.

$$f_i(T) = A_i T^3 + B_i T^2 + C_i T + D_i$$

Coolant fit function	**n**	**A**	**B**	**C**	**D**
Density (kg m^{-3})	2	0	-1.4226E-2	1.4122E+1	-2.6930E+3
Specific heat (j kg^{-1} K^{-1})	3	9.8485E-3	-1.6399E+1	9.1187E+3	-1.6882E+6
Thermal conductivity (W m^{-1} K^{-1})	2	0	-1.2024E-5	1.1846E-2	-2.2804E+0
Dynamic viscosity 10^{-6} (kg m^{-1} s^{-1})	2	0	-8.0952E-4	5.7224E-1	2.9672E+1

Tab. 16 – Coolant fit function coefficients

PbLi fit function	n	A	B	C	D
Density (kg m^{-3})	1	0	0	-1.1890E+0	1.0520E+4
Specific heat (j kg^{-1} K^{-1})	1	0	0	-9.0000E-3	1.9474E+2
Thermal conductivity (W m^{-1} K^{-1})	1	0	0	1.9600E-2	1.9463E+0

Tab. 17 – PbLi fit function coefficients

Eurofer fit function	n	A	B	C	D
Density (kg m^{-3})	1	0	0	-3.6100E-1	7.8743E+3
Specific heat (j kg^{-1} K^{-1})	3	5.3333E-6	-8.7371E-3	4.9838E+0	-4.3883E+2
Thermal conductivity (W m^{-1} K^{-1})	2	0	6.5000E-5	-9.0810E-2	6.0915E+1

Tab. 18 – Eurofer steel fit function coefficients

Specific isobar heat capacity trends of the computed fit functions are reported in Fig. 34 and Fig. 35.

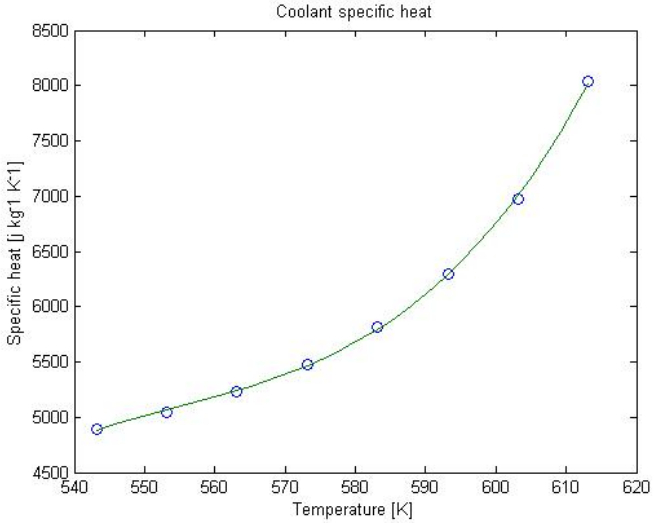

Fig. 34 – Coolant specific heat

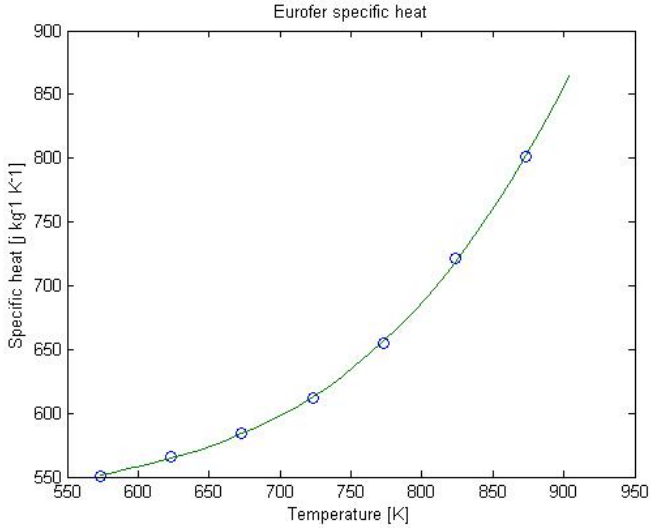

Fig. 35 – Eurofer specific heat

The PbLi dynamic viscosity (μ) is implemented according with the following formula [30]:

$$\mu_{PbLi} = 1.87 \cdot 10^{-4} \cdot e^{\frac{11640[j \cdot mol^{-1}]}{T \cdot R}} (Pa \cdot s)$$

The tungsten properties are assumed constant in the model, as they have a weak dependence at the temperatures of interest (Tab. 19). Moreover, the temperature range is small because it is concentrated in a thin layer, having a thickness of 2 mm: this makes the hypothesis acceptable.

Density (kg m^{-3})	19300
Specific heat (j kg^{-1} K^{-1})	145
Thermal conductivity (W m^{-1} K^{-1})	125

Tab. 19 – Tungsten thermal properties [31]

4.5 Thermal loads and boundary conditions

The FW surface is subjected to a power deposition due to particles and radiations arising from plasma. This is modelled with a non-uniform heat flux imposed on the external surface.

Each element of the FW surface has a normal heat flux calculated by multiplying the nominal heat flux value of 0.5 MW/m^2 for the cosine of the angle between the radial and the surface normal directions (see Fig. 36).

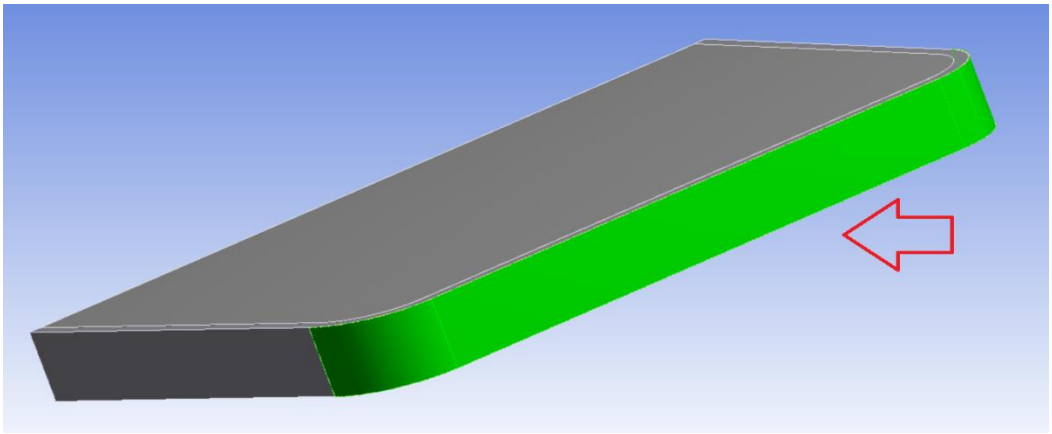

Fig. 36 – Heat flux on the FW surface

Moreover, a radial distribution of heat power volumetric density is applied to simulate the power deposited by neutrons and photons. To this purpose, the heat power density calculated for PPCS-A WCLL outboard blanket [28] has been scaled with the factor of 1.05/2.56 according to DEMO average Neutron Wall Loadings (NWLs) [19]

Subsequently, it is modified to reflect the different arrangement of the plates between the module of the PCCS-A and the ENEA WCLL2015.OB4 module [10] (radial-poloidal stiffening plate which are replaced by radial-toroidal stiffening plate).

To assess the value of volumetric generation in the zones with only Eurofer steel in the PCCS-A WCLL geometry, a data fitting is used with an exponential function in the previous and in the next interval to these areas (the coefficients are summarized in Tab. 20 and Tab. 21).

$$f_k(r) = A_k \cdot e^{-B_k \cdot r} \; ; \; k = 1,2,3,4,5 \; fitting \; functions$$

$$[r_i; g_i] \; ; \; i = 1 + 5(k-1), \ldots . \; 5k \; data \; fitting \; ;$$

$$r_i \; radial \; position \; [mm]$$

$$g_i \; power \; density [W \cdot cm^{-3}]$$

k	A	B
1	1.4268E+1	8.6154E-3
2	9.6954E+0	7.3515E-3
3	7.3074E+0	6.3612E-3
4	6.4129E+0	6.1855E-3
5	3.9015E+0	5.5710E-3

Tab. 20 – Coefficients exponential fit for PbLi

k	A	B
1	3.5500E+0	1.0302E-2
2	2.5419E+0	9.2355E-3
3	2.4883E+0	8.9725E-3
4	1.4492E+0	7.9107E-3
5	4.0000E-3	0

Tab. 21 – Coefficients exponential fit for Eurofer

The heat power density values that are not defined in the PbLi domain in the WCLL PPCS-A distribution were evaluated using the obtained fitting functions. The highest value is considered for precautionary reasons.

$$g^*_k = Max[f_k(r^*_k); f_{k+1}(r^*_k)]$$

$$r^* = [190.4; 357.8; 525.2; 692.6]$$

Therefore, the heat power volumetric density is implemented in Eurofer, Tungsten and PbLi domain of the model, as summarized in Tab. 22. The volumetric density, implemented in CFX through CEL language, are reported in Appendix C.

Thickness (mm)	Rin (mm)	Rout (mm)	Eurofer/tungsten power density (W/cm^3)	PbLi power density (W/cm^3)
6.7	0	6.7	8.704	0.000
3	6.7	9.7	5.229	0.000
17.3	9.7	27	7.887	0.000
32	27	59	2.539	11.152
32	59	91	1.690	7.444
32	91	123	1.210	5.681
32	123	155	0.886	4.446
31.4	155	186.4	0.677	3.646
8	**186.4**	**194.4**	0.531	2.913
32	194.4	226.4	0.402	2.280
32	226.4	258.4	0.279	1.645
32	258.4	290.4	0.205	1.288
32	290.4	322.4	0.156	1.042
31.4	322.4	353.8	0.123	0.886
8	**353.8**	**361.8**	0.106	0.780
32	361.8	393.8	0.090	0.705
32	393.8	425.8	0.066	0.550
32	425.8	457.8	0.049	0.447
32	457.8	489.8	0.037	0.369
31.4	489.8	521.2	0.029	0.312
8	**521.2**	**529.2**	0.024	0.269
32	529.2	561.2	0.021	0.234
32	561.2	593.2	0.016	0.185
32	593.2	625.2	0.012	0.152
32	625.2	657.2	0.008	0.123
31.4	657.2	688.6	0.008	0.107
8	**688.6**	**696.6**	0.006	0.092
32	696.6	728.6	0.004	0.078
32	728.6	760.6	0.004	0.062
32	760.6	792.6	0.004	0.053
34.4	792.6	827	0.004	0.045

Tab. 22 – Heat power volumetric density in Pbli and Eurofer domains

The volumetric generation in the coolant was not considered, because it is negligible if compared with the amount of heat exchanged by convection heat transfer.

This can be shown through an energy balance between the inlet and outlet sections of the coolant. It is reported an estimate of the volumetric generation and the enthalpy flow of

water refrigerating a channel of FW zones. The volumetric generation is highest in these channels being invested by the maximum neutron flux.

.

$$\dot{H} = \dot{G} + \dot{Q}$$

$$\dot{H} = \dot{m} \cdot \Delta h \cong 12300\ W$$

$$\dot{G} = \int_V \dot{g}(V)\, dV \cong \dot{g}_0 \cdot S \cdot L \cong 600\ W$$

$$\dot{Q} = \int_A \vec{q}'' \cdot \overrightarrow{dA}$$

$$\dot{H} \cong \dot{Q}$$

It is noted that the contribution of volumetric generation is relatively small compared to the superficial heat exchange, thus volumetric generation will be assumed negligible for the whole domain of the coolant.

Periodic boundary conditions are imposed on the radial-toroidal plates being the same surface, while the side wall is considered adiabatic in order to take into account the presence of the other blanket modules (see Fig. 37).

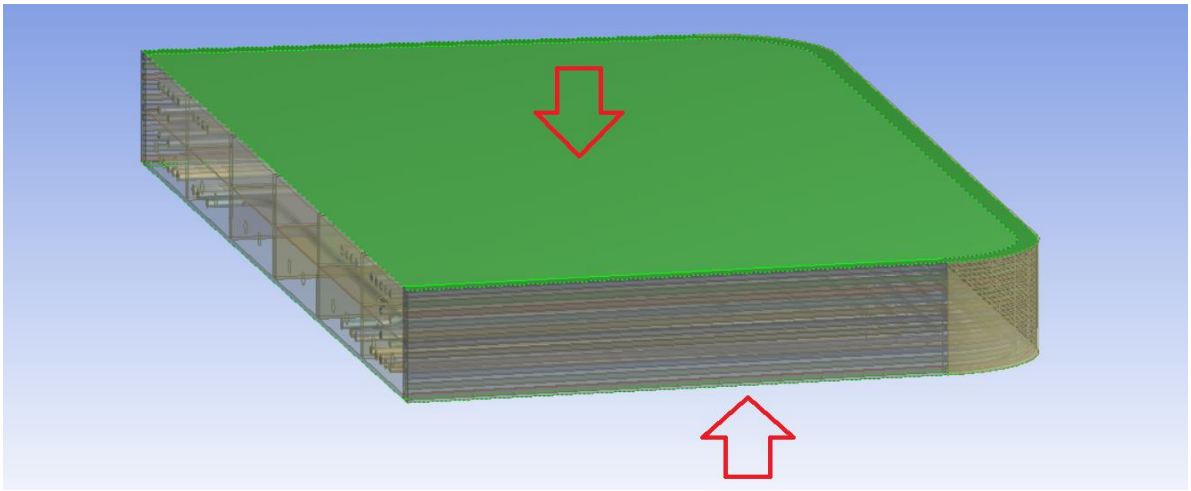

Fig. 37 – Periodic boundary conditions

These operating conditions are applied in all simulations, with the exception of simulations Sim V and Sim VI. For these, the operating conditions are described in sections 5.5 and 5.6.

4.6 Inlet conditions set-up

The inlet conditions are summarized in Tab. 23 in accordance with Ref. [10]. These are kept the same in the simulations.

The total flow rate of the FW coolant is divided equally across channels in each simulation (Fig. 38). Specific assumptions set in CFD analyses from SIM-I to SIM-VII are described in detail in sections 5.1, 5.2, 5.3, 5.4, 5.5, 5.6 and 5.7.

Coolant BZ T_inlet (°C)	285
Coolant BZ P (MPa)	15.5
Coolant FW T_inlet (°C)	285
Coolant FW P (MPa)	15.5
PbLi T_inlet (°C)	325
PbLi P (MPa)	0.5
PbLi Mass Flow (kg/s)	0.146

Tab. 23 – Inlet conditions

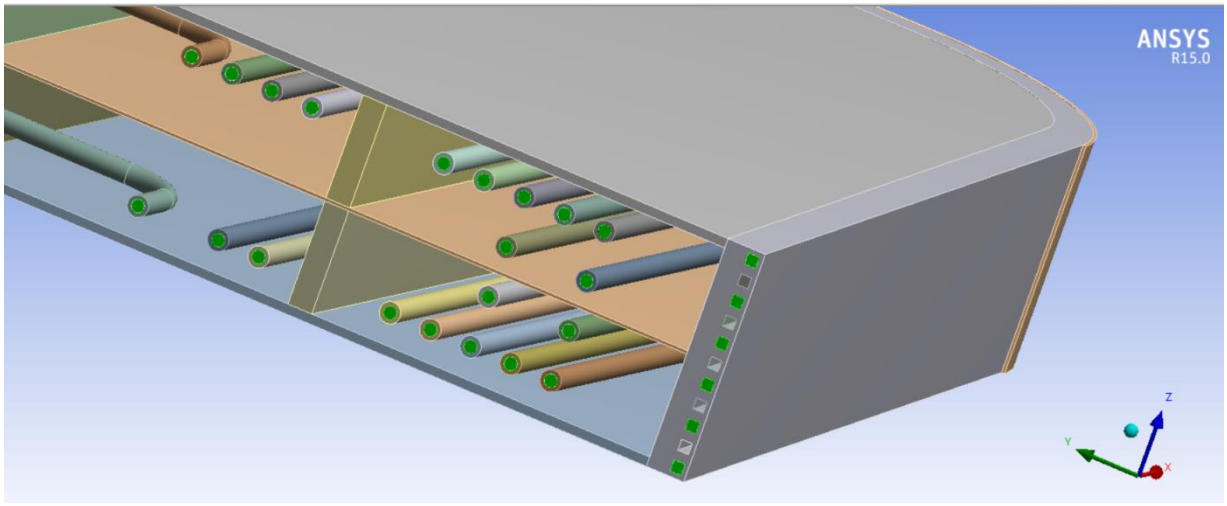

Fig. 38 – FW zone and BZ coolant inlets

5 SIMULATIONS RESULTS

5.1 Sim I: results and analysis

In SIM-I (and SIM-II), the coolant flow rates in the FW and BZ zones are taken from WCLL Design Description Document [10]. The total coolant flow rate of equatorial outboard module is divided by 16 since the model is 1\16 of the total module. Furthermore, a constant flow distribution is assumed in the FW cooling loop and the same is for the BZ cooling loop. The input data are reported in Tab. 24.

Coolant BZ Mass Flow (kg/s)	1.15
Coolant FW Mass Flow (kg/s)	0.609

Tab. 24 – Coolant mass flow rates (Sim I-II)

5.1.1 Analyses of results

The results of the simulation are hereafter discussed with focus on temperature field in the Eurofer steel, PbLi and coolant domains.

A significant thermal gradient arises in both radial and toroidal directions within the Eurofer domain, due to the external heat flux, heat transfer inside the cooling tubes with PbLi flowing in the BZ and the volumetric density of nuclear power.

The range of temperatures within the solid structure is wide, going from 286.5 to 530.5 °C (see Fig. 39). In particular, the maximum temperature of 530.5 °C (Tab. 25) is predicted in the baffle plate. This temperature is below the Eurofer temperature limit, which is 550 °C. This temperature in the baffle plate does not jeopardize the strength of the module because this has not structural function. The baffle plate is used to separate the channels and to allow the PbLi passing through the module in the correct way.

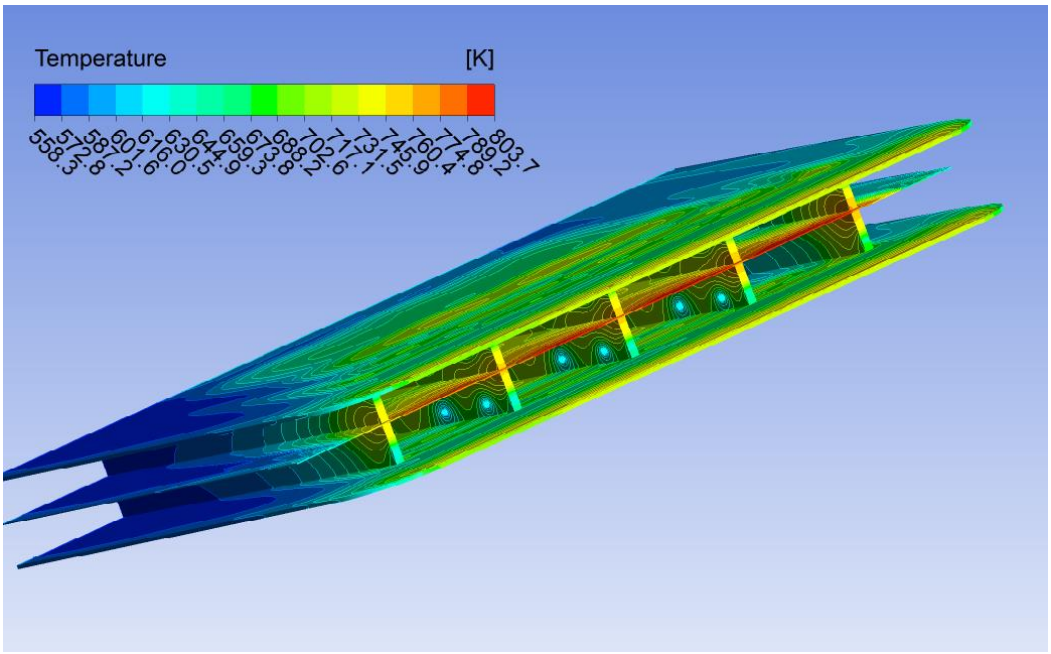

Fig. 39 – Eurofer temperature in stiffening plates and baffle plate domain (Sim I)

Fig. 40 shows the temperature of the poloidal radial stiffening plate between the fourth and fifth channel. The maximum temperature is in the area of the baffle plate and the presence of a symmetry plane can be observed. This is linked to the tubes position.

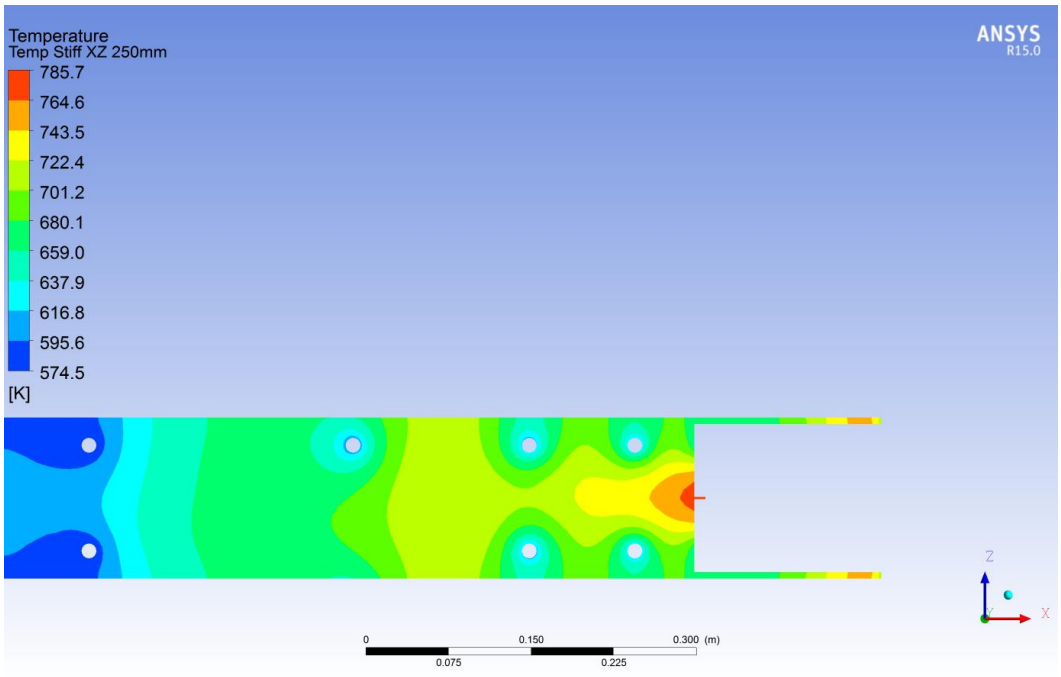

Fig. 40 – Eurofer temperature in stiffening plate in poloidal – radial plane (Sim I)

T Eurofer	
T_min stiff (°C)	286.5
T_max stiff (°C)	530.5
T_ave stiff (°C)	371.2

Tab. 25 – Eurofer temperature (Sim I)

Results suggest that the FW thermal field is quite uniform along the poloidal and toroidal directions due to the countercurrent FW coolant flow that makes the temperature homogeneous (Fig. 41). In this region, the maximum temperature reached in the Eurofer steel is 444.4 °C.

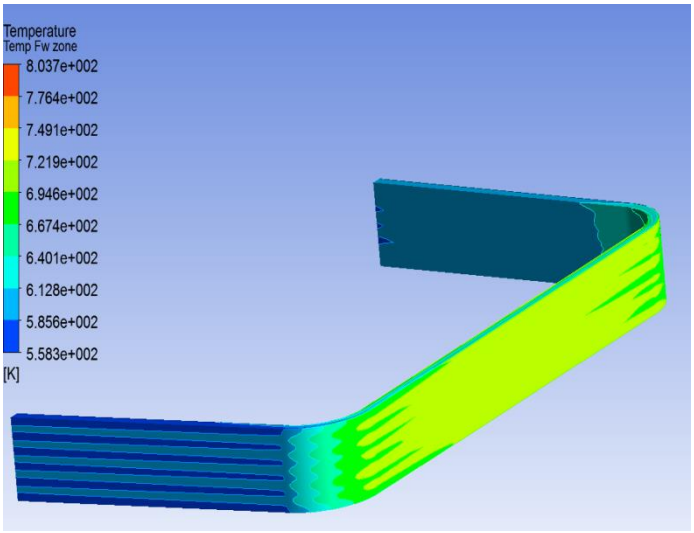

Fig. 41 – Eurofer temperature in FW zone (Sim I)

The maximum PbLi temperature computed in the simulation is 548.5 °C (Tab. 26), lower than the 550°C limit. It is possible to further reduce this value by modifying the tubes arrangement in the area closest to the FW with the possibility of adopting staggered tube bundle arrangement.

The average outlet PbLi temperature is 314.9 °C, lower than the target temperature set at 325 °C but above the eutectic PbLi melting point (235 °C). This is due to an un-balance of energy between deposited energy and removed. This problem can be fixed by optimizing the mass flow rate distribution in the tube, or adjusting tubes arrangement by shifting the involved tube in the radial direction. It should be also noted that the energy deposited in the box inner manifold and in the back manifold region is neglected.

An area cooler can be noted at the BZ coolant entrance due to co-current cooling loop configuration, see area (see Fig. 42).

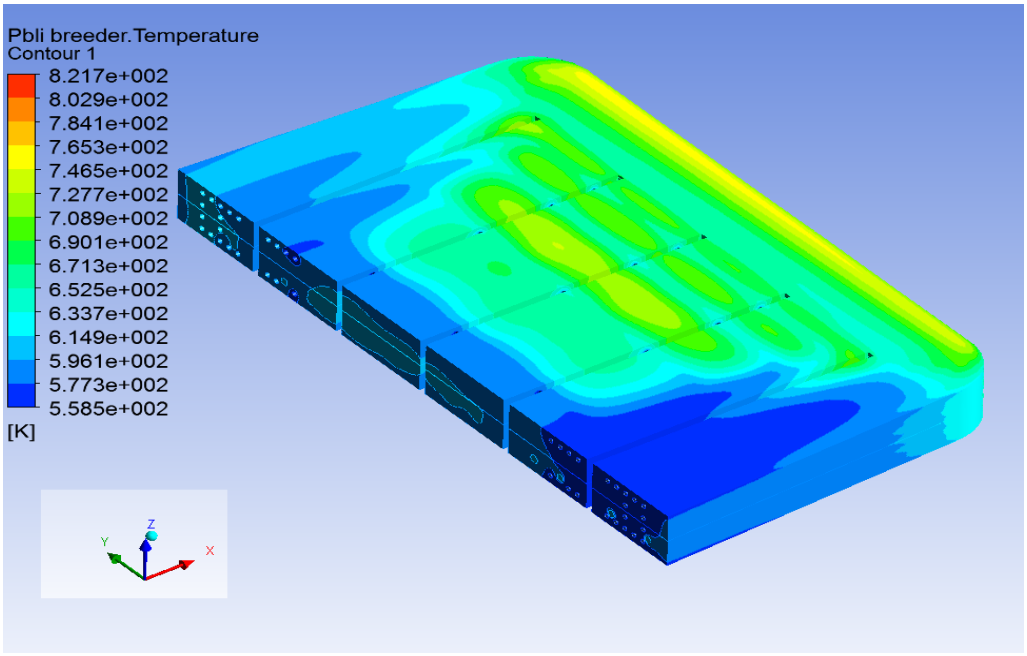

Fig. 42 – PbLi temperature in 3D domain (Sim I)

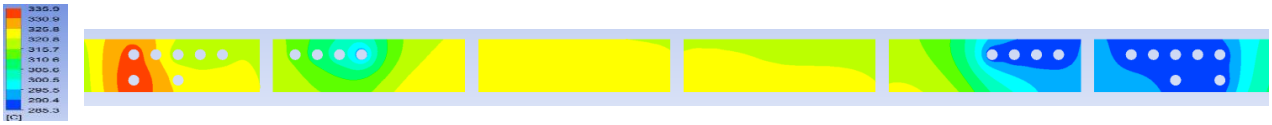

Fig. 43 – PbLi outlet temperature in a poloidal – toroidal plane (Sim I)

There is a considerable difference in the outlet temperature of PbLi in toroidal direction. The minimum temperature is found close to the entrance of the coolant, while the maximum temperature is observed in the area close the coolant exit (Fig. 43). This temperature difference cannot be avoided because it is linked to the coolant co-current configuration, at most it can be reduced up to a value of about 40 degrees which would be the temperature difference between inlet and outlet of the coolant.

T PbLi (°C)	
T_min PbLI	285.4
T_max PbLi	548.5
T_ave PbLi	378.5
T_outlet ave	314.9
T_outlet max	335.9
T_outlet min	285.4

Tab. 26 – PbLi temperature details (Sim I)

Analyzing the PbLi temperature in a poloidal – radial plane centred in the channel (Fig. 44), a significant thermal gradient arises in both radial and poloidal direction due to the radial power distribution and cooling tubes arrangement.

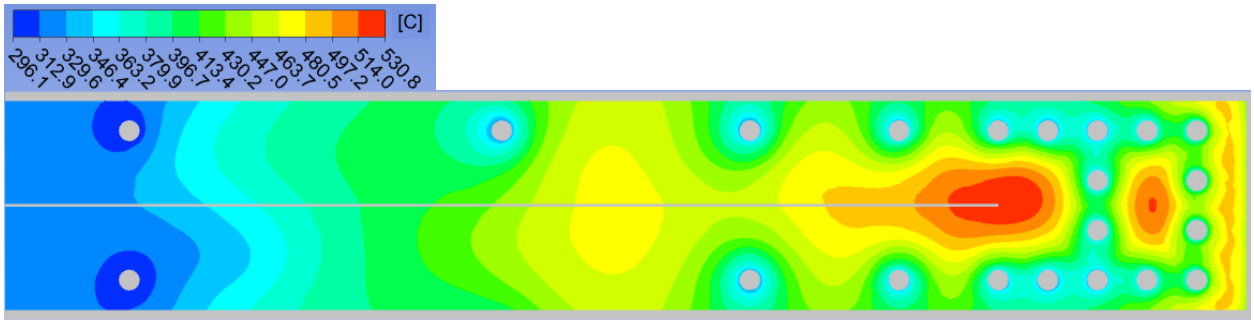

Fig. 44 – PbLi temperature in a poloidal-radial plane centred in the channel (Sim I)

The maximum velocity is 5.5 mm/s and it is reached in the inlet section of the breeding zone. The minimum average velocity (0.25 mm/s) allows to avoid significant MHD-effects.

The velocity field inside the module has the main velocity in the radial direction, in most of the module. At the end of the baffle plate the main flow path is in poloidal direction because in that area the fluid bends and goes back, again, in the radial direction towards the exit. It is observed that the component of the velocity in toroidal direction is very low than the other components.

Significant sections (Fig. 45) are considered into PbLi domain in order to show the velocity field.

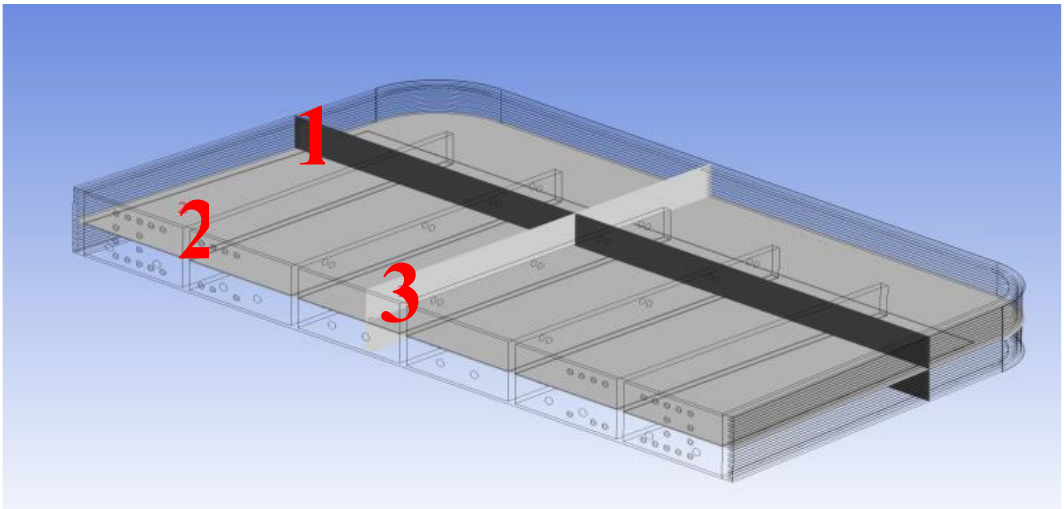

Fig. 45 – Plane section 1, 2 and 3

The tubes arrangement influences PbLi flow field inside the module, in fact zones with higher velocity are found where a greater portion of the channel is occupied by the tubes (Fig. 46).

As can be seen from the Fig. 47 and Fig. 48, the fluid rotates almost near the end of the baffle plate, leaving stagnant zones close to the FW.

Therefore, almost stagnant zones are possible in an area where the maximum production of tritium is expected, being maximum the neutron flux.

Hence, modifications of the baffle plate are suggested for a better fluid flow distribution. Nevertheless, bringing the baffle plate closer to the FW means increasing the volumetric heat generation within this solid structure and therefore a different arrangement of the cooling tubes to avoid temperatures above the critical Eurofer temperature.

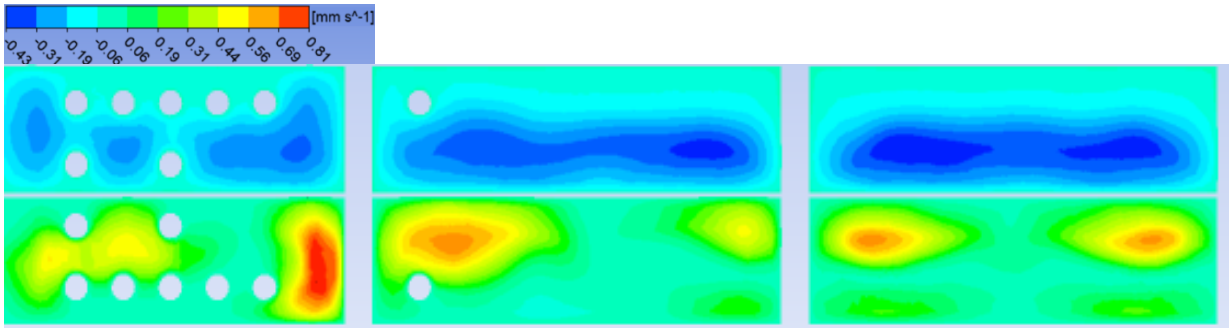

Fig. 46 – PbLi radial velocity in a poloidal-toroidal plane (section 1) (Sim I)

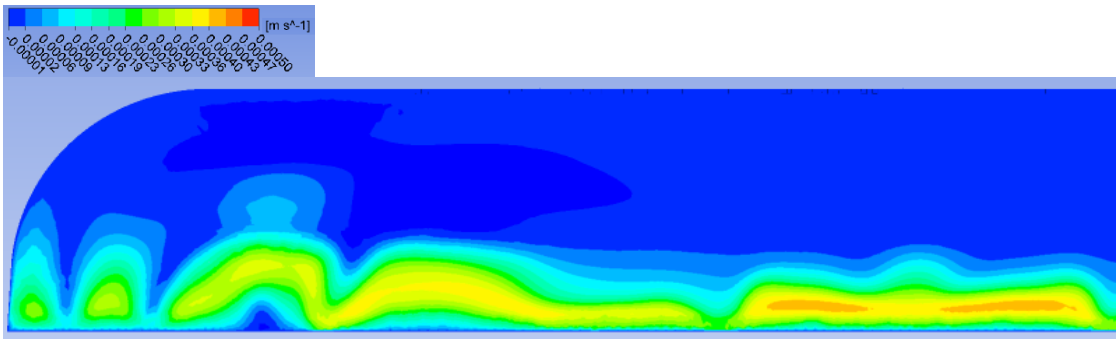

Fig. 47 – Pbli poloidal velocity in a radial-toroidal plane (section 2) (Sim I)

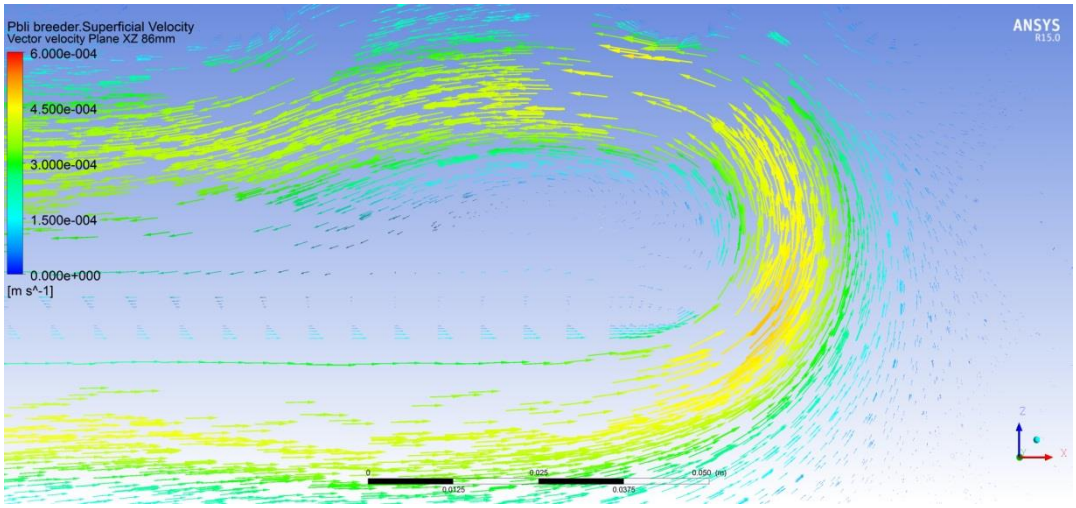

Fig. 48 – PbLi velocity vector distribution in a radial-poloidal plane (section 3) (Sim I)

Water coolant outlet temperatures are not homogenous and too spread from the target value of 325 °C, as reported in Tab. 27 and showed in Fig. 49. This temperature distribution is not acceptable because in some tubes the temperature is close to saturation temperature (that is about 345 °C at 155 bar). On the contrary, others tubes have low temperatures, e.g. the tube identified as BZ-9 reaches 290. 4 °C. The coolant flowing in FW absorbs more heat than estimated analytically. This is due to the simplified assumption done for evaluating these flow rates (i.e. adiabatic conditions between breeding and FW zones).

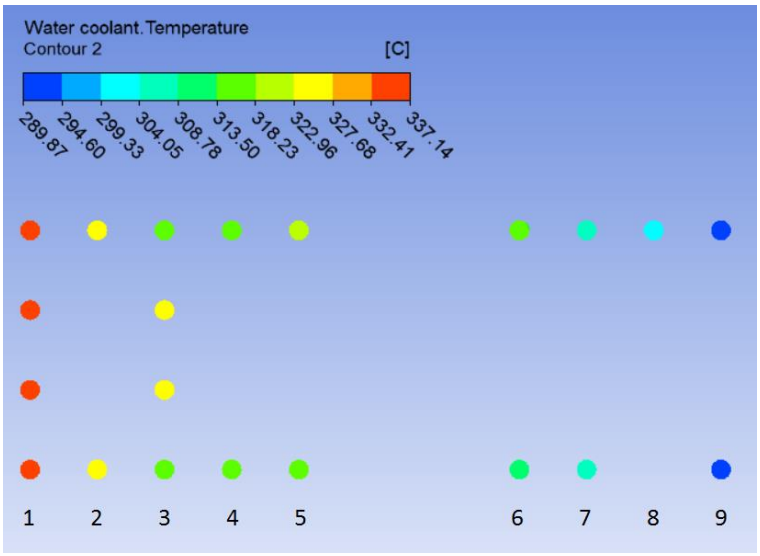

Fig. 49 – BZ coolant outlet temperature (Sim I)

T_Coolant outlet (°C)	
T_ave FW	332.4
T_ave BZ 1	335.6
T_ave BZ 2	325.7
T_ave BZ 3	320.1
T_ave BZ 4	315.2
T_ave BZ 5	318.0
T_ave BZ 6	313.3
T_ave BZ 7	306.6
T_ave BZ 8	301.2
T_ave BZ 9	290.4

Tab. 27 – Water coolant average outlet Temperature (Sim I)

Therefore, the inlet of the tubes has to be orificed in order to homogenize the coolant temperature at outlet. The coolant velocity is lower than the limit value (7 m/s), and the pressure drops are summarized in Tab. 28:

Coolant Velocity	
Vel_ave coolant inlet FW (m/s)	1.49
Vel_ave coolant inlet BZ (m/s)	1.47
Pressure Drops	
Average Coolant FW (Pa)	7193
Average Coolant BZ (Pa)	4723

Tab. 28 – Coolant velocity and pressure drops (Sim I)

5.1.2 *Highlights from the analysis*

- The simulation is set-up with the water coolant flow available in DDD 2016 and constant uniform distribution in BZ tubes.
- In stationary condition, a thermal flux is calculated from the BZ to the FW zone.
- The evaluation based on the analytical solution of mass flow rate in the two water cooling loops (i.e. BZ and FW) is not satisfactory.
- The maximum PbLi and structural steel temperatures are below the limit (i.e. 550°C).
- "Quasi" stagnant PbLi zones are calculated close to FW

5.2 Sim II: results and analysis

The water coolant inlet flow rate are the same of SIM-I. Details are reported in section 5.1.

5.2.1 *Analyses of results*

The buoyancy forces are activated in the simulation II. This option implies that a source term is added to the momentum equations as follows:

$$S_{Mz} = (\rho - \rho_{ref})g$$

The density difference $(\rho - \rho_{ref})$ is evaluated using the Full Buoyancy model, which evaluates this term directly. This option is set in case the density is function of temperature.

This simulation did not achieve the convergence; in fact, the residual RMS error values are about 10^{-3}. Moreover, the monitor points of PbLi velocity and temperature did not reach a steady solution, as shown in Fig. 50.

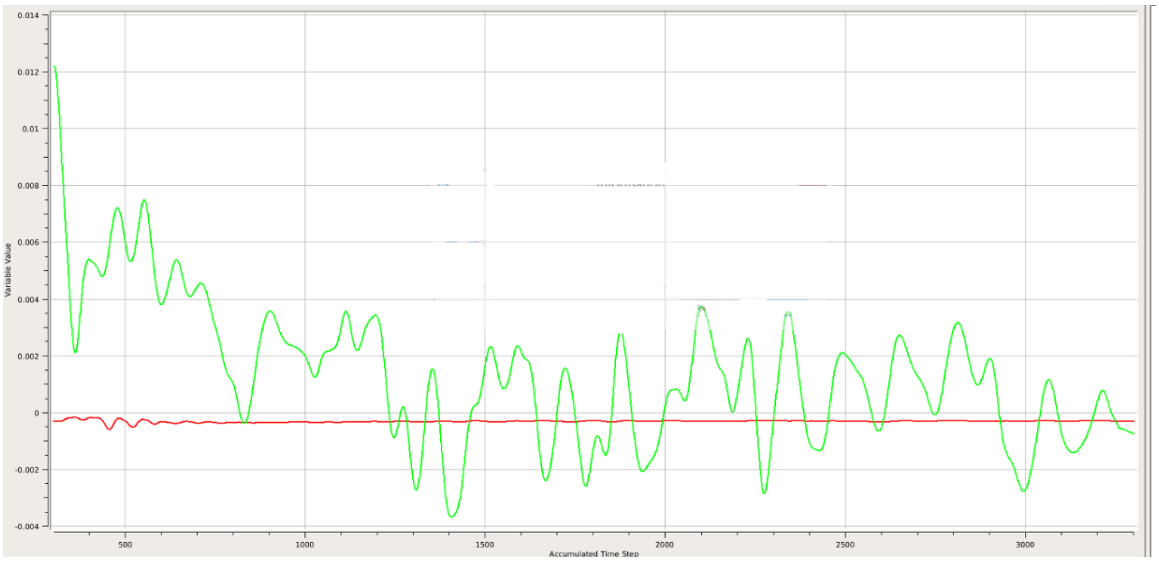

Fig. 50 – Velocity fluctuations as a function of the time step (Sim II)

The problem is related to the insufficient number of the elements in some areas of the domain. Indeed, the mesh is realized with inflation layers at the PbLi\solid material interface and using coarser elements in the zones furthest this interface. High temperature gradients are generated due to the volumetric generation also in the zones distant from tubes and plates walls. In these areas vortices are established, whose simulation requires large number of elements. Considering the required number of elements, an up-graded mesh has been set-up, but the calculation has not been launched waiting for the availability of the cluster.

5.2.2 Highlights from the analysis

- The simulation does not achieve convergence if the buoyancy forces are activated. This implies that the mesh of CFD model shall be further refined a greater degree of detail of the grid is required to describe the PbLi domain.
- Refined mesh is set-up and tested. Simulation will be carried out when larger computational resources will be available.

5.3 Sim III: results and analysis

The flow rates flowing in the BZ tubes are estimated analytically using a "manifold approach" (the pressure drops between inlet and outlet of each tube are the same).

$$\Delta P_i = costant$$

The total flow rate is set for the calculation.

$$\sum_i \dot{m}_i = \dot{m}_{tot} = 0.920 \ kg/s$$

Only the distributed pressure drops along the fluid path are taken into consideration, thus the local pressure drops due to inlet, exit and curvature of the fluid inside the tubes are neglected.

$$\Delta P_i = \frac{\rho \cdot u^2{}_i \cdot f_i \cdot L_i}{2 \cdot D} \ [31]$$

For the Moody friction factor (f), the Petukhov correlation has been used as it is exploitable for the smooth surface condition in a large Reynolds number range.

$$f = (0{,}790 \cdot ln(Re) - 1.64)^{-2} \qquad 3000 \leq Re \leq 5 \cdot 10^6 \ [31]$$

The Petukhov correlation has been approximated by the f * function within a more restricted Reynolds range $[40000 - 250000]$.

$$f^* = 0.2068 Re^{-0{,}212}$$

In this way, it is possible to explicit the velocity in each tube as a function of the pressure drops, in order to obtain the mass flow rates in each tube as a function of pressure drops, $\dot{m}_i = g_i(\Delta P)$.

$$u_i = \left(\frac{\Delta P}{0.1034 \cdot L_i \cdot \rho^{0{,}788} \cdot D^{-1{,}212} \cdot \mu^{0{,}212}}\right)^{1/1{,}788}$$

$$\dot{m}_i = \rho \cdot u_i \cdot \frac{\pi \cdot D^2}{4}$$

$$\dot{m}_{tot} = \sum_i \dot{m}_i = \sum_i g_i(\Delta P) \rightarrow \sum_i g_i(\Delta P) - \dot{m}_{tot} = 0$$

This equation is solved iteratively and the findings are reported in Tab. 32. The fluid properties are assumed constant at the temperature of 305 °C (see Tab. 29, Tab. 30 and Tab. 31).

$$\dot{m}_i = g_i(\Delta P)$$

Density (kg/m^3)	71593
Dynamic viscosity (Pa s)	8.655E-05

Tab. 29 – Coolant reference

Diameter (m)	0.008
n. tubes	21

Tab. 30 – Tubes reference

	Length (m)	**n_tubes**
L_1	2.807	4
L_2	2.689	2
L_3	2.571	4
L_4	2.453	2
L_5	2.359	2
L_6	2.052	2
L_7	1.806	2
L_8	1.432	1
L_9	0.898	2

Tab. 31 – Tubes lengths

j	**m_BZ** (kg/s)
1	0.148
2	0.076
3	0.156
4	0.080
5	0.082
6	0.088
7	0.095
8	0.054
9	0.141

Tab. 32 – BZ coolant flow rates (Sim III)

5.3.1 Analyses of results

The flow rates have been calculated analytically and inserted as inlet conditions in the simulation. These produce the pressure drops between input and output in the various arrays of tubes in the range of 2878 -3072 Pa, as summarized in Tab. 33. This range is quite small, so the flow rates calculated analytically are not very different from the "real" flow in the presence of a manifold.

The average velocities of the coolant in the different arrays are between [1.03 to 2.02 m/s]. There is a high difference of velocity between the different tubes, but the maximum values are below the limit value (i.e. 7 m/s).

Array	Temperature outlet (°C)	Pressure Drops (Pa)	Velocity (m/s)
1	351.0	3072	1.03
2	339.4	3055	1.06
3	332.0	2994	1.08
4	325.2	2937	1.11
5	326.9	3018	1.14
6	319.5	2923	1.22
7	309.8	2900	1.32
8	301.6	2878	1.50
9	289.3	2892	1.96
FW	324.1	10891	2.02

Tab. 33 – Coolant results (Sim III)

With these flow rates, the distribution of the coolant outlet temperature in the BZ is not appropriate. Large differences between the arrays are found and troubling temperature values are reached, in particular in the arrays closer to the FW. In fact, saturated conditions are reached in the array 1 and therefore not allowed conditions for the operation are established.

The liquid temperatures observed are above the saturation temperature, because the CFD does not model the two-phase conditions.

PbLi reaches the maximum temperature of 563.4 °C (Tab. 34) and exceeds the limit value. The peak temperature is always located in the area between the tubes arrays 1, 2 and 3, as seen in Fig. 51.

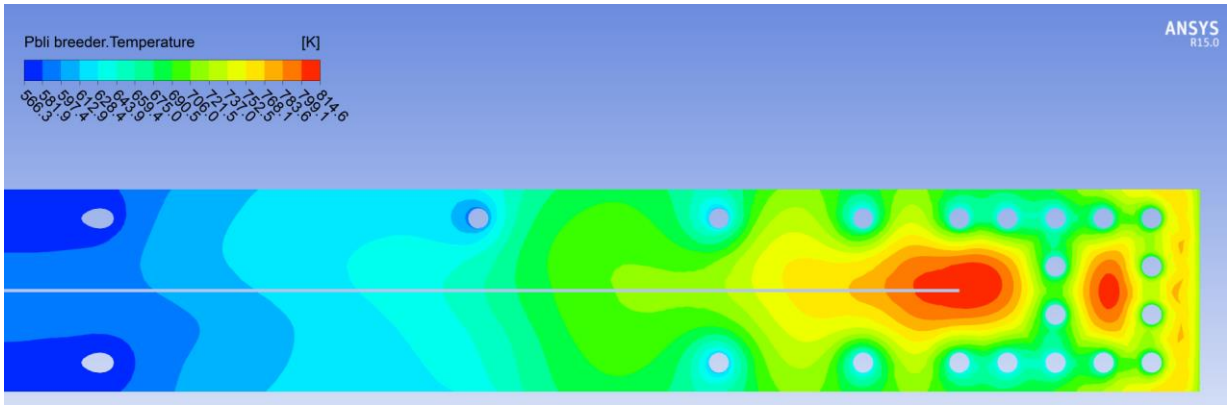

Fig. 51 – PbLi in the poloidal-radial plane centred in the 5th elementary channel (Sim III)

Pbli	(°C)
T_max	563.4
T_min	285.4
T_volume ave	382.8
T_outlet_average	315.6
T_outlet max	350.7
T_outlet min	285.4

Tab. 34 – PbLi temperature details (Sim III)

The maximum temperature in the Eurofer is 540.2 °C (Tab. 35) , that is a value similar to those found in previous simulations. This is because the flow rates of the coolant are similar in the arrays 4 and 5, which are the tubes closest to the structure having the highest temperature.

Temperature Eurofer (°C)	**Stiffening Plate**
T_max	540.2
T_min	286.5
T_ave	374.7

Tab. 35 – Eurofer steel temperature (Sim III)

5.3.2 Highlights from the analysis

- The simulation is set-up with the manifolds assumption upstream and downstream tubes.
- Analytical evaluation of flow rates in the presence of manifolds provides good approximation of calculated flow.
- Saturated conditions are reached in array 1 of BZ tubes.
- Maximum PbLi temperature is higher than T limit (550°C).
- Orifices are required to optimize the flow, thus improving the temperature field in the module.

5.4 Sim IV: results and analysis

The mass flow rates flowing in BZ tubes and in FW channels are calculated considering the deficit or surplus of enthalpy flow of simulation I compared to the target conditions.

$\Delta \dot{H}_j = \dot{m}_j^0 \Delta h_j = \dot{m}_j^0 \cdot \bar{c_p}(\Delta T_j) \cdot \Delta T_j$;

$\Delta T_j = T_j^0 - T_{target}$

$$\Delta\dot{m}_j = \frac{\Delta\dot{H}_j}{\bar{c_p}(\Delta T_{target})}$$

$$\dot{m}_j^I = \dot{m}_j^0 + \Delta\dot{m}_j$$

The resulting coolant flow rates in each tubes array computed with the previous methodology is reported in Tab. 36.

Furthermore, the total flow rate of FW is: $\dot{m}_{FW} = 0.780\ kg/s$

j	**m_BZ** (kg/s)
1	0.293
2	0.110
3	0.187
4	0.078
5	0.087
6	0.075
7	0.056
8	0.021
9	0.013

Tab. 36 – BZ coolant flow rates (Sim IV)

5.4.1 Analyses of results

The mass flow rates have enabled to homogenize the coolant outlet temperature in the different arrays of tubes and in the FW channels as shown in Tab. 37.

To ensure these flow rates it is necessary to orifice the BZ cooling loop to balance pressure differences present among the various arrays of tubes.

The different between the maximum pressure drop and the pressure drop calculated for each array is the additional pressure drop to insert in the tubes to achieve the calculated mass flow rates.

$$\Delta p_i^* = max|\Delta p_i| - \Delta p_i$$

$$\Delta p_i^* = k_i \frac{1}{2}\rho U_i^2$$

Array	**Temperature outlet** (°C)	**Pressure Drops** (Pa)	**Velocity** (m/s)
1	325.5	9889	2.04
2	325.0	5664	1.53
3	324.9	4056	1.30
4	324.7	2805	1.08
5	325.8	3338	1.21
6	325.1	2232	1.04
7	324.2	1177	0.78
8	323.2	570	0.58
9	320.4	47	0.18
FW	323.5	10873	2.02

Tab. 37 – Main results related to the coolant (Sim IV)

The maximum temperature of the PbLi is found out in the area between the first and the second tubes array nearest the FW. The maximum value calculated is 543.9 °C (Tab. 38) and it is lower compared to the Sim I. This is because the coolant flowing into the cooling tubes is at a lower temperature. The maximum PbLi outlet temperature is increased compared to the Sim I, reaching the value of 361.4 °C. On the contrary form the previous simulations, this value occurred in the fourth and fifth array of channels (as reported in Fig. 52). Moreover, the average PbLi outlet temperature increases reaching 332.4 °C and exceeds the target value. Instead the minimum PbLi outlet temperature remains 285.4 °C and it is in proximity of the coolant temperature at the inlet tubes.

Fig. 52 – PbLi outlet temperature in a poloidal – toroidal plane (Sim IV)

Considering these results, the solution is to set a larger coolant flow rate in the array 9, in order to reach the target temperature. The aim is to cool the PbLi down mainly in the zones near the exit from the module; this effect will be more effective in the central cells. The result will be a reduction of the temperature difference between the zones getting closer to the limit value of approximately 40 °C and bringing the average PbLi outlet temperature close to the design value.

PbLi	(°C)
T_max	543.9
T_min	285.4
T_volume ave	388.4
T_outlet_average	332.4
T_outlet max	361.4
T_outlet min	285.4

Tab. 38 – PbLi temperature details (Sim IV)

As regards the Eurofer temperatures, it is noted that the maximum computed temperature is always found out in the baffle plate and it reaches the value of 540.1 °C (Fig. 53). This temperature is increased compared to Sim I since the coolant flow rate is lower. Anyway, the temperature remains below the limit value. The maximum temperature of the Eurofer steel computed in FW zones is 432.9 °C (Tab. 39), because the flow rate of the FW channels is increased.

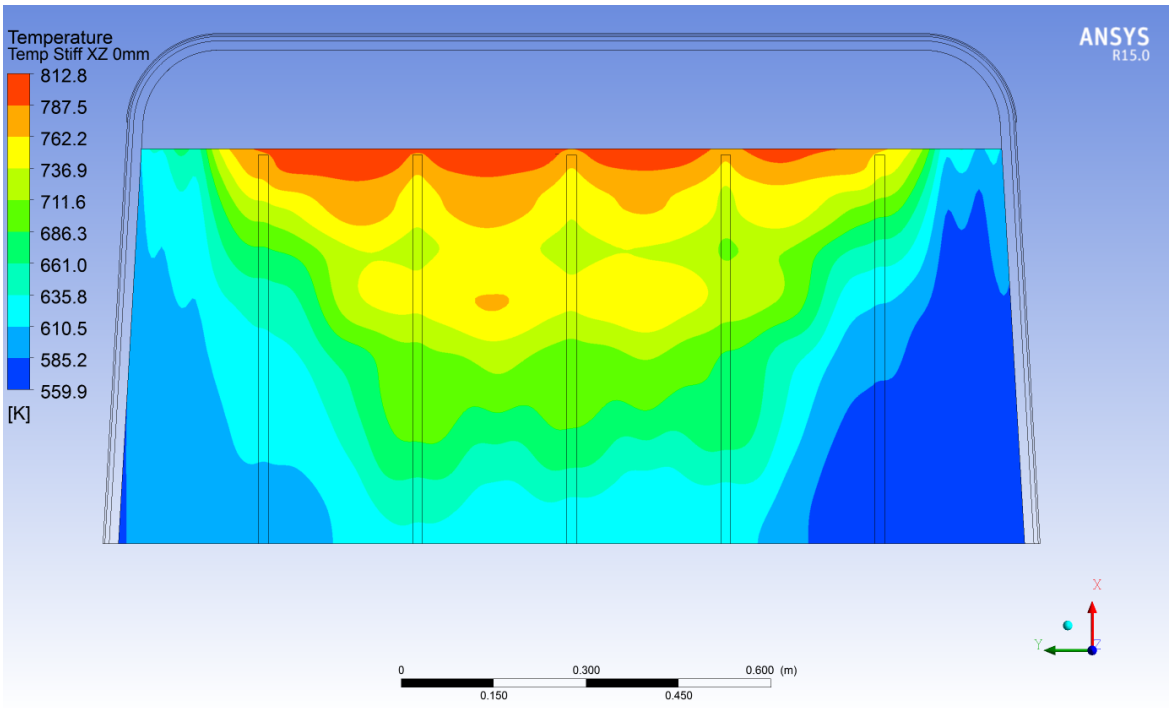

Fig. 53 – Temperature in the middle of the baffle plate (Sim IV)

The maximum stiffening plate temperature is 476.4 °C. This value is located between the cooling tubes array 7 and 8 (Fig. 54). The outcome is to that a reduction of the distance between these two arrays of tubes will improve the uniformity of temperature. However, the value is not a concern because below the limit.

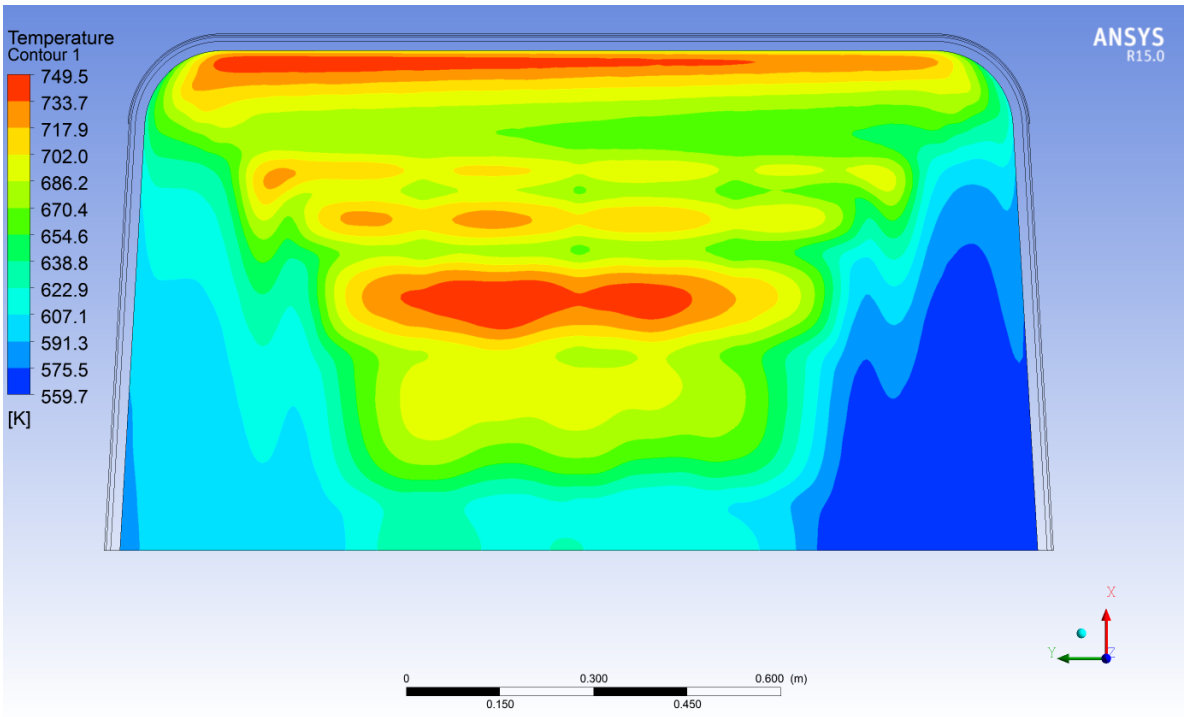

Fig. 54 – Temperature stiffening plate in radial – toroidal plane (Sim IV)

Eurofer temperature (°C)	**Plates**	**Tubes**	**FW zone**
T_max	540.1	385.5	432.9
T_min	286.5	285.2	285.5
T_ave	383.1	327.1	343.1

Tab. 39 – Eurofer steel temperature (Sim IV)

5.4.2 Highlights from the analysis

- Proper orifices are assumed to homogenize the coolant outlet temperature in the different arrays of tubes and in the FW channels.
- Maximum PbLi and steel temperature is calculated below the T limit (550°C).
- Maximum FW surface temperature is reduced.

5.5 Sim V: results and analysis

The aim of Sim V is to assess the limit value of heat flux on the FW surface acceptable for the Eurofer material: this limit is 550 °C.

A simplified analytical approach is carried out in order to assess the theoretical limit value and to get a first indication about the order of magnitude of this heat flux limit.

A one-dimensional multi-material approach is chosen in the radial direction taking into account the tungsten and the Eurofer steel (Fig. 55).

Within the domain, a constant power volumetric generation is considered, consistently with the estimated value used in the CFD simulation (see section 4.5 for details). The heat flux is set at the interface of the tungsten/ plasma and a wall temperature at the interface Eurofer/coolant is calculated.

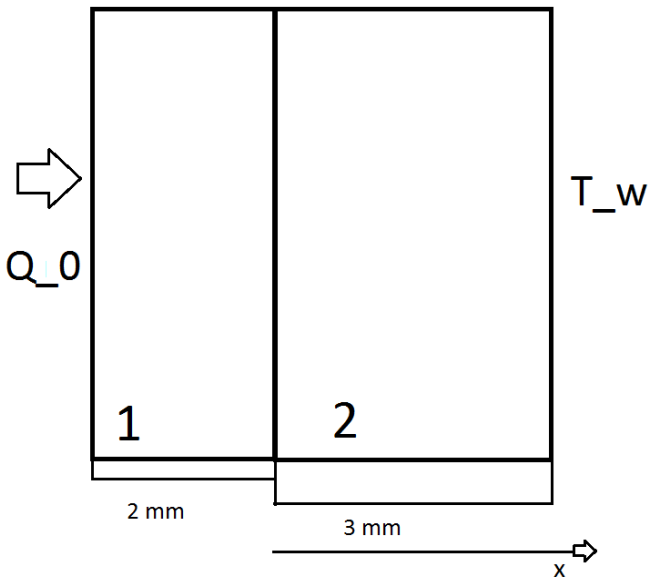

Fig. 55 – Simplified geometry for analytical discussion

$$\begin{cases} \dfrac{d^2T}{dx^2} = -\dfrac{g_0}{k}; \quad 0 < x < L_{steel} \\ -k\left.\dfrac{dT}{dx}\right|_{x=O} = \dot{Q}_I = g_0 L_{Tung} + \dot{Q}_0 \\ T|_{x=L_{eurofer}} = T_{wall} \end{cases}$$

Change of variable:

$$\theta(x) = T(x) - T_{wall}$$

$$\theta(x) = \frac{g_o}{2k}\left({L_{steel}}^2 - x^2\right) + \frac{\dot{Q}_I}{k}(L_{steel} - x)$$

Obviously:

$$Max\,[\theta(x)] = \theta(0) = \frac{g_o}{2k}{L_{steel}}^2 + \frac{\dot{Q}_I}{k}L_{steel}$$

$$T(0) = \frac{g_o}{k}\left(\frac{{L_{steel}}^2}{2} + L_{steel}L_{tung}\right) + \frac{\dot{Q}_0}{k}L_{steel} + T_{wall}$$

The limit value of $\dot{Q}_0$ is calculated as:

$$\dot{Q}_0{}^* = \left(T_{limit} - T_{wall} - \frac{g_o}{k}\left(\frac{L_{steel}{}^2}{2} + L_{steel}L_{tung}\right)\right)\frac{k}{L_{steel}}$$

$$T(0) = T_{limit} = 550°C$$
$$T_{wall} = 325\ °C$$
$$g_o = 1 \cdot 10^{-7}\frac{W}{m^3}$$
$$k = 30\frac{W}{m \cdot K}$$
$$L_{steel} = 3 \cdot 10^{-3}m$$
$$L_{tung} = 2 \cdot 10^{-3}m$$
$$\dot{Q}_0{}^* = 2.22\ MW/m^2$$

$\dot{Q}_0{}^*$ is obtained in ideal conditions of heat transfer (infinity convective heat transfer between the coolant and the wall), and without taking into account the space among the tubes in the structure. This limit calculated with realistic geometry and best estimate models will be lower.

Starting from the value obtained by the simplified analytical discussion, sensitivity analyses have been conducted to identify the heat flux limit.

Afterwards, the case with a nominal heat flux of 1.5 MW/m^2 on the FW surface and with a volumetric generation described in section 4.5 is considered.

The mass flow rates required to refrigerate the slice of the module must be re-calculated through an energy balance:

$$\dot{H}_{tot} = \dot{G}_{BZ} + \dot{G}_{FW} + \dot{Q}_{FW}$$
$$\dot{G}_{BZ} = \int_{V_{BZ}} g_0 \cdot dV \cong 258000\ W$$
$$\dot{G}_{FW} = \int_{V_{FW}} g_0 \cdot dV \cong 34000\ W$$
$$\dot{Q}_{FW} = \int_{S_{FW}} q'' \cdot dS \cong 318000\ W$$
$$\dot{m}_{coolant} = \frac{\dot{H}_{tot}}{\Delta h_{coolant}} = 2.71\ kg/s$$

The global coolant mass flow rate has been calculated (2.71 kg/s) and subsequently the FW channels flow rate have been calculated considering BZ flow rate as in Sim III.

$$\dot{m}_{BZ} = \sum_i \dot{m}_{BZ,i} = 0.92 \ kg/s$$

$$\dot{m}_{FW} = \dot{m}_{coolant} - \dot{m}_{BZ} = 1.79 \ kg/s$$

5.5.1 Analyses of results

The maximum temperature in Eurofer steel is found in the FW zone at the interface between Eurofer and tungsten (Fig. 56). The calculated value is 559 °C and exceeds the limit value of 550 °C. This results in a heat flux equal to 1.5 MW/m^2 on the FW surface that is excessive and is not tolerable from thermal point of view.

However, the limit value of heat flux will not differ a lot from the set value since the Eurofer temperature limit has been exceeded by only 9 °C.

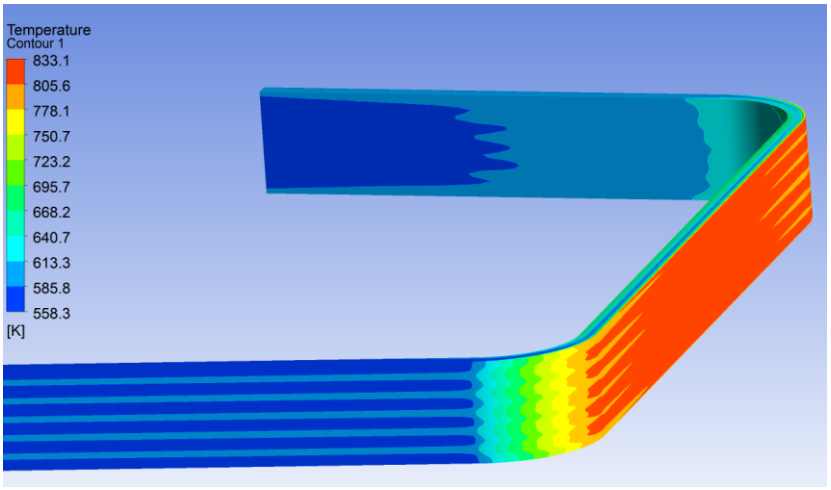

Fig. 56 – FW zone temperature (Sim V)

Temperature (°C)	**Stiffening**	**FW Zone**	**Tungsten**
T max	540.0	559.0	581.9

Tab. 40 – Solid domain temperature (Sim V)

The Eurofer steel temperature trend in proximity of FW surface is shown in Fig. 57, which represents a radial-poloidal cross section in the symmetry plane. In this plane the coolant flow path from inlet in the channel is equal and, therefore, a periodic temperature shape is observed in the different channels having the same pitch of the square tubes.

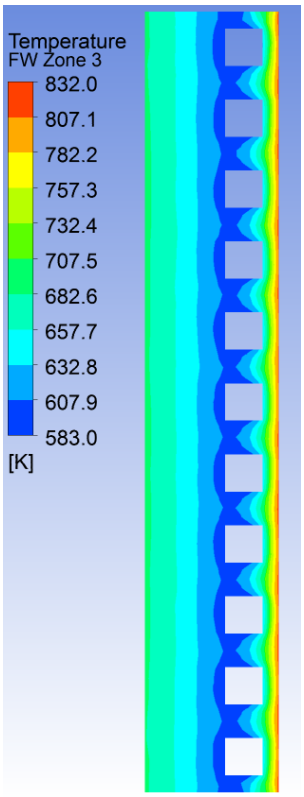

Fig. 57 – Poloidal – radial section of the FW zone (Sim V)

The coolant at the exit sections of the FW channels has a temperature of about 323 °C, which is satisfactory but slightly below the target (325 °C). The average velocity in the channels is 4.64 m/ s (postulated limit is 7m/s), which implies that modifications in mass flow rate are possible, if needed. The pressure drops calculated in the square channel path is 48.46 kPa (Tab. 41).

Coolant FW	
T_ave outlet (°C)	323.1
Velocity (m/s)	4.64
Pressure Drop (Pa)	48460

Tab. 41 – FW zone coolant details (Sim V)

5.5.2 Highlights from the analysis

- The maximum heat load capacity of the First Wall surface with respect to the Eurofer temperature limit is about 1.5 MW/m^2.
- Larger values are possible decreasing the thickness from cooling tubes and FW boundary.

5.6 Sim VI: results and analysis

Fluid dynamic analysis is conducted accounting for the PbLi domain standalone model in order to study the design of the breeder path exiting from the blanket module. Original design postulates only two parallel exit, located in the upper part of the central square breeder channels. This implies PbLi flowing in the four peripheral channels shall cross the stiffening plates for being routed outside. Fig. 58 shows the connection between the upper return channels, crossing the vertical stiffening plates.

The simulation is carried out with an isothermal temperature of 325 °C, hence in absence of thermal loads described above. PbLi inlet flow rate is set according the conceptual design specifications (i.e. 0.146 kg/s).

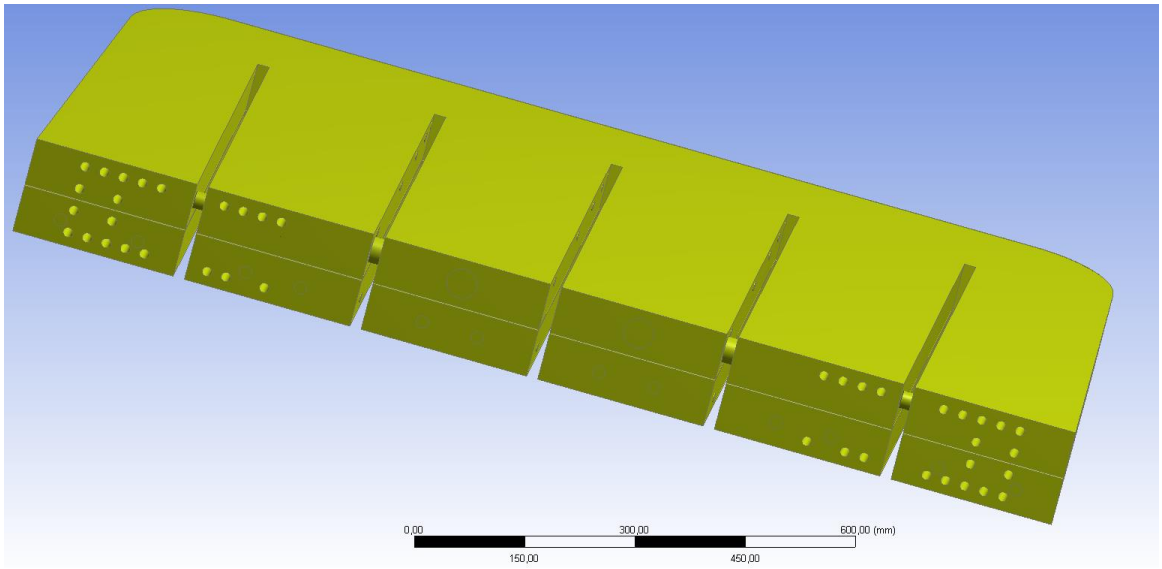

Fig. 58 – PbLi domain (Sim VI)

The radial-poloidal stiffening plates have been drilled to allow the fluid exiting from the middle part (Fig. 59 and Fig. 60) and the sections are sized by setting a velocity of 5 mm/s.

$$A = \frac{\dot{m}}{\rho \cdot U_{limit}} \quad ; \quad r = \sqrt{\frac{A}{\pi}}$$

$$U_{limit} = 5\,mm/s\,;\ \rho = 9600\ \ kg/s$$

Assuming that the flow rate of one channel passes through the plate hole it is evaluated that:

$$\dot{m}_I = \frac{1}{6}\dot{m}_{PbLi};\ \dot{m}_{II} = \frac{1}{3}\dot{m}_{PbLi}$$

$$r_I = 12\ mm; r_{II} = 18\ mm$$

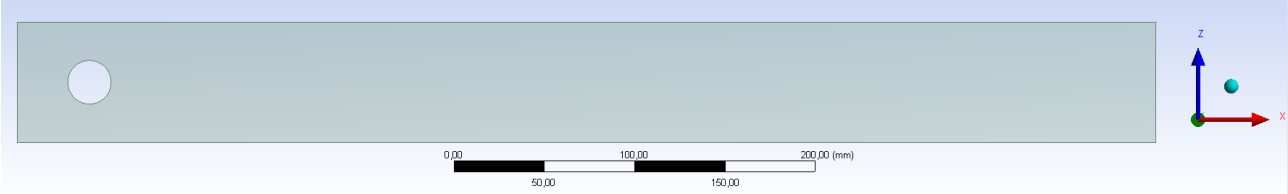

Fig. 59 – Hole 1 in the stiffening plate

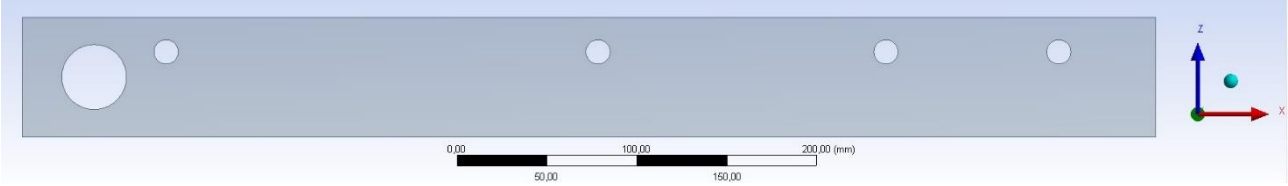

Fig. 60 – Hole 2 in the stiffening plate

Similarly, for the PbLi output from the module, two circular sections are sized: one for each of the two central channels (Fig. 61):

$$r_{out} = 21\ mm$$

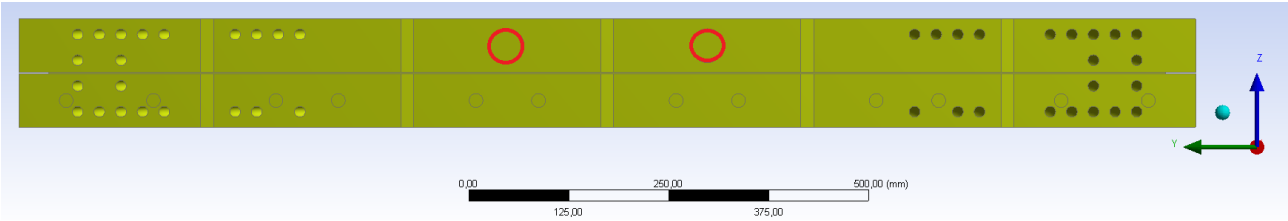

Fig. 61 – PbLi outlet (Sim VI)

A structural analysis will be conducted to verify that the module in the new configuration, with a part of the structural material removed, would be able to safely withstand the thermo-mechanical loads in normal operation and over pressurization scenarios.

5.6.1 Analyses of results

The PbLi flow rates passing through the holes are respectively 0.0009 kg/s and 0.0085 kg/s. The calculated values are lower than the postulated values of 0.0243 kg/s and 0.0486 kg/s, where PbLi flow rate feeding the side channels passes through the toroidal holes, in the upper part of the module, reaching the central channels and, then, the exit.

According with the simulation, this does not occur because cross flow from peripheral towards the central channels (i.e. toroidal direction) is observed before, in proximity of the FW. Fig. 62 highlights the stream in the toroidal direction calculated by CFX.

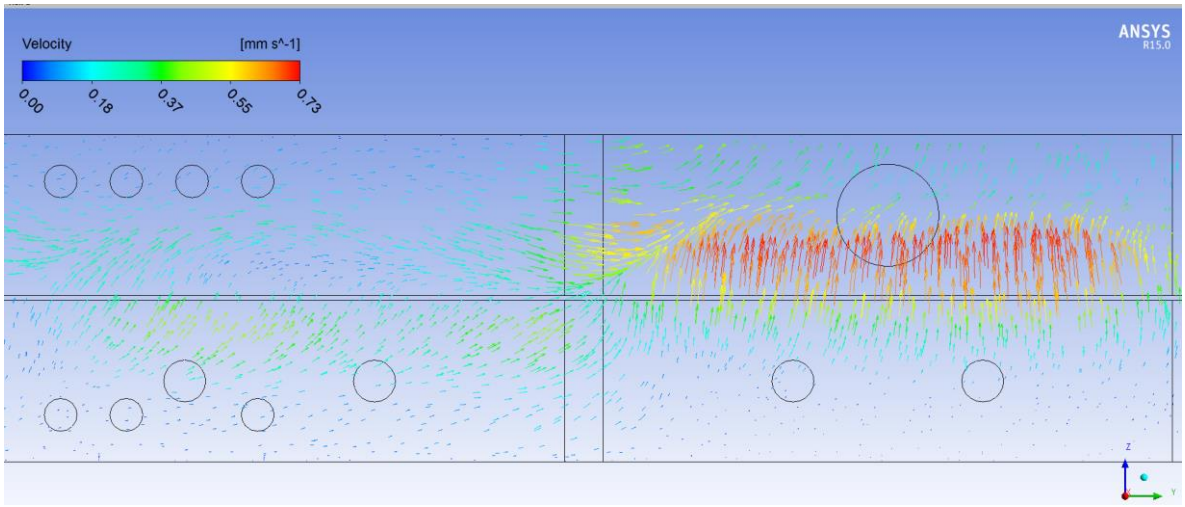

Fig. 62 – Velocity vector in poloidal-toroidal plane (680 mm) (Sim VI)

Fig. 63 and Fig. 64 show the crossing velocity of the holes, resulting lower than in the design.

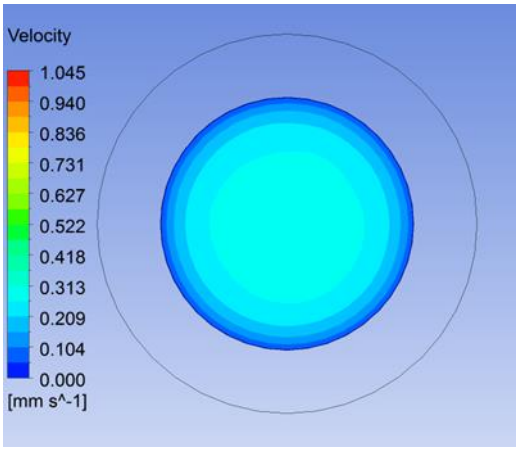

Fig. 63 – Velocity in hole 1 (Sim VI)

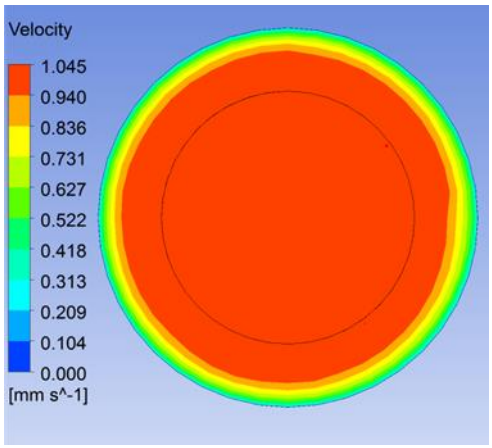

Fig. 64 – Velocity in hole 2 (Sim VI)

The flow rates calculated in the upper return channels are very different as can be seen in Fig. 65. The flow rates are considerably non-homogeneous, in fact, by calculating the ratio between the flow channel and the nominal one the following percentages are obtained: 3.7, 31.2, and 265.1%, respectively for the channels from the outside inwards, where this faction is evaluated as

$$\frac{\dot{m}_{channel}}{\dot{m}_{nomin}}$$

The ratio between the maximum and minimum flow rate is 70; this non-uniformity of flow is excessive and not sustainable. It implies that design modifications or countermeasures are required.

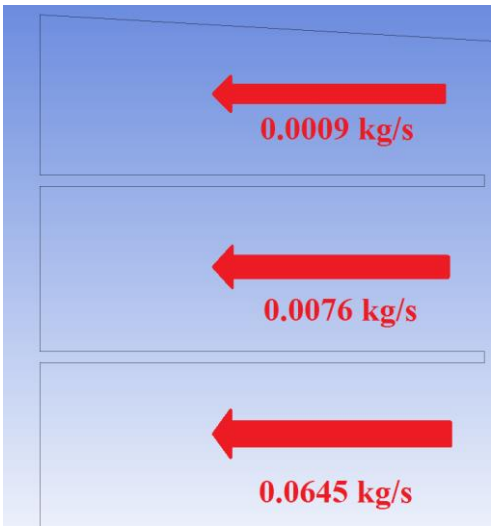

Fig. 65 – Pbli mass flow in the outlet channels (Sim VI)

The radial component of PbLi velocity over the output channels are represented at different poloidal-toroidal planes (600, 400 and 200 mm from the exit) in Fig. 66.

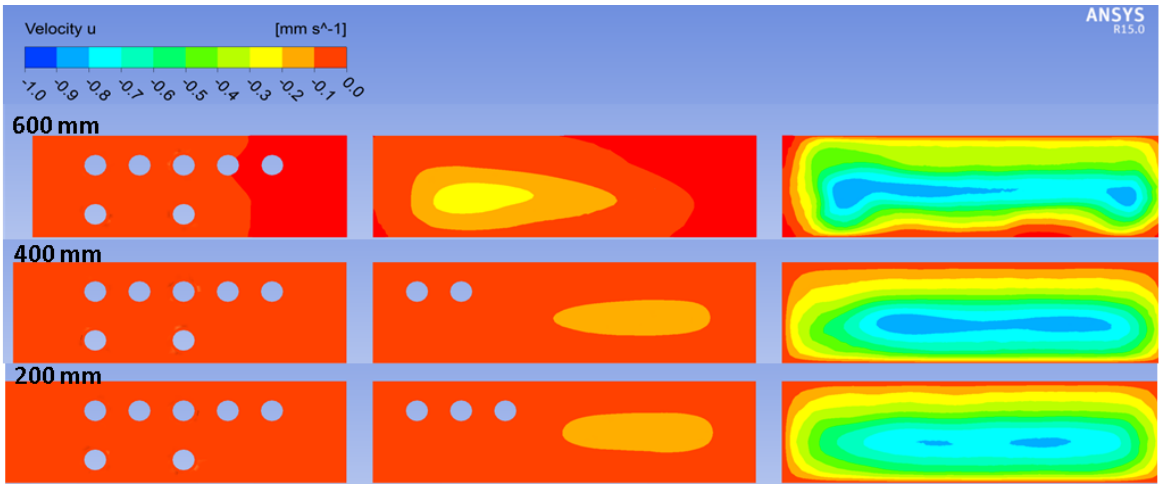

Fig. 66 – PbLi radial velocity in poloidal-toroidal planes (Sim VI)

It is evident the relevant velocity differences between the side channels and the center channel. The fluid in the side channels is almost stagnant, so the residence time of the PbLi will be larger than the design value. This may involve an accumulation of tritium in the breeding blanket overpassing the threshold limit. Besides current limits are defined for the PbLi system, it should be noted that a specific limit will be defined for the safety analyses: this limit will be connected, with the postulated frequency of breeding blanket failure and the retention capability of the containment building, according with the ALARA approach. Therefore, this reference solution must be carefully reviewed.

The possible solutions to reduce the over mentioned problems are

1) to increase the flow areas of the connections between peripheral channels and central one and to decrease the cross section flow areas in the zone closer to FW;

2) to review the design of the PbLi manifold, allowing the fluid exiting from each toroidal channel, symmetrically.

5.6.2 Highlights from the analysis

- PbLi exit path from the central channels breeder module shall be reviewed.
- Two possible solutions are identified:
    1. increasing the breeder square channels toroidal connections;
    2. proposing an alternative solution where the exit is possible in more/all channels.

5.7 Sim VII: results and analysis

22 tubes are adopted and arranged in a radial-toroidal-radial direction in a configuration symmetrical to the baffle plate and to the poloidal-radial plane at half height of the module. The adopted solution is more compact: in fact, only 6 arrays of tubes are considered instead of previous nine (Fig. 67) With this configuration, the inlet and the outlet of the coolant from the back plate of the WCLL module is placed only through the PbLi side square channels. This solution improves the water manifolds geometry and optimize the space of the manifolds in the back space of the module. Indeed, the water manifolds have reduced the overall toroidal dimensions. Moreover, the PbLi has the option to leave the module through the central and semi-lateral channels, and only the PbLi outer channels are routed through the stiffening plates. One solution may be to introduce a tube which bypasses the coolant collector (for this purpose the space between the coolant tubes has been left).

The geometry of the FW zone is not changed.

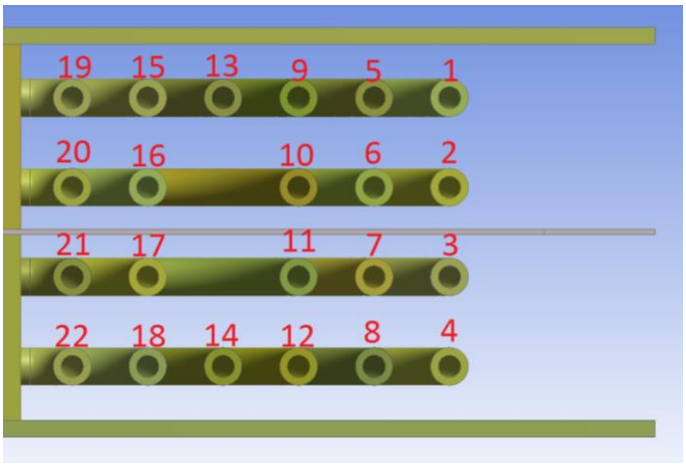

Fig. 67 – New tubes arrangement in poloidal- toroidal section

Another significant change is the radial length of the baffle plate, which is increased from 640 mm to 680 mm to enhance the fluid flow near the interface PbLi/FW zone. In order to avoid the increase of the volumetric heat generation within the solid structure, tubes 10 and 11 are placed for the baffle plate cooling (see Fig. 68).

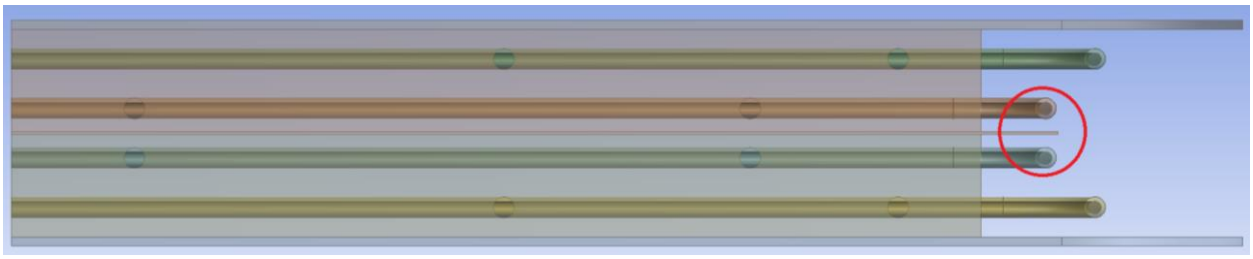

Fig. 68 – Baffle plate detail with coolant tubes

Two tubes are added close the FW since the maximum of the PbLi temperature is foreseen in this area (Fig. 69). This solution will also result in a lower heat flux for the tubes from the breeder zone, closer to the FW (1, 2, 3, 4). This is an important advantage because a lower flow rate than in the reference design will be required to achieve the outlet design temperature of coolant outlet. This implies that reduced differences of areas in the orifices at the inlet of the tubes.

The cooling tubes layout is reported in Fig. 70.

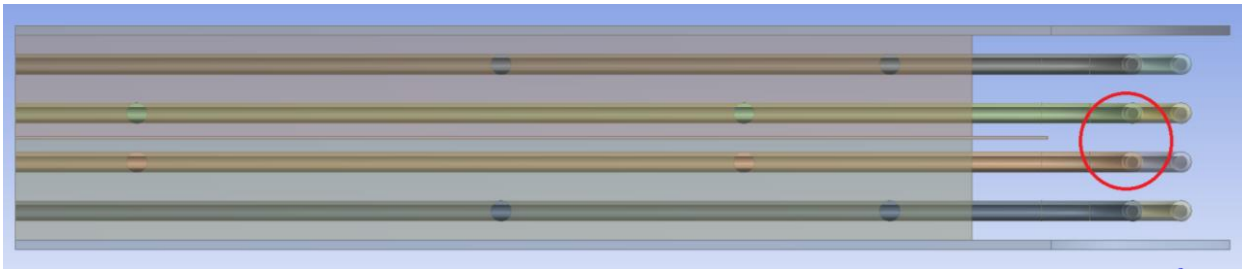

Fig. 69 – Tubes details close to FW

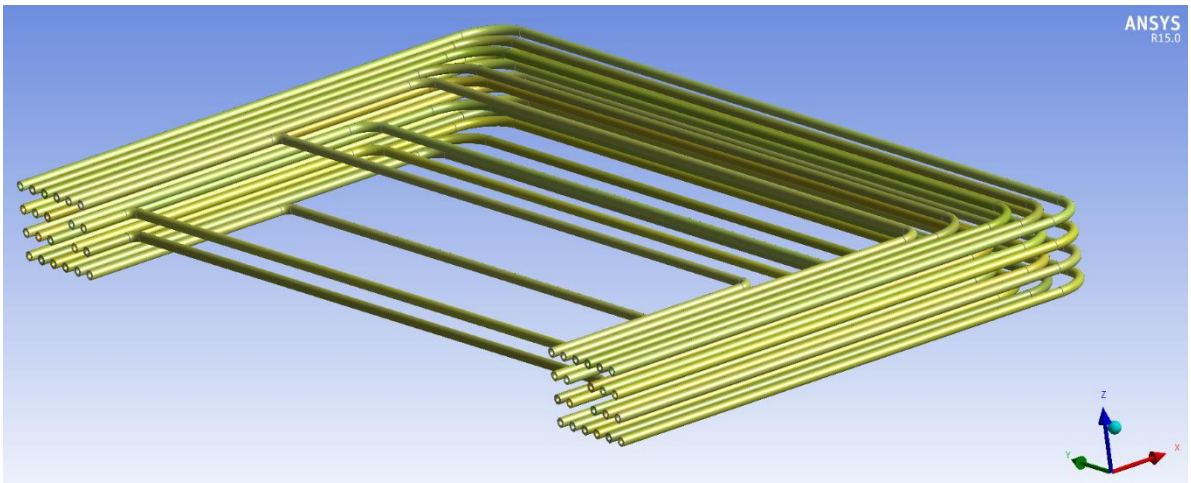

Fig. 70 – Improved tubes arrangement

The flow rates flowing in the BZ tubes are estimated analytically using the same methodology described in 5.3.The lengths of tubes used in the calculation are given in Tab. 42

Tubes	Length (m)
1-2-3-4	2.859
5-6-7-8	2.741
9-12	2.623
10-11	2.559
13-14	2.441
15-18	2.259
16-17	2.067
19-22	1.693
20-21	1.213

Tab. 42 – Improved layout tubes lengths

$$\sum_{i=1}^{22} \dot{m}_i = \dot{m}_{tot} = 0.920 \ kg/s$$

The coolant flow rates in the breeding zone are reported in Tab. 43.

Tubes	m_BZ (kg/s)
1 2 3 4	0.037
5 6 7 8	0.038
9 12	0.039
10 11	0.039
13 14	0.040
15 18	0.042
16 17	0.044
19 22	0.049
20 21	0.059

Tab. 43 – Breeding zone coolant flow rates (Sim VII)

5.7.1 Analyses of results

According with the coolant flow rates imposed in the simulation (see Tab. 43), the pressure drops between input and output sections in the arrays of tubes are between 2.845 kPa and 3.021 kPa. This range is quite satisfactory; therefore, the flow rates evaluated analytically provide a good approximation of the operating condition in presence of a manifold (Tab. 44).

The average velocities of the coolant in the different arrays of the BZ are from 1.02 to 1.64 m/s, whereas, the average coolant velocity flowing in the FW channels is 2.02 m/s. These values are acceptable and well below the maximum allowable value of 7 m/s.

Compared to previous Sim III, the maximum velocity is reduced (see for comparison Tab. 33) and also averaged values between the different tube arrays are decreased. The most significant change regards the arrays 8 and 9, because the length of these tubes is changed significantly. Hence, this improved layout of the cooling tubes provides a homogeneous flow distribution.

Moreover, the temperature reached by the coolant in the closest arrays to the FW have been significantly reduced: for the first array it is decreased from 351 to 344.9 °C, while for the second array it has changed from 339.4 to 335.2 °C. This is due to the introduction of two new tubes in this area.

Although the distribution of the coolant temperature of the BZ is improved, high values of coolant temperature are reached. Also for this configuration orifices are required to reduce flow rates distortions and to route the needed flow rate where it needed, thus improving the temperature field in the module. Moreover, considering the modifications discussed above, it expected a reduction of pressure drops.

The FW coolant reaches an output temperature of about 324 °C (Tab. 44). This value is similar to previous simulations since the configuration of the FW zone is not changed and the same thermal loads are set.

Array	**Tubes**	**Temperature outlet** (°C)	**Pressure Drop** (Pa)	**Velocity** (m/s)
1	1 2 3 4	344.9	3021	1.02
2	5 6 7 8	335.2	2941	1.04
3	9 12	333.8	2943	1.07
4	10 11	332.0	2924	1.08
5	13 14	328.5	2893	1.11
6	15 18	322.2	2943	1.17
7	16 17	312.6	2845	1.22
8	19 22	301.0	2904	1.36
9	20 21	290.1	2899	1.64
FW		324.1	10897	2.02

Tab. 44 – Coolant results (Sim VII)

The maximum PbLi temperature computed in the simulation is 523.1 °C (Tab. 41). This value is lower than the limit temperature of RAMF material (i.e. 550 °C) and then the

value calculated in Sim III (i.e. 563.4 °C). A reduction of about 40 ° C is due to the layout of the tubes.

The PbLi peak temperature is calculated between the first array of tubes and the FW zone, also hot zones are found between the fifth and sixth array of tubes near the baffle plate (Fig. 71).

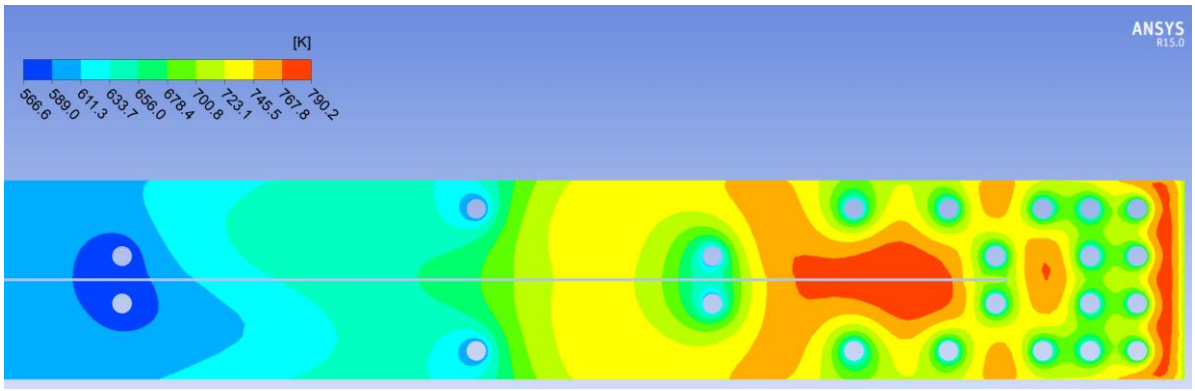

Fig. 71 – Poloidal-radial section centred in the fourth channel (central channel) (Sim VII)

PbLi	**Temperature** (°C)
T_max	523.1
T_min	285.3
T_volume average	384.1
T_outlet average	318.9
T_outlet max	343.9
T_outlet min	285.3

Tab. 45 – PbLi temperature details (Sim VII)

The temperature of the PbLi ranges from 285.3 to 523.1 °C, as can be seen in Fig. 71, Fig. 72, Fig. 73, Fig. 74 and Fig. 75.

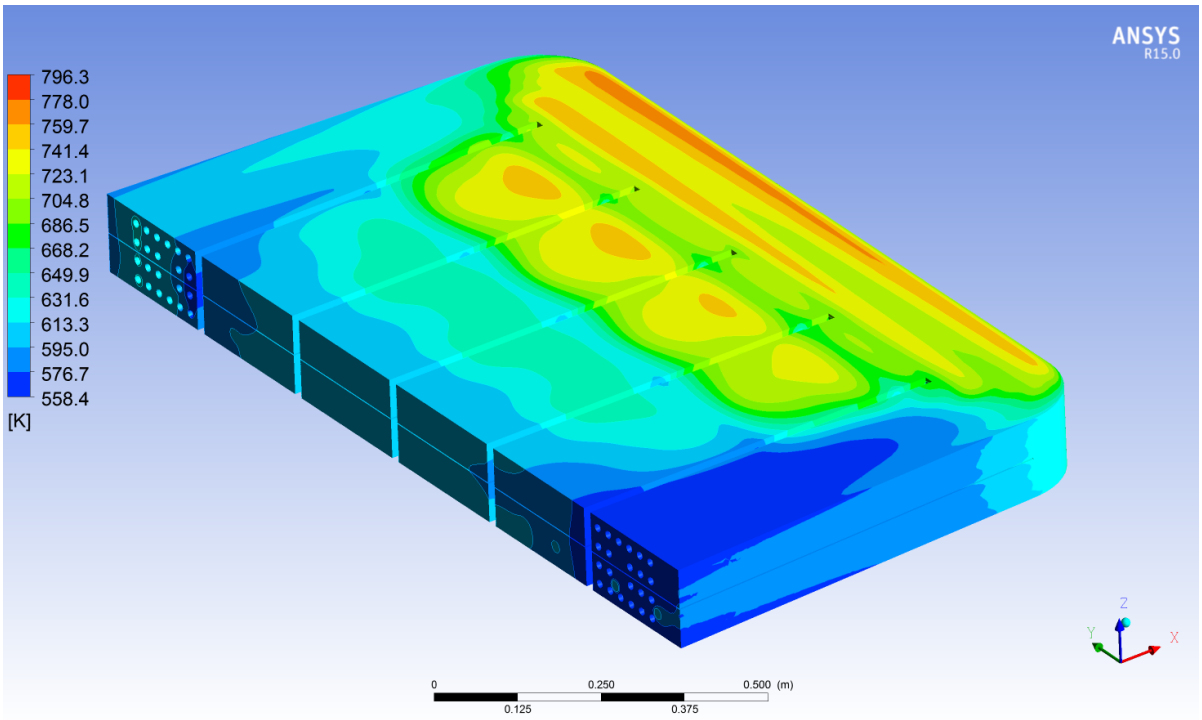

Fig. 72 – PbLi temperature in 3D domain (Sim VII)

Significant temperature gradients are observed in different directions:

- radial, due to the radial distribution of the volumetric density of nuclear deposited heat power imposed to the model;
- toroidal, due to the co-current cooling loop system;
- poloidal, due to cooling tubes arrangement (Fig. 73, Fig. 74, Fig. 75).

The effect of radial distribution of heat power is shown in Fig. 71.The effect of the cooling loop system produces a cooler area, as showed in Fig. 72, where the coolant inlet pipes are placed.

The effect of the tubes arrangement is highlighted in Fig. 73, which shows the higher temperatures in the central part because the tubes (array eight) occupy the upper part of the channel. The same effect can be seen in Fig. 75 and is linked to the effect of the array 6. On the contrary, Fig. 74 evidences hottest areas are in the upper part because the tubes (array seven) occupy the lower part of the channel.

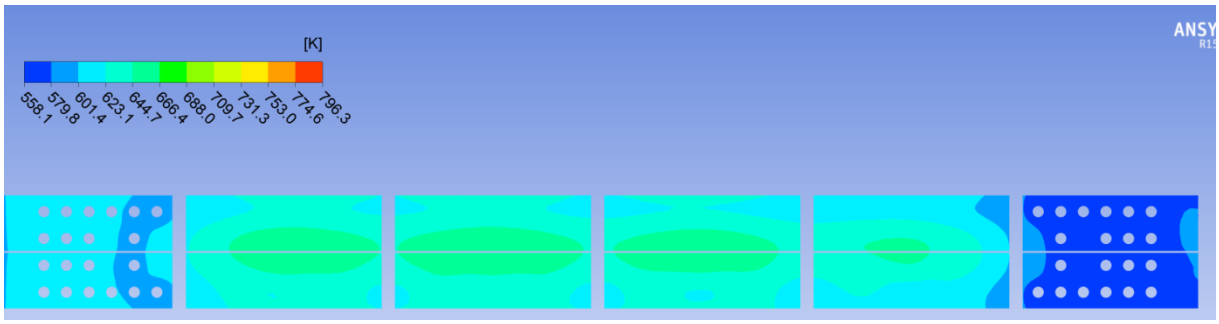

Fig. 73 – PbLi temperature in a poloidal-toroidal plane (300 mm from PbLi inlet, Sim VII)

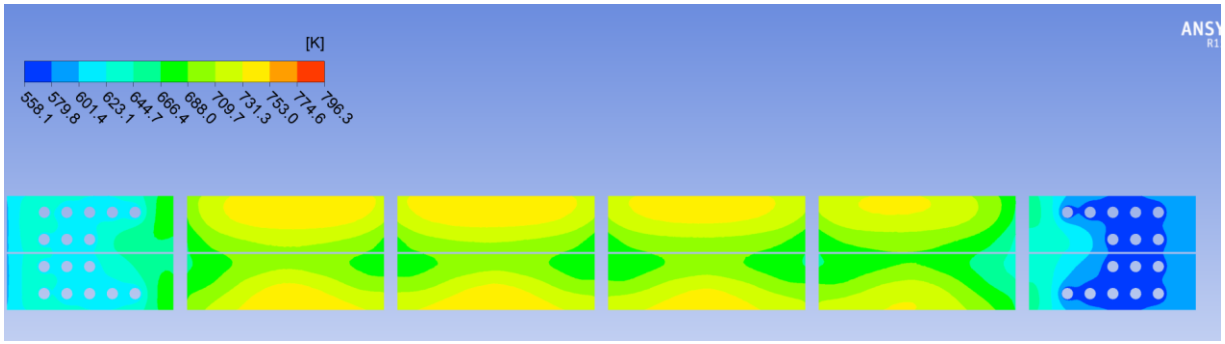

Fig. 74 – PbLi temperature in a poloidal-toroidal plane (500 mm from PbLi inlet, Sim VII)

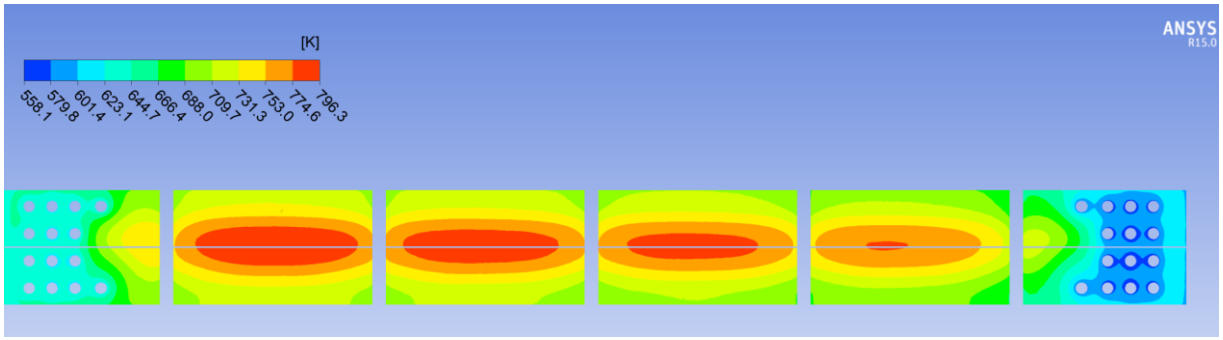

Fig. 75 – PbLi temperature in a poloidal-toroidal plane (600 mm from PbLi inlet, Sim VII)

The maximum PbLi outlet temperature is decreased to a value of 343.9 °C (Tab. 45) compared to the third simulation (350.7 °C in Tab. 34). Moreover, the average PbLi outlet temperature increases reaching 318.9 °C and get closer to the target value. Hence, this improved configuration implies an enhanced PbLi output temperature distribution (see Fig. 76).

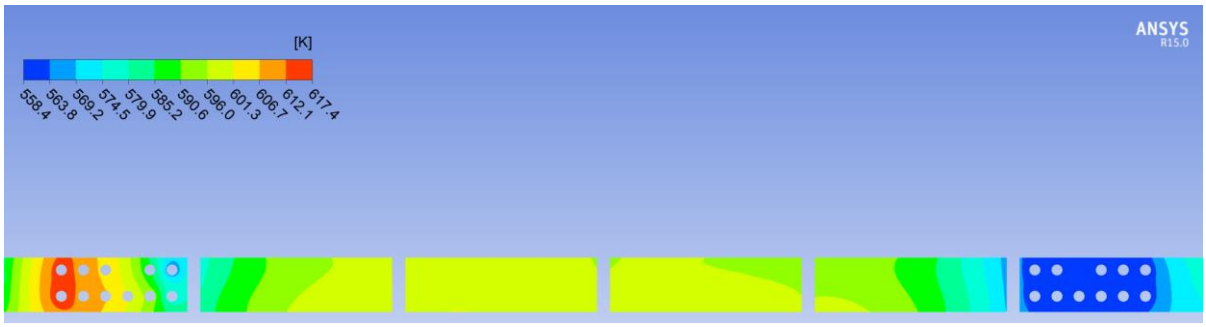

Fig. 76 – PbLi outlet temperature in a poloidal – toroidal plane (Sim VII)

The maximum temperature of the plates is reduced of about 20 degrees, from 540.2 (Tab. 46) to 522.9 °C (Tab. 35). The peak temperature has shifted from the edge of the baffle plate to an internal zone. This is linked to the new position of the cooling tubes belonging to array 4 (Fig. 77 and Fig. 78). An hot spot temperature of about 500 °C is calculated in the upper side of the poloidal-radial plate, in the zone close to the FW (Fig. 79 and Fig. 80).

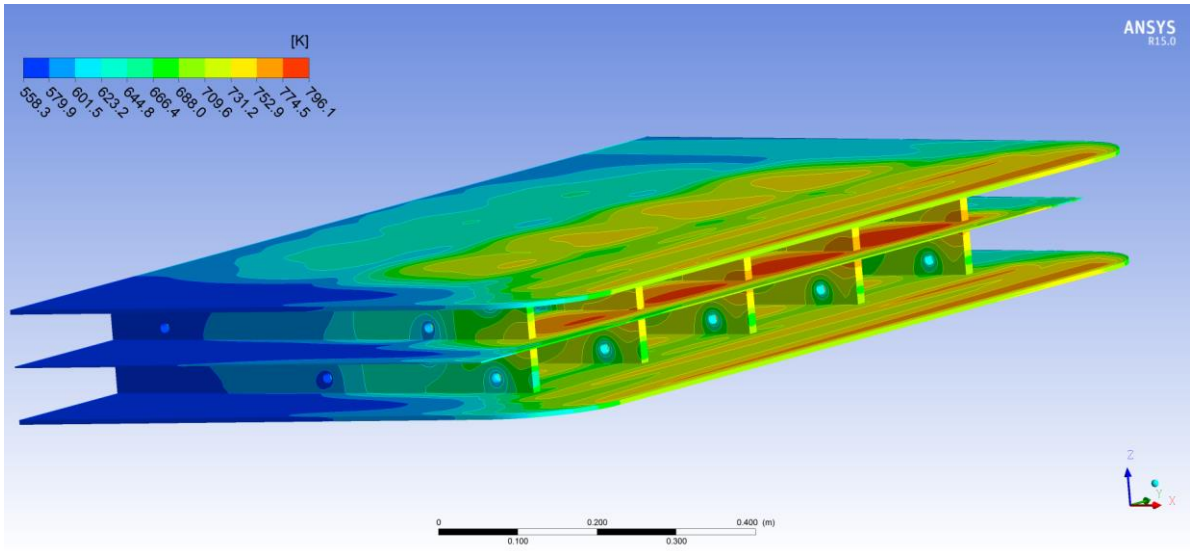

Fig. 77 – Eurofer temperature in stiffening plates and baffle plate (Sim VII)

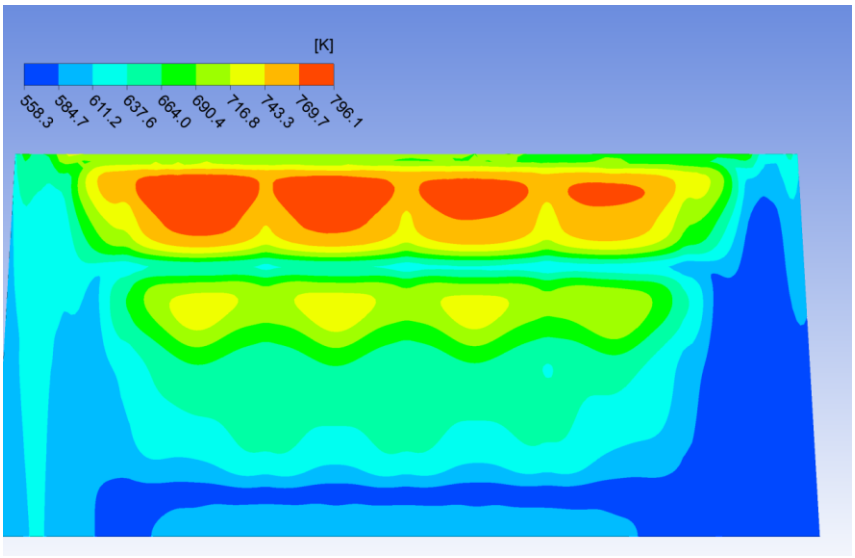

Fig. 78 – Temperature in the baffle plate (Sim VII)

The average temperature in the structures is increased from 374.7 °C (Tab. 35) to 380.4 °C (Tab. 46), because the cooling tubes of the arrays 3 and 6 are moved towards the baffle plate.

This change is the reason why the average temperature increases. Indeed, the toroidal-radial plates have higher temperatures, on the contrary a reduction is observed in the baffle plate, which has lower thickness.

Eurofer temperature (°C)	**Stiffening Plates**
T_max	522.9
T_min	285.9
T_ave	380.4

Tab. 46 – Eurofer steel temperature (Sim VII)

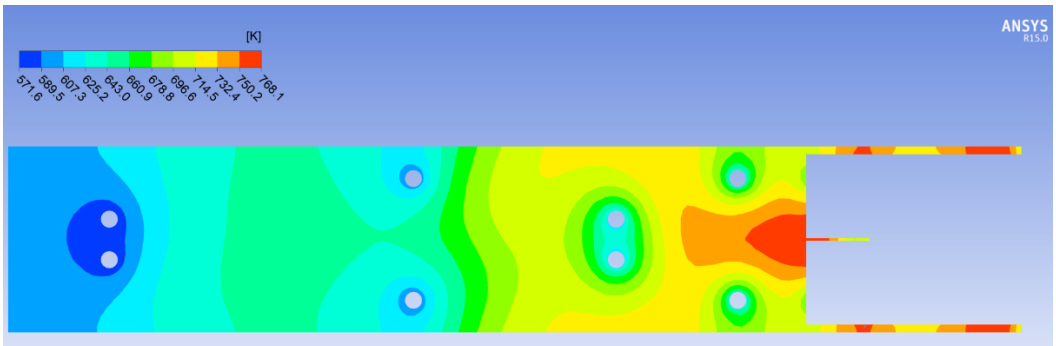

Fig. 79 – Eurofer temperature in stiffening plate in poloidal – radial plate (between the fourth and fifth channel, Sim VII)

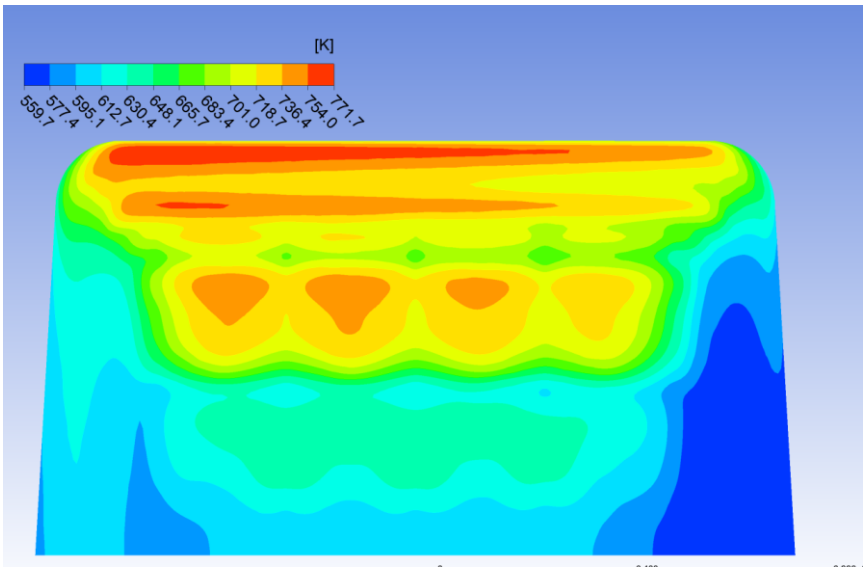

Fig. 80 – Temperature stiffening plate (radial – toroidal, Sim VII)

The tubes arrangement influences PbLi flow field inside the module, in fact zones with higher velocity are found where more tubes are present (see Fig. 81 and Fig. 82).

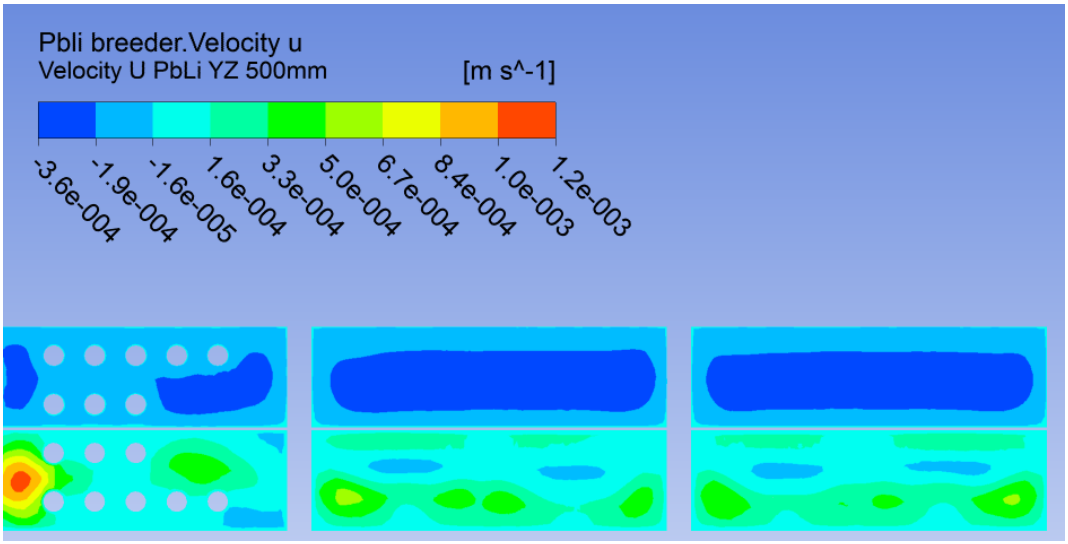

Fig. 81 – PbLi radial velocity in a poloidal-toroidal plane (500 mm from PbLi inlet, Sim VII)

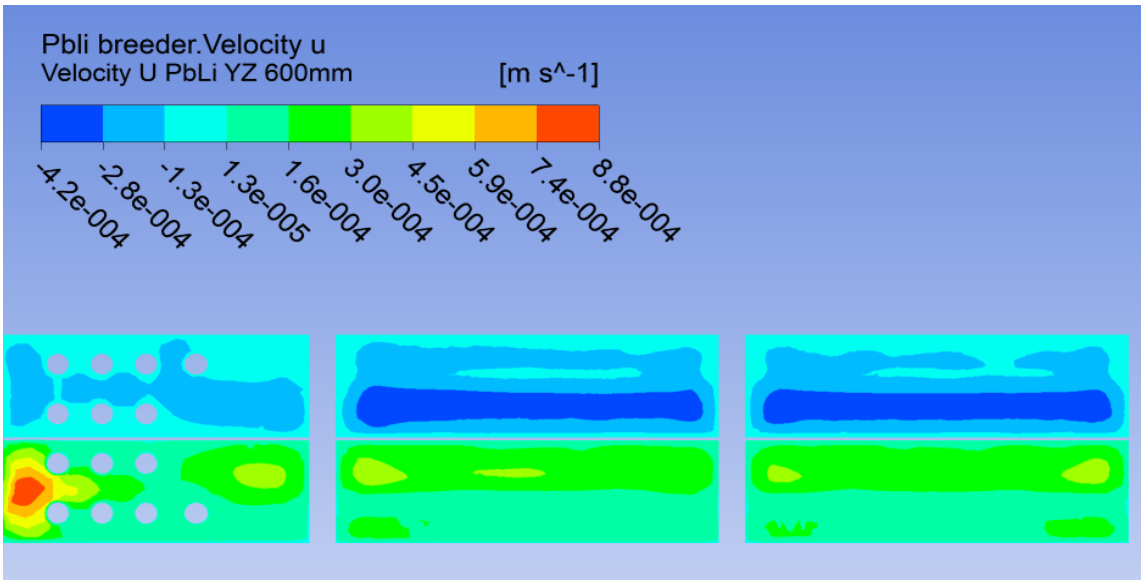

Fig. 82 – PbLi radial velocity in a poloidal-toroidal plane (600 mm from PbLi inlet, Sim VII)

In comparison with the first simulation (Sim I), the repositioning of the baffle plate has allowed a better PbLi flow distribution close to FW reducing stagnant zones (Fig. 83). However, the simulation evidences zones where "quasi stagnant" conditions are achieved (Fig. 84). It must be stressed that being the buoyancy forces not active, the real velocity field may be different, thanks the poloidal temperature differences.

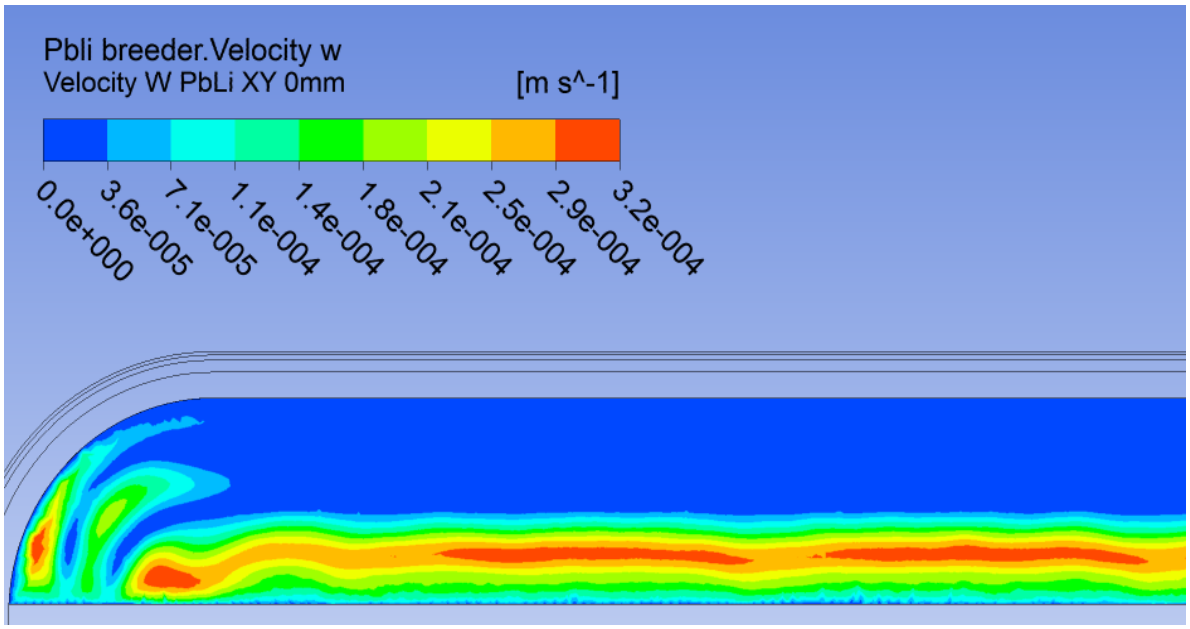

Fig. 83 – PbLi poloidal velocity in radial-toroidal middle plane (Sim VII)

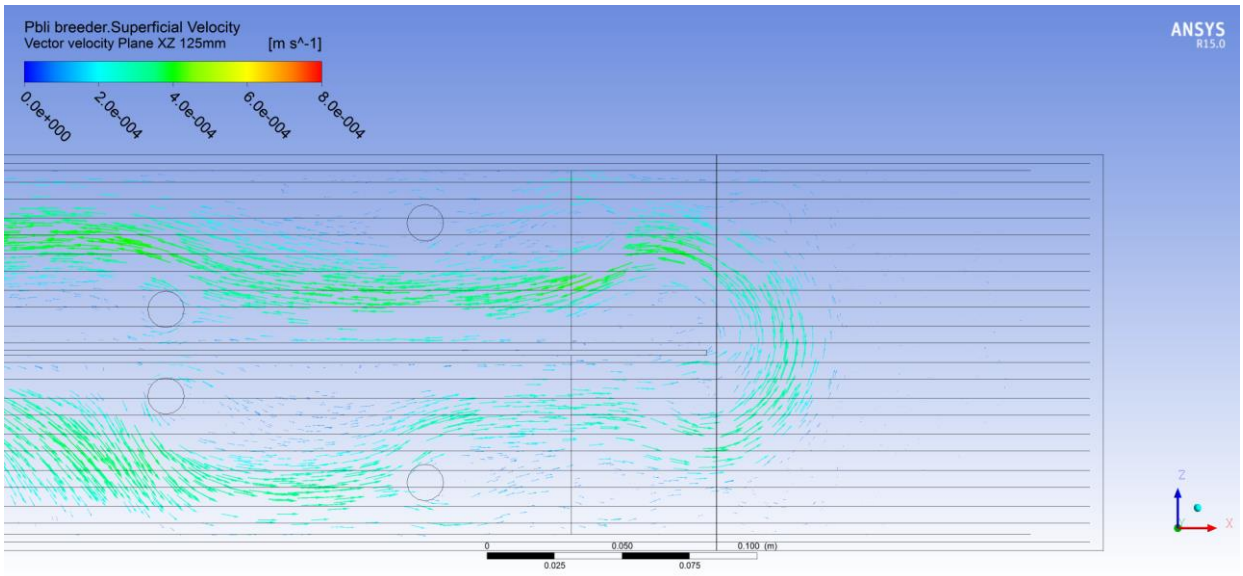

Fig. 84 – PbLi velocity in radial-poloidal plane (Sim VII)

5.7.2 Highlights from the analysis

- Layout of tubes in BZ is improved with respect the original design.
- Improved layout of cooling tubes provides a more homogeneous distribution of flows in BZ tubes with the manifold approach.
- Maximum coolant temperature is significantly reduced and the outlet coolant temperatures are more homogeneous in the various arrays of tubes.
- Orifices are still required to improve the temperature field in the module.
- Maximum PbLi and steel temperature are significantly reduced
- The increased radial length of the baffle plate has reduced PbLi "quasi" stagnant zones close to FW.

6 CONCLUSIONS

The objective of the activity was the thermo-hydraulic assessment of the WCLL breeding blanket. The analyses were conducted to assess the water cooling pipes layout; the PbLi inlet and outlet orifices; the PbLi temperature and flow pattern; and the water coolant temperature and pipes pressure drops.

Computational thermal and fluid-dynamic models by ANSYS CFX (ver. 15.0) were developed and run. The three dimensional mesh models a toroidal-radial slice of the central outer segment equatorial module. It includes six breeder cells in the toroidal direction. Solid structures (EUROFER97 and tungsten) and fluid domains (PbLi and coolant) are considered. Seven analyses are presented changing the water coolant inlet conditions, the first wall heat load and the tubes and baffle plate layout, in order to optimize the thermal field in the module.

The results have demonstrated that the first version of the WCLL breeding blanket design, based on DEMO-2015 data and having horizontal tubes layout, has promising thermal-hydraulic features. Structural material temperature field shows values below the limit and a margin of 30°C is calculated, if the hot spot is considered. The analyses have also pointed out areas for improvements. Margin exists to enhance the design further, optimizing the layout and the coolant mass flow rate distribution of the tubes, as well as the manifolds.

Regarding the water cooling system, breeding zone and first wall, the following conclusions apply.

- The CFD calculations have showed the limits of the analytical evaluation of the overall mass flow rate, based on the energy balance. Indeed, this is done assuming no heat exchange at the FW / BZ boundary. Starting from the performed analysis and considering different inlet conditions and tubes layout, it has been possible to enhance the cooling capability. Improvements are still possible optimizing the orifices strategy.
- Results based on the reference cooling tubes arrangement demonstrated that there is margin for improvements. In particular, the reference layout connected, upstream and downstream, with two manifolds and without orifices evidenced temperatures

of the PbLi and solid structure above the threshold limit of 550°C and saturated conditions inside the tubes.

- Proper orifices at inlet of cooling tubes can be used to enhance the temperatures of the coolant at the outlet section. Moreover, this solution reduces PbLi and structures temperatures below the temperatures limits. These conditions are achieved respecting the velocity constraints.
- The maximum value of the heat load capacity of the First Wall is calculated lower than but close to 1.5 MW/m^2. Structural analysis in normal operating mode and in accident conditions shall confirm this value.

- An improved layout of the breeding zone cooling tubes is proposed and analysed. Results show a better distribution of the coolant flow rate and the outlet coolant temperatures, as well as a reduction of the maximum coolant velocity with consequent decrease of pressure drops.

The following outcomes apply to the analyses of the PbLi system.

- The results have demonstrated that current design, having the PbLi routed out from the central module channels, has limits. Modifications may be applied (i.e. increasing the cross connections through the stiffening plates), which might compromise the structural integrity of the module, when the over-pressurization scenario is considered. The solution shall be re-considered and reviewed.
- The improved layout of the breeding zone cooling tubes has enhanced temperature distribution in PbLi and structures. The maximum temperature is 523 °C, about 30 °C lower than the limit (550 °C).
- Notwithstanding this, differences persist, even though mitigated, between the PbLi temperatures along the toroidal direction. This implies that countermeasures shall be taken to increase the PbLi temperature of the colder part.
- Increasing the baffle plate length, the "quasi" stagnant zones is reduced. These results are conservative and, further analyses are needed activating the buoyancy forces.

The activity has provided feedbacks to designers, highlighting pro and cons of current WCLL breeding blanket design from thermal-hydraulic point of view.

Follow-up activities shall focus on: 1) the review of the PbLi manifold, and the increase of minimum PbLi temperature in the module (changing the cooling path and having inlet and

outlet tubes mixed together in the same breeding zone, or increasing the coolant inlet temperature) and 2) the detailed analysis of the PbLi local flow paths due to buoyancies and/or magnetic field. Moreover, further cooling tubes configurations can be exploited to enhance the temperature filed of the module.

LIST OF REFERENCES

[1] EFDA "Fusion Electricity, A roadmap to the realisation of fusion energy", November 2012.

[2] Fusion power program, "BLANKET COMPARISON AND SELECTION STUDY FINAL REPORT", ANL/FPP-84-1, vol 1-3, US, 1985.

[3] L. Giancarli et alii, "Reference concept selection for EU water-cooled Pb-17Li DEMO blanket", CEA Report (1993).

[4] L. Giancarli et alii, "European reference design of the water-cooled lithium lead blanket for a demonstration reactor", Fusion Technology (1994), 1079-1085.

[5] L. Giancarli et alii, "Development of the EU water-cooled Pb-17Li blanket", Fusion Engineering and Design. 39-40 (1998), 639-644.

[6] P. Sardain et alii, "Power plant conceptual study – WCLL concept", Fusion Engineering and Design 69 (2003) 769-774.

[7] J. Aubert et alii, "Development of the water cooled lithium lead blanket for DEMO", Fusion Engineering and Design 89 (2014) 1386-1391.

[8] J. Aubert et alii, "Preliminary design of a Water Cooled Lithium Lead blanket concept for DEMO reactor", CEA Report for TA WP13-DAS-02 (2013).

[9] G. Aiello et alii, "HCLL blanket 2014 Design Description Document", WPBB-DEL-D1B02.

[10] WCLL Design Description Document, under preparation.

[11] G. McCracken and P. Stott, "Fusion the energy of the Universe", Elsevier Academic Press, 2005.

[12] J. Freidberg, "Plasma Physics and Fusion Energy", Cambridge University Press, 2007.

[13] N. Cerullo, "Lezioni di Ingegneria dei Reattori a Fusione".

[14] www.Iter.org , [online] .

[15] IAEA, "Summary of the ITER final design report" Vienna, 2001.

[16] G. Federici et alii, "Overview of EU DEMO design and R&D activities", Fusion Engineering and Design 89 (2014) 882–889.

[17] J Aubert, et alii, "Preliminary design of a Water Cooled Lithium Lead blanket concept for DEMO reactor", WP13-DAS-02-T03.

[18] D. Stork, "DEMO and the Route to Fusion Power", Intl School of Fusion Technology, 2009.

[19] DEMO Reference Design April 2015

[20] L.V. Boccaccini, “EU blanket design and R&D for DEMO”, 2nd EU–US DCLL Workshop, 2014 UCLA.

[21] M. Dalle Donne (Ed.), “European DEMO BOT Solid Breeder Blanket”, KfK 5429, Forschungszentrum Karlsruhe, 1994.

[22] S. Hermsmeyer, et alii., “Lay-out of the He-cooled solid breeder model B in the European power plant conceptual study”, Fusion Eng. Des 69 (2003) 281–287.

[23] D. Carloni et alii, “Helium Cooled Blanket Design Development”, WP13-DAS-02-T04.

[24] L.V. Boccaccini et alii, “Objectives and status of EUROfusion DEMO blanket studies”, Fusion Engineering and Design.

[25] P. Sardain, et alii., “The European power plant conceptual study: Helium-cooled lithium–lead reactor concept”, Fusion Eng. Des. 81 (2006) 2673–2678.

[26] S. Malang, K. Schleisiek, “Dual Coolant Blanket Concept”, KfK-Report 5424, 1994.

[27] P. Norajitra, et al., “Conceptual design of the dual-coolant blanket in the frame of the EU power plant conceptual study”, Fusion Eng. Des. 69 (2003) 669–673.

[28] Y. Chen et alii, “The EU Power Plant Conceptual Study-Neutronic Design Analyses for Near Term and Advanced Reactor Models”.

[29] Ansys CFX – Solver Theory Guide.

[30] Mas de Vallas et alii, “Lead–lithium eutectic material database for nuclear fusion technology”, Journal of nuclear materials, 2008.

[31] F. P. Incropera et alii, “Principles of HEAT AND MASS TRANSFER” 7th edition.

APPENDIX A – MATERIALS DATA FITTING

```
%POLYFIT Eurofer97 steel
%fitting nell'intervallo di temperatura [573.15-873.15]
T=[573.15 673.15 773.15 873.15];
%roS densità [kg m^-3]
roS=[7666 7633 7596 7558];
RoS=polyfit(T,roS,1);
t=573.15:10:903.15;
RoS_=polyval(RoS,t);
figure
plot(T,roS,'o',t,RoS_)
title('Eurofer density')
xlabel('Temperature [K]')
ylabel('density [kg m^-3]')
%lamS conducibilità termica [W m^-1 K^-1]
lamS=[30.2 29.3 29.5 31.2];
LamS=polyfit(T,lamS,2);
LamS_=polyval(LamS,t);
figure
plot(T,lamS,'o',t,LamS_)
title('Eurofer Thermal conductivity')
xlabel('Temperature [K]')
ylabel('Thermal conductivity [W m^-1 K^-1]')
%T1 vettore Temperatura [K]
T1=573.15:50:873.15;
%cpS calore specifico [j kg^-1 K^-1]
cpS=[551 566 584 612 655 721 801];
CpS=polyfit(T1,cpS,3);
CpS_=polyval(CpS,t);
figure
plot(T1,cpS,'o',t,CpS_)
title('Eurofer specific heat')
xlabel('Temperature [K]')
ylabel('Specific heat [j kg^-1 K^-1]')
%POLYFIT Pb15.7Li
%fitting nell'intervallo di temperatura [573.15-973.15]
%T2 vettore temperatura [K]
T2=573.15:50:973.15;
%roP densità [kg m^-3]
roP=[9839 9779 9720 9661 9601 9542 9482 9423 9363];
RoP=polyfit(T2,roP,1);
t2=573.15:10:973.15;
RoP_=polyval(RoP,t2);
figure
plot(T2,roP,'o',t2,RoP_)
title('PbLi density')
xlabel('Temperature [K]')
ylabel('density [kg m^-3]')
%lamP conducibilità termica [W m^-1 K^-1]
lamP=[13.18 14.16 15.14 16.12 17.10 18.08 19.06 20.04 21.02];
LamP=polyfit(T2,lamP,1);
LamP_=polyval(LamP,t2);
figure
```

```
plot(T2,lamP,'o',t2,LamP_)
title('PbLi Thermal conductivity')
xlabel('Temperature [K]')
ylabel('Thermal conductivity [W m^-1 K^-1]')
%cpP calore specifico [j kg^-1 K^-1]
cpP=[190 189 189 188 187 187 187 187 186];
CpP=polyfit(T2,cpP,1);
CpP_=polyval(CpP,t2);
figure
plot(T2,cpP,'o',t2,CpP_)
title('PbLi specific heat')
xlabel('Temperature [K]')
ylabel('Specific heat [j kg^-1 K^-1]')
%Polifit coolant
%fitting nell'intervallo di temperatura [543.15-613.15] K [270-
340] °C
%T3 temperatura [K]
T3=543.15:10:613.15;
%roC densità [kg m^-3]
roC=[782 765 747 727 705 680 651 616];
RoC=polyfit(T3,roC,2);
t3=543.15:2:613.15;
RoC_=polyval(RoC,t3);
figure
plot(T3,roC,'o',t3,RoC_)
title('Coolant density')
xlabel('Temperature [K]')
ylabel('density [kg m^-3]')
%lamC conducibilità termica [W m^-1 K^-1]
lamC=[0.607 0.593 0.577 0.559 0.539 0.516 0.491 0.462];
LamC=polyfit(T3,lamC,2);
LamC_=polyval(LamC,t3);
figure
plot(T3,lamC,'o',t3,LamC_)
title('coolant Thermal conductivity')
xlabel('Temperature [K]')
ylabel('Thermal conductivity [W m^-1 K^-1]')
%cpC calore specifico [j kg^-1 K^-1]
cpC=[4895 5043 5232 5481 5818 6290 6977 8036];
CpC=polyfit(T3,cpC,3);
CpC_=polyval(CpC,t3);
figure
plot(T3,cpC,'o',t3,CpC_)
title('Coolant specific heat')
xlabel('Temperature [K]')
ylabel('Specific heat [j kg^-1 K^-1]')
%muC viscosità dinamica 10^-6 [Kg m^-1 s^-1]
muC=[102 98.2 94.9 91.7 88.3 84.5 80.4 76];
MuC=polyfit(T3,muC,2);
MuC_=polyval(MuC,t3);
figure
plot(T3,muC,'o',t3,MuC_)
title('Coolant Dynamic viscosity')
xlabel('Temperature [K]')
ylabel('Dynamic viscosity 10^-6 [Kg m^-1 s^-1]')
```

APPENDIX B - MATERIALS CEL EXPRESSION

CpCoolant

```
if(T>543.15[K] && T<=613.15 [K], (9.8485[K^-3]*10^-3*T^3-
16.39861[K^-2]*T^2+9118.681[K^-1]*T-1.6882247*10^6)*1[J * kg^-
1*K^-1],0[J * kg^-1*K^-1])+if(T>613.15 [K],8021.5[J * kg^-1*K^-
1],0[J * kg^-1*K^-1])+if(T<=543.15[K],4883[J * kg^-1*K^-1],0[J *
kg^-1*K^-1])
```

DynViscoCoolant

```
if(T>543.15[K] && T<=613.15[K],(-8.095238[K^-2]*10^-
4*T^2+0.5722429[K^-1]*T+29.67213)*10^-6*1[kg*m^-1*s^-1],0[kg*m^-
1*s^-1])+if(T>613.15 [K],7.62*10^-5*1[kg*m^-1*s^-1],0[kg*m^-1*s^-
1])+if(T<=543.15[K],0.000101667[kg*m^-1*s^-1],0[kg*m^-1*s^-1])
```

LambdaCoolant

```
if(T>543.15[K] && T<=613.15[K],(-1.2024[K^-2]*T^2*10^-5+1.1846[K^-
1]*T*10^-2-2.2804)*1[W*m^-1*K^-1],0[W*m^-1*K^-
1])+if(T>613.15[K],0.46252[W*m^-1*K^-1],0[W*m^-1*K^-
1])+if(T<=543.15[K],0.606534[W*m^-1*K^-1],0[W*m^-1*K^-1])
```

RhoCoolant

```
if(T>543.15[K] && T<=613.15[K],(-1.4226[K^-2]*10^-2*T^2+14.122[K^-
1]*T-2693)*1[kg*m^-3],0[kg*m^-3])+if(T>613.15[K],617.598[kg*m^-
3],0[kg*m^-3])+if(T<=543.15[K],780.525[kg*m^-3],0[kg*m^-3])
```

CpPbLi

```
if(T>573.15[K] && T<=973.15[K],(194.74[K] -9*10^-3*T) * 1 [J* kg^-
1* K^-2] ,0[J* kg^-1* K^-1])+if(T>973.15[K],185.982[J* kg^-1* K^-
1],0[J* kg^-1* K^-1])+if(T<=573.15[K],189.582[J* kg^-1* K^-1],0[J*
kg^-1* K^-1])
```

DynViscoPbLi

```
if(T>573.15[K] && T<=973.15[K],(1.87*10^-
4)[Pa*s]*exp(11640[J*mol^-1]
/(T*R)),0[Pa*s])+if(T>973.15[K],0.000788162[Pa*s],0[Pa*s])+if(T<=5
73.15[K],0.00215102[Pa*s],0[Pa*s])
```

LambdaPbLi

```
if(T>573.15[K] && T<=973.15[K],(1.96 [K^-1]*10^-
2*T+1.9463)*1[W*m^-1*K^-1],0[W*m^-1*K^-
1])+if(T>973.15[K],21.02[W*m^-1*K^-1],0[W*m^-1*K^-
1])+if(T<=573.15[K],13.18[W*m^-1*K^-1],0[W*m^-1*K^-1])
```

RhoPbLi

```
if(T>573.15[K] && T<=973.15[K],(-1.189[K^-1]*T+10520)*1[kg*m^-
3],0[kg*m^-3])+if(T>973.15[K],9362.92[kg*m^-3],0[kg*m^-
3])+if(T<=573.15[K],9362.92[kg*m^-3],0[kg*m^-3])
```

CpEurofer

```
if(T>573.15[K] && T<=873.15 [K],(-4.3883*10^2+4.9838[K^-1] *T-
8.7371[K^-2]*10^-3*T^2+5.3333[K^-3]*10^-6*T^3)*1[J * kg^-1*K^-
1],0[J * kg^-1*K^-1])+if(T>873.15[K],801.968[J* kg^-1* K^-1],0[J*
kg^-1* K^-1])+if(T<=573.15[K],551.644[J* kg^-1* K^-1],0[J* kg^-1*
```

```
K^-1])
```

LambdaEurofer

```
if(T>573.15[K] && T<=873.15[K],(60.915-9.081[K^-1]*10^-2*T+6.5[K^-
2]*10^-5*T^2)*1[W*m^-1*K^-1],0[W*m^-1*K^-
1])+if(T>873.15[K],31.1796[W*m^-1*K^-1],0[W*m^-1*K^-
1])+if(T<=573.15[K],30.2198[W*m^-1*K^-1],0[W*m^-1*K^-1])
```

RhoEurofer

```
if(T>573.15[K] && T<=873.15[K],(-0.361[K^-1]*T+7874.3)*1[kg*m^-
3],0[kg*m^-3])+if(T>873.15[K],7559.09[kg*m^-3],0[kg*m^-
3])+if(T<=573.15[K],7667.39[kg*m^-3],0[kg*m^-3])
```

APPENDIX C – POWER DENSITY CEL EXPRESSION

Pbli Power density

```
(if(x>0 [mm] && x<=34.4 [mm], 0.045, 0)+if(x>34.4 [mm] && x<=66.4
[mm], 0.053, 0)+if(x>66.4 [mm] && x<=98.4 [mm], 0.062,
0)+if(x>98.4 [mm] && x<=130.4 [mm], 0.078, 0)+if(x>130.4[mm] &&
x<=138.4 [mm], 0.092, 0)+if(x>138.4 [mm] && x<=169.8 [mm], 0.107,
0)+if(x>169.8 [mm] && x<=201.8 [mm], 0.123, 0)+if(x>201.8 [mm] &&
x<=233.8 [mm], 0.152, 0)+if(x>233.8 [mm] && x<=265.8 [mm], 0.185,
0)+if(x>265.8 [mm] && x<=297.8 [mm], 0.234, 0)+if(x>297.8 [mm] &&
x<=305.8 [mm], 0.269, 0)+if(x>305.8 [mm] && x<=337.2 [mm], 0.312,
0)+if(x>337.2 [mm] && x<=369.2 [mm], 0.312, 0)+if(x>369.2 [mm] &&
x<=401.2 [mm], 0.447, 0)+if(x>401.2 [mm] && x<=433.2 [mm], 0.550,
0)+if(x>433.2 [mm] && x<=465.2 [mm], 0.705, 0)+if(x>465.2 [mm] &&
x<=473.2 [mm], 0.780, 0)+if(x>473.2 [mm] && x<=504.6 [mm], 0.886,
0)+if(x>504.6 [mm] && x<=536.6 [mm], 1.042, 0)+if(x>536.6 [mm] &&
x<=568.6 [mm], 1.288, 0)+if(x>568.6 [mm] && x<=600.6 [mm], 1.645,
0)+if(x>600.6 [mm] && x<=632.6 [mm], 2.280, 0)+if(x>632.6 [mm] &&
x<=640.6 [mm], 2.913, 0)+if(x>640.6 [mm] && x<=672 [mm], 3.646,
0)+if(x>672 [mm] && x<=704 [mm], 4.446, 0)+if(x>704 [mm] && x<=736
[mm], 5.681, 0)+if(x>736 [mm] && x<=768 [mm], 7.444, 0)+if(x>768
[mm] && x<=800 [mm], 11.152, 0))*1 [W*cm^-3]
```

Eurofer Power density

```
(if(x>0 [mm] && x<=34.4 [mm], 0.004, 0)+if(x>34.4 [mm] && x<=66.4
[mm], 0.004, 0)+if(x>66.4 [mm] && x<=98.4 [mm], 0.004,
0)+if(x>98.4 [mm] && x<=130.4 [mm], 0.004, 0)+if(x>130.4[mm] &&
x<=138.4 [mm], 0.006, 0)+if(x>138.4 [mm] && x<=169.8 [mm], 0.008,
0)+if(x>169.8 [mm] && x<=201.8 [mm], 0.008, 0)+if(x>201.8 [mm] &&
x<=233.8 [mm], 0.012, 0)+if(x>233.8 [mm] && x<=265.8 [mm], 0.016,
0)+if(x>265.8 [mm] && x<=297.8 [mm], 0.021, 0)+if(x>297.8 [mm] &&
x<=305.8 [mm], 0.024, 0)+if(x>305.8 [mm] && x<=337.2 [mm], 0.029,
0)+if(x>337.2 [mm] && x<=369.2 [mm], 0.037, 0)+if(x>369.2 [mm] &&
x<=401.2 [mm], 0.049, 0)+if(x>401.2 [mm] && x<=433.2 [mm], 0.066,
0)+if(x>433.2 [mm] && x<=465.2 [mm], 0.090, 0)+if(x>465.2 [mm] &&
x<=473.2 [mm], 0.106, 0)+if(x>473.2 [mm] && x<=504.6 [mm], 0.123,
0)+if(x>504.6 [mm] && x<=536.6 [mm], 0.156, 0)+if(x>536.6 [mm] &&
x<=568.6 [mm], 0.205, 0)+if(x>568.6 [mm] && x<=600.6 [mm], 0.279,
0)+if(x>600.6 [mm] && x<=632.6 [mm], 0.402, 0)+if(x>632.6 [mm] &&
x<=640.6 [mm], 0.531, 0)+if(x>640.6 [mm] && x<=672 [mm], 0.677,
0)+if(x>672 [mm] && x<=704 [mm], 0.886, 0)+if(x>704 [mm] && x<=736
[mm], 1.210, 0)+if(x>736 [mm] && x<=768 [mm], 1.690, 0)+if(x>768
[mm] && x<=800 [mm], 2.539, 0)+if(x>800[mm] &&
x<=817.3[mm],7.887,0)+if(x>817.3[mm] &&
x<=820.3[mm],5.229,0)+if(x>820.3[mm] && x<=827[mm],8.704,0))*1
[W*cm^-3]
```